PROBE FOR PORTABLE LASER INDUCED BREAKDOWN SPECTROSCOPY OF MOLTEN ALUMINUM AND CRYOLITE

Úlfar Karl Arnórsson

Thesis

B.Sc. Mechanical and Energy Engineering

2014

Author: Úlfar Karl Arnórsson
Social ID: 151288-2789
Instructor: Sveinn Hinrik Guðmundsson

Tækni- og verkfræðideild
School of Science and Engineering

Tækni- og verkfræðideild

Heiti verkefnis:

Probe for portable laser induced breakdown spectroscopy of molten aluminum and cryolite

Námsbraut:

B.Sc. Vél- og orkutæknifræði

Tegund verkefnis:

Lokaverkefni í tæknifræði B.Sc.

Önn:

Haust, 2014

Námskeið:

VT LOK 1012

Höfundur:

Úlfar Karl Arnórsson

Umsjónarkennari:

Indriði Sævar Ríkharðsson

Leiðbeinandi:

Sveinn Hinrik Guðmundsson

Fyrirtæki/stofnun:

DTE ehf. – Dynamic Technology Equipment ehf.

Ágrip:

Við álframleiðslu þarf að fylgjast stöðugt með hreinleika álsins ásamt efnafræðilegri byggingu raflausnarinnar sem notuð er til að rafgreina áloxíð í hreint ál. Í dag er sýni tekið af raflausninni og álbráðinni, sýnin eru steypt og meðhöndluð áður en það fer í greiningu á rannsóknarstofu. Ferlið er langt og stýringar keranna vinna stöðugt eftir gömlum upplýsingum. Í þessu verkefni eru vandamálin við að beita „laser induced breakdown spectroscopy“ eða LIBS tækni til frumefnagreiningar á álbráð og raflausn í álframleiðslu skoðuð. Orkumiklum leysigeisla er er skotið í gegnum ljósleiðara sem tengist í próbu sem stungið er ofan í fljótandi álbráðina sem og raflausnina. Geislinn fer í gegnum linsur sem sjá til þess að brennipunktur geislans lendi á yfirborði fljótandi málmsins og rafgas er myndað. Ljósið frá rafgasinu er síðan flutt aftur til baka í gegnum ljósleiðarann í litrófsgreini þar sem frumefnagreining fer fram. Með þessu styttist ferlið verulega og upplýsingaflæði til framleiðslustýringanna eykst. Þetta leiðir til mikils orkusparnaðar, minnkunar á losun gróðurhúsalofttegunda og meiri gæða.
Aðaláherslan í þessu verkefni er hönnun á próbu sem þolir hitastigið og tæringuna sem er til staðar í kerjunum. Próban þarf að skapa samskonar aðstæður fyrir hverja greiningu til þess að samræmi sé í öllum greiningum. Til þess að oxíð húð myndist ekki á álbráðinni er óvirku gasi blásið inn í próbuna. Þrýstistýring var hönnuð til að stjórna gasþrýstingnum inni í próbunni til þess að yfirborð bráðarinnar haldist í brennipunkti geislans.

Dagsetning:

03.12.2014

Lykilorð íslensk:

LIBS, próba, bráð, ál

Lykilorð ensk:

LIBS, probe, molten, aluminum.

Dreyfing:

opin ☐ **lokuð** X **til: 03.12.17**

Probe for Portable Laser Induced Breakdown Spectroscopy of Molten Aluminum and Cryolite

Úlfar Karl Arnórsson

24 ECTS thesis submitted to the School of Science and Engineering at Reykjavík University in partial fulfillment of the requirements for the degree of

Bachelor of Science in Mechanical and Energy Engineering

Student:

Úlfar Karl Arnórsson	Date

Supervisor:

Indriði Sævar Ríkharðsson	Date

Instructor:

Sveinn Hinrik Guðmundsson	Date

Abstract

In modern aluminum smelters there is a constant need for monitoring the purity of the aluminum being made and the chemical composition of the electrolyte used to drive the chemical reaction to produce aluminum from alumina. The process of sampling and analysing these parameters today takes a long time and the process control is constantly working with old information.

In this thesis the problems of applying laser induced breakdown spectroscopy on molten aluminum and cryolite in aluminum smelters is explored. A high intensity laser beam is transferred through an optical fiber to a probe where the laser beam is focused upon the molten material and micro plasma is generated. The emission from the micro plasma is then viewed back through the optical fiber with a spectroscope and elemental analysis is performed. This should result in gains in process understanding, efficiency, material quality and environmental factors.

The main focus of this thesis is the design of a probe that is resistant to the heat and corrosion in the pots. The probe needs to keep conditions as similar as possible for all analysis. To prevent oxidization of the aluminum melt a noble gas is purged inside the probe and a pressure control system was designed to control the surface of the molten material around the focal point of the lens.

“The science of today is the technology of tomorrow.”
Edward Teller

Contents

List of Equations

List of Figures

List of Tables

1 Introduction

Modern aluminum smelters follow the principles of the Hall-Héroult process. This process involves taking alumina (Al_2O_3) and dissolving it in molten cryolite (Na_3AlF_6). A carbon electrode works as an anode and sends direct current through the electrolyte. The steel shell of the pot is lined with refractory thermal insulation and at the bottom the aluminum produced works as a cathode where the current is lead through a carbon block and exits the pot through a bus bar [1]. This is called electrolysis which is used to drive the chemical reaction that is breaking alumina into its primary element aluminum and then carbon dioxide (see (1), (2) and (3), the aluminum sinks to the bottom because at liquid state the aluminum is denser than the cryolite while at solid state the opposite is true as seen in Table 1. The oxygen moves up and oxidizes the carbon anode and carbon dioxide is produced. The anode dissolves and the distance between the anode and cathode needs to be controlled to withhold the right resistance with the optimal voltage around 4.2V [2].

$$\overbrace{2Al_2O_3}^{\text{Alumina}} + \overbrace{3C}^{\text{Carbon anode}} = \overbrace{4Al}^{\text{Aluminum}} + \overbrace{3CO_2}^{\text{Carbon dioxide}} \tag{1}$$

$$\overbrace{6O^{2-} + 3C = 3CO_2 + 12e^-}^{\text{Anode}} \tag{2}$$

$$\overbrace{4Al^{3+} + 12e^- = 4Al}^{\text{Cathode}} \tag{3}$$

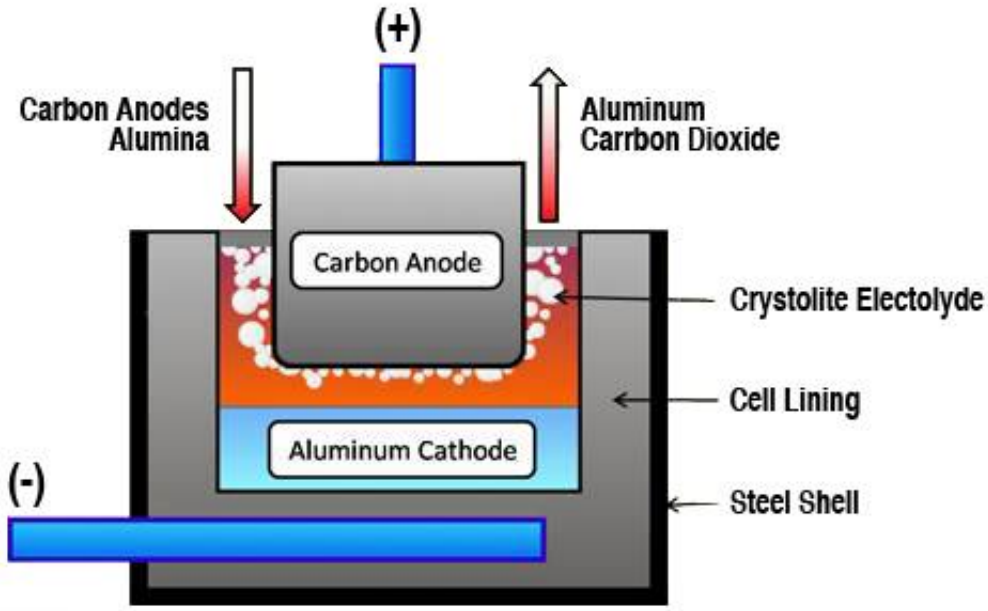

Fig. 1. Hall Héroult process [1].

	Room temperature	**960**$^{\circ}C$
Aluminum	2710 [$\frac{kg}{m^3}$] [3]	2365 [$\frac{kg}{m^3}$] [4]
Na_3AlF_6	2900 [$\frac{kg}{m^3}$] [3]	2100 [$\frac{kg}{m^3}$] [5]

Table 1. Density of aluminum and cryolite in molten and solid state.

For this process to work efficiently, power, quality and environmentally all material and thermal balances need to be controlled thoroughly. In the semi-closed loop control of the temperature and material balance the feedback is delayed up to 24 hours. With the method used today, a sample of the bath and aluminum are taken by hand and solidified. These samples need to be prepared and sent to a laboratory where the samples are machined, grounded and categorized before elemental and crystal structure analysis is performed. This process can take from 6 to 24 hours, depending on the size of the smelter [6], and by that delaying the feedback to the control system drastically. Because of this delay the output of the control loop is based on old information and because the properties of the cell changes dynamically in time the input to the cell more often overshoots the desired output causing an unsteady system. The system then tries to correct the overshoot up to a day later with the same results. This feedback delay causes the system to never fully accomplish optimal operating conditions [7]. Because of the complexity of the process there is always a chance of sample mix-up and the data being registered to a different pot.

To get real time data from the bath and aluminum, DTE (Dynamic Technology Equipment) are developing PEA Aluminum (Portable Elemental Analysis Aluminum). The idea is to use LIBS technology (Laser Induced Breakdown Spectroscopy), where a high intensity laser beam is focused on the molten electrolyte and aluminum and micro plasma is generated. By viewing the emission from the plasma, back through a fiber optic with a spectrometer, the composition of elements can be determined, essentially taking the process that is used today and compressing it down to seconds. An employee will go from pot to pot with the portable device and at each pot the employee will insert a probe into the bath material and the laser is discharged. Then he will do the same for the aluminum and raw data will go to a cloud, via wireless connection, where the algorithmic calculations take place and feedback is than sent to the process control and by that provide *in-situ* measurements of the elemental composition.

The gains of *in-situ* information are huge. The obvious ones are saving labor hours, laboratories and equipment but looking at the possible gains in process understanding, efficiency, material quality and environmental factors are far greater. If you look at the solution Alcoa have made, seen in section 2.2, they guarantee that current efficiency is up by 0.5%, voltage usage is down by 35 mV, AlF_3 savings are 5% and still to established 100-150 day pot life improvement [8]. Only looking at the electrical savings and assuming 4.5 V over each pot, a current of 200 kA and that the price per MWh is around $25 you can see that energy savings for one pot in a year are 100 MWh that becomes $2500 a year. If this was in a mediocre sized aluminum smelting company with 500 pots the savings related only to energy would be around 1.25 million dollars. To put that in perspective the energy savings alone in an aluminum smelter this size are equal to the energy needed to produce around 3700 tons of aluminum.

Gains by using the STARprobe discussed in 2.2

- 0.5% current efficiency (proven)
- 35 mV voltage savings (proven)
- 5% AlF3 savings (proven)
- 100-150 day pot life improvement (still to be established)
- One time capital cost saving (X-ray equipment) (proven)
- Labor savings for sampling/analysis (proven)
- Improved understanding by operators (proven) [8]

Estimated energy savings	
Electric current	200 kA
Voltage (single pot)	4.5 V
Electric price	$25 per Mwh
Energy savings in a year	100.4 MWh
Savings	$2500 per year

Table 2. Estimated energy savings per pot.

In this report the focus will be on the design and development of a working prototype of the probe. The laser pulse is transferred through an optical fiber to the probe where the focal point of the beam is adjusted with lenses. The energy of the beam is focused on the surface to get high-energy plasma emission, therefore the length from the focusing lens to the surface of the material being analysed is critical for constant signal readings and repeatability. The probe also needs to be able to handle high temperatures and highly corrosive environment.

The two main problems of the probe design are broken into two parts. The problem of controlling the length from the focus lens to the liquid material, described in section 3.2, will be issued by making a small prototype made from plexiglass where the only input will be pressure by gas as a function of the depth in liquid material. The problem of transferring and focusing the laser beam onto the liquid material and capturing the emission radiation back will then be issued by making a prototype from steel, which can be used in experimental setups and, with little modification, also in liquid materials.

2 Theoretical Backround

2.1 Parameters to Achieve

There are numerous parameters that need to be measured to be able to control the cell's electrolysis, aluminum quality, cell life, overall efficiency, emission of undesirable gases, anode carbon consumption etc.

Superheat is the difference between bath temperature and the liquidus temperature of the bath composition seen in (4). Liquidus temperature is the temperature where solid material starts to precipitate in the liquid melt. The liquidus line can be seen in Fig. 4 between the liquid phase and the semi-solid phases meeting in the eutectic point. The effects of controlling the superheat are essential. The current efficiency is affected by the superheat, i.e. the lower the superheat, the higher the current efficiency, although alumina solubility decreases when superheat is too low. It is optimal to keep the density ratio of aluminum and bath as high as possible, as said before the density of aluminum is greater at liquid state. This automatically separates the aluminum from the bath after electrolysis occurs and the molten cryolite protects the aluminum from oxidization. So the higher the temperature of the bath the higher the density ratio is. But as said before the current efficiency decreases with high superheat and the decomposition of the carbon anodes increases so there is a fine line in controlling the bath temperature. To control the superheat, additives are used to lower the liquidus temperature primarily AlF_3, CaF_2 and sometimes other [9].

$$\Delta T = T_B - T_L \tag{4}$$

ΔT: Superheat, T_B: Bath temperature, T_L: Liquidus temperature [10]

Cryolite ratio seen in (5) is actually a measurement of the pureness of the cryolite as pure cryolite has a CR ratio of three as seen by finding the common denominator of cryolite composition $Na_3AlF_6 \rightarrow 3NaF \cdot AlF_3$. By adding excess aluminum fluoride to the cryolite the ratio lowers but the current efficiency increases. Modern smelters are working at a ratio of two to three. By looking at the phase diagram in Fig. 2 you can see that the liquidus temperature is also related to the cryolite ratio.

$$CR = \frac{n_{NaF}}{n_{AlF_3}} \tag{5}$$

CR: Cryolite ratio, n_{NaF}: Number of sodium fluoride moles, n_{AlF_3}: Number of aluminum fluoride moles [11]

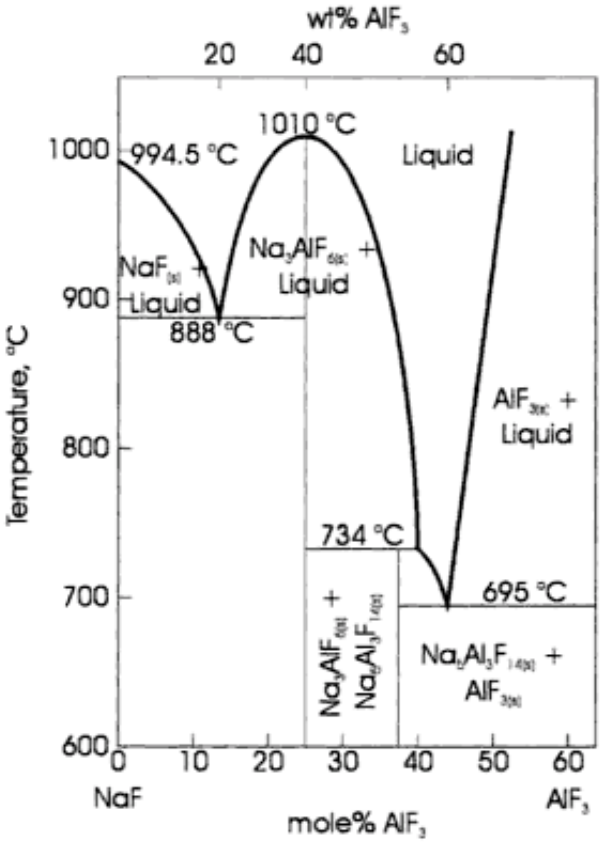

Fig. 2. $NaF - AlF_3$ Phase diagram [12].

As said before the Hall-Héroult process works by dissolving alumina in the bath by using electrolysis. The optimal concentration of alumina is around 2-5%. If the alumina concentration is too high there is a risk of the anode effect where the oxygen from the electrolysis of alumina (Al_2O_3) reacts with the carbon anode and a film of carbon dioxide separates the electrolyte from the anode resulting in higher resistance and therefore voltage.

Aluminum smelters produce primary aluminum with a purity of 99.7-99.9%. The purity controls the price and for applications like electrical conductors, capacitors, etc. the purity is essential for low resistance. To be able to get this high purity the process control needs information about trace elements in the aluminum produced. The trace elements typically shown in analysis are iron and silicon and in smaller amount zinc, magnesium, manganese, titanium, copper, chromium, gallium, sodium, lithium, calcium, vanadium and boron [13]. Sodium, lithium, calcium and magnesium can be removed by passing chlorine gas through the molten aluminum. Oxides and carbides can be removed with filters. Other elements are removed by further refinement. If iron levels rise there is a risk of leakage from the steel shell so by knowing these levels operators can determine if the shell should be shut down and re-insulated.

2.2 Alcoa STARprobe

Over the last 10 to 15 years Alcoa has developed a tool to measure four of the control parameters required to feed the control system of the pots. This device is called STARprobe, which stands for **S**uperheat, **T**emperature, **A**lumina concentration and cryolite **R**atio and it delivers almost *in-situ* measurements of these parameters. This device only measures key parameters in the bath but not the aluminum [6].

2.2.1 Theory

In order to get the material characteristics, Alcoa relies on DTA or differential thermal analysis. DTA works by monitoring the thermal energy that the sample is releasing by comparing the temperature over time with a reference material. The probe seen in Fig. 3 is lowered in to the liquid bath and kept there for a couple of minutes for the tip to get to a thermal equilibrium state with the bath. When the probe is pulled up, the sample slot, marked (116) on the right in Fig. 3, is filled with liquid bath and the solid matter that the probe is made of is at the same temperature as the sample. Type-K thermocouples, marked 22-a and 22-b on the right side in Fig. 3, monitor the temperatures over time. Every time the bath sample goes through a phase transformation a temperature difference occurs compared to the reference material. This way they are able to measure the heat release rate from the sample and detect phase transformations.

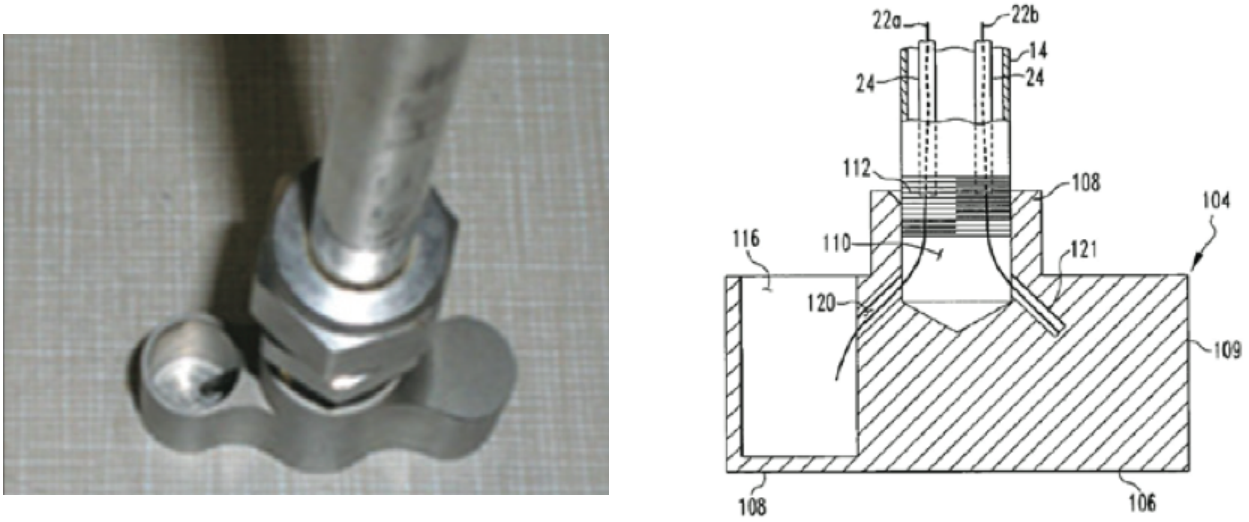

Fig. 3. STAR probe tip [7].

The cryolite ratio, see (5), is related to the thermal release during the phase transformation therefore by monitoring the temperature difference of the sample and the reference material it is possible to calculate the ratio. To measure the superheat the temperature at the first occurrence of phase change from liquid bath, seen in (6) and the phase diagram in Fig. 4, is registered and the difference from original temperature and that temperature is the superheat.

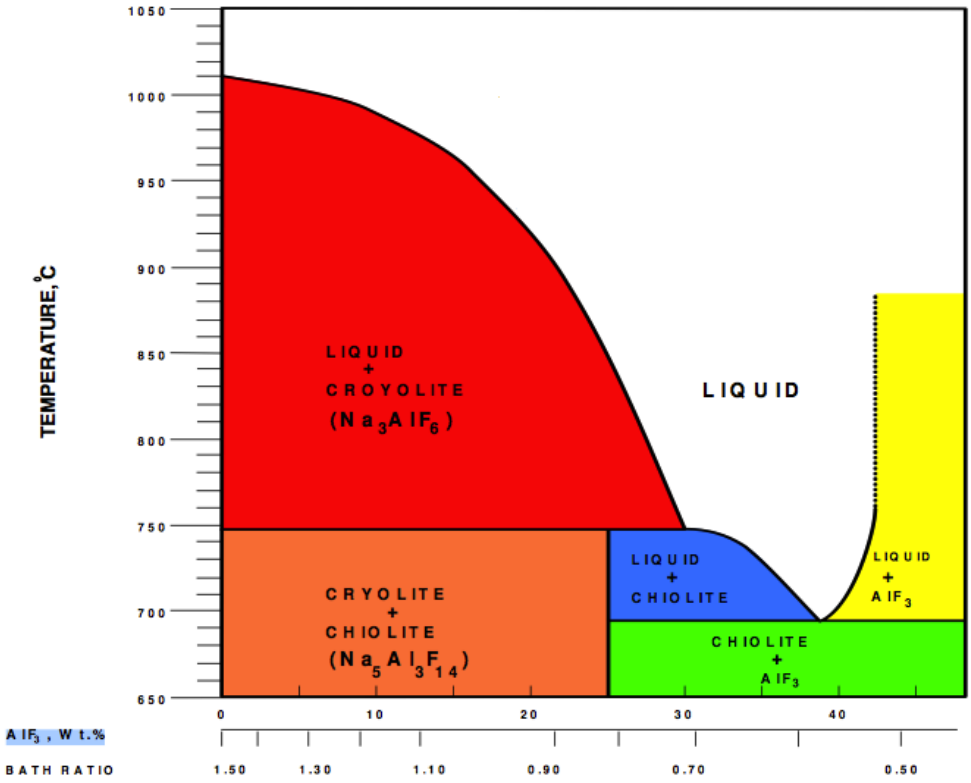

Fig. 4. $Na_3AlF_6 - AlF_3$ Phase diagram [6].

$$Liq.Bath \rightarrow Na_3AlF_6 + Liq.(var.XS \quad ALF_3) \tag{6}$$

When the bath liquidus, or the temperature of the first phase transformation increases, the aluminum concentration also increases this and the fact that the magnitude of a peak of heat release between $800 - 900°C$ is related to it, ables the Alcoa STARprobe to measure the aluminum concentration.

Alcoa developed a new cell controller to take advantage of this new measurement method. Reported improvements according to Dr. M. Dupuis (2013) are: 0.5% improved current efficiency, 35mV voltage savings, 5% AlF_3 savings, a one time capital cost saving (X-ray equipment), labor savings for sampling/analysis, and improved understanding by operators, as well as a potential of 100-150 day pot life improvement (still being tested) [8].

2.3 LIBS of Molten Aluminum Alloy

As said before laser induced breakdown spectroscopy or LIBS is an elemental analysis method where a high intensity laser beam is focused on a sample to produce micro plasma for spectroscopic analysis. Theoretically LIBS can analyse all matter in all states, which makes it optimal for elemental analysis of molten aluminum or bath material. As this is a known fact there have been some experiments with elemental analysis of molten aluminum alloy but none have been made so robust that they could be used for industrial usage. At the Diagnostic Instrumentation and Analysis Laboratory, Mississippi State University, Awadhesh, Yueh and Singh [14], published their work on LIBS of molten aluminum alloy. They were able to measure concentrations of several additives in the aluminum melt by using Fe as a reference element. All experiments were done in a laboratory furnace with optimal conditions.

2.3.1 Experiment Setup

Following Fig. 5, the Nd:YAG laser (Big Sky CFR-400 532 nm) discharges a beam through a lens with a focal length of 10 cm, 5 mm behind the focal point the beam enters the optical fiber (Thorlabs FG-1.0-UAT UV to visible transmission 1000$\pm$25 μm) through a 0.8 mm pinhole. After the fiber the beam is collimated in a plano-convex lens with a focal length of 15 cm. The parallel beam is then focused with a plano-convex lens with focal length of 5 cm, 75 cm behind the collimating lens. To protect the probe, control the distance from the focal point to material and prevent oxidization of the aluminum Ar and N_2 was purged inside the probe and as seen in Fig. 6 below the collimating lens, the outlet is eight equal sized holes below the focus lens. The pressure control of the gas was primitive, the inlet flow rate was constant at 1.5-3 L/min and the outlet constant at 100-600 mL/min. This was found to be sufficient to get good signal readings in a laboratory setup. The emission light is then captured through the same optical fiber and delivered to the spectrograph and the data sent to the computer.

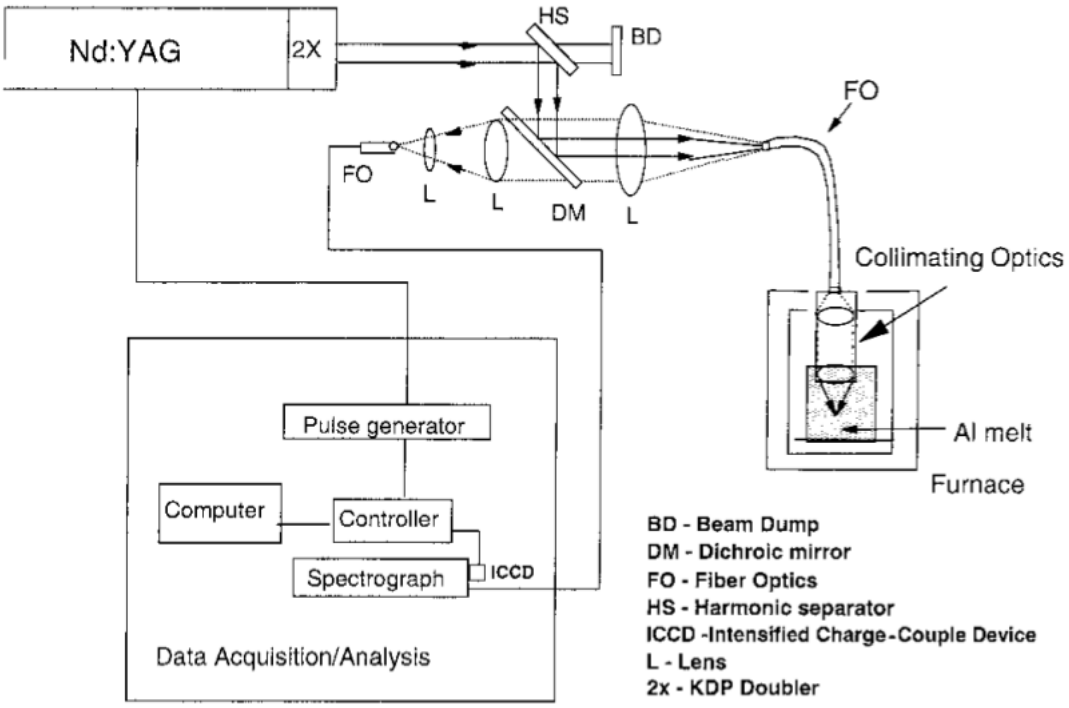

Fig. 5. Experimental setup [14].

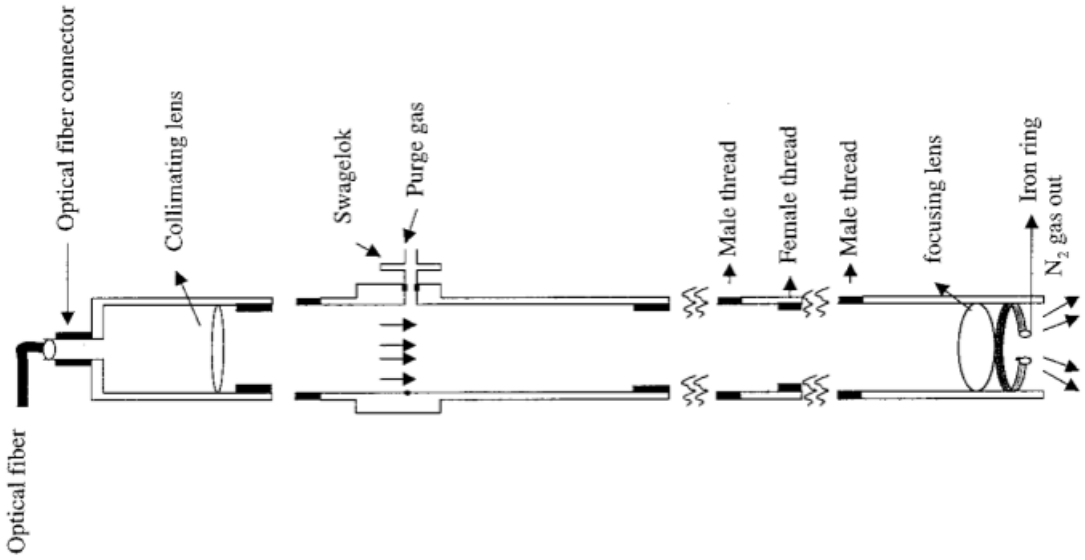

Fig. 6. Schematic diagram of the probe used in the experiment [14].

Cr, Cu, Mg, Mn, Si, Zn, etc. were detected in the aluminum melt. The Ar gas proved to be a better choice giving higher signal to backround ratio (S/B) and higher signal to noise ratio (S/N). It could also be shown that it is not possible to apply calibration curves from solid samples to the molten ones, because the calibration curve is afflicted by the melting point of the element.

3 Focus of Development and Limits

When designing a measurement or analytical device; accuracy, repeatability, reproducibility and stability are topics that need to be confronted. The necessary accuracy of a measurement device needs to be determined beforehand and the device then designed to meet that requirement. The main focus of the probe design is on repeatability, reproducibility, stability and robustness. The probe needs to maintain the same conditions for all measurements to be able to get the same results from multiple measurements of the same sample, regardless of who performs the measurements. The human factor also has to be taken into account, i.e. that the procedure will not be completely followed as planned.

3.1 Transfer of Light

The laser beam is supposed transfer through the fiber optics, collimate in the first plano-convex lens and then focus in the second lens. Everything needs to be concentric for the lens to work as supposed therefore manufacturing accuracy is essential. The emitting light explodes in random directions so in order to capture as much as possible of the emitting light the surface of the inside of the probe should not absorb much light.

3.2 Conditions Inside The Probe

By focusing the laser beam onto a small area, the energy per square mm [$\frac{mJ}{mm^2}$] or mol [$\frac{mJ}{mol}$] increases. One disadvantage of focusing the laser onto a small area is that the liquid material may not be homogeneous so the emission's spectral lines may reflect wrong information statistically, so there is a fine line between the optimal energy per area and signal readings with information that reflects the right results. By increasing the laser energy it is possible to explore more area and therefore the deviation from the focal point can be bigger. Fig. 7 shows how area A (in Fig. 7), that the laser beam is focused on, is a function of the deviation D (in Fig. 7). Therefore to control the maximum area the deviation needs to be controlled.

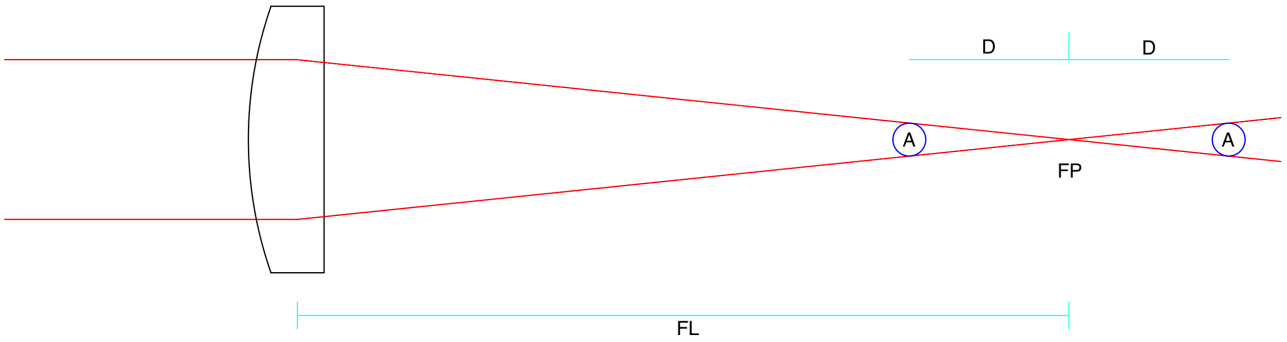

Fig. 7. Schematic drawing of the laser beam being focused by a plano convex lens. (a) FL: focal length, (b) A: area and (c) D: deviation.

When analysing the aluminum melt it is essential to have direct access to the melt because the emission from the melt will only withhold information about the surface. This is why it is important that the melt will not oxidize with the atmosphere. By purging inert gas inside the probe it is possible to lower the chance of oxidization.
When the probe is submerged into the liquid the pressure at the tip increases as seen in (7) and given a constant amount of gas inside the probe according to Boyle's Law seen in (8) the volume of the air or gas inside the probe will decrease. Looking at the ideal gas law the only way to compensate for the change in volume due to pressure change is to control the amount of gas inside the probe or control the heat. If not compensated for the length from the focus lens to the liquid surface will change with depth, and the slope of the pressure will not always be the same do to change in the density when the tip of the probe goes through the bath and into the aluminum.

$$P_{tip} = P_{atm} + \rho * g * h \tag{7}$$

P_{tip} : *Pressure at the tip,* P_{atm} : *Atmospheric pressure,* ρ : *Density of liquid,* g : *Gravitational acceleration,* h : *Depth in liquid*

$$PV = k \tag{8}$$

P*: Pressure,* V*: Volume,* k*: Constant*

$$PV = nRT \tag{9}$$

P*: Pressure,* V*: Volume,* n*: Amount of gas in mol,* R*: Universal gas constant (*$8.314\frac{J}{molK}$*),* T*: Temperature in kelvin*

3.3 Heat and Corrosion

The operating temperature of the molten aluminum and electrolyte is around 950$^\circ C$ [1] so the materials of the probe should have their solidus line well above 1000$^\circ C$.

Corrosion of metals is essentially metal atoms being oxidized, losing electrons, and leaving the solid metal as seen in (10). For this to happen the electric circuit needs to be a closed loop so the electrons can travel to another metal ion or another material as seen in (11) and (12) [3]. This means that the electrolyte in aluminum smelting speeds up corrosion of metals rapidly.

$$M \rightarrow M^{m+} + me^- \tag{10}$$

M : *Metal atom,* m : *Number of lost electrons,* e^- : *Electrons, [15]*

$$N + ne^- \rightarrow N^{n-} \tag{11}$$

N : *Non-metallic element,* n : *Number of lost electrons,* e^- : *Electrons, [15]*

$$G^{m+} + me^- \rightarrow G \tag{12}$$

G : *Metal ion,* m : *Number of lost electrons,* e^- : *Electrons, [15]*

3.4 Size and Weight

The length of the probe should be enough so that the employee operating it can submerge the tip of the probe below the electrolyte and into the molten aluminum. The best way to get a reference for this length was to examine the sample equipment used today. The author and instructor went to Norðurál (Nov. 5, 2014), a partner company of DTE, at Grundartangi, Iceland and the sample equipment was examined. The length decided to start with should be around 1.5 meters and should that be enough so that the operating employee should not have to lean into the pot for sampling.

In modern aluminum smelters safety is a priority. Although the probe is in it's early stages of development it is good to design it according to the standards that the probe must meet. One of these requirements is that the probe must not be too heavy for a person to operate it properly without causing harm to himself. The issue with the weight limit was addressed by looking at the Applications Manual for The Revised NIOSH Lifting Equation [16] to get some reference weight that the probe should not exceed.

The RWL or recommended weight limit seen in (13) is a way to calculate the recommended weight a person should lift and by looking at Table 3, it can be seen that the base point weight is 23 kg. To get a sense for the maximum weight a person should lift in a certain situation, the base point is multiplied by several constants that are functions of physical posture while lifting. The RWL does not apply if any of the following occur:

- Lifting/lowering with one hand
- Lifting/lowering for over eight hours
- Lifting/lowering while seated or kneeling
- Lifting/lowering in a restricted workplace
- Lifting/lowering unstable objects
- Lifting/lowering while carrying, pushing or pulling
- Lifting/lowering with wheelbarrows or shovels
- Lifting/lowering with high speed motion (fasted than about 30 inches/second)
- Lifting/lowering with unreasonable foot/floor coupling (<0.4 coefficient of friction between the sole and the floor)

None of the above should occur while operating the device except maybe carrying the device while lifting it.

The assumptions that were made are that the probe would be held at maximum 40 cm from body (H in Fig. 8), the maximum height of lifting would be 150 cm (V in Fig. 8), the maximum vertical travel of the device should be no more than 35 cm, the twist of the body while lifting should not exceed 45 degrees (A in Fig. 8), the frequency of lifting should not exceed two times per minute for a maximum of two hours and the hand to device coupling or handle should qualify as good. As seen in Table 3 the multiplier for all these assumptions is about 0.33, which means that the probe should not exceed 7.6 kg.

$$RWL = LC \times HM \times VM \times DM \times AM \times FM \times CM \tag{13}$$

Description	**Symbol**	**Equation**	**Parameters**	**Value**
Load constant	LC	$23kg$		
Horizontal multiplier	HM	$\frac{25}{H[cm]}$	40 cm	0.625
Vertical multiplier	VM	$1 - 0.003(\|V[cm] - 75\|)$	150 cm	0.775
Distance multiplier	DM	$0.82 + \frac{4.5}{D[cm]}$	35 cm	0.949
Asymmetric multiplier	AM	$1 - 0.0032A[deg]$	45 deg	0.856
Frequency multiplier	FM	From Table 5 in [16]		0.84
Coupling multiplier	CM	From Table 7 in [16]		1
SUM				0.33

Table 3. RWL parameters [16].

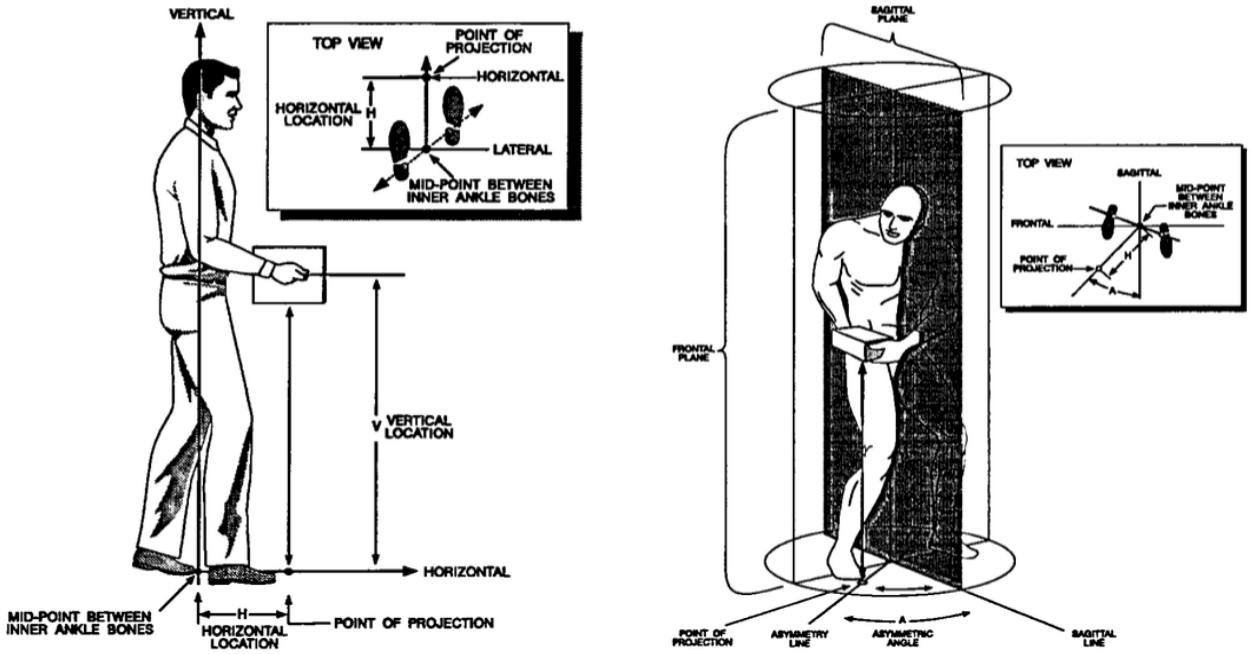

(a) Hand location.

(b) Angle of asymmetry.

Fig. 8. RWL Graphic representation [16].

4 Pressure Control Design

As discussed in section 3.2 the conditions inside the probe needs some kind of an inert gas to prevent oxidization of the aluminum with the oxygen in the atmosphere. The pressure of the gas inside the probe needs to be precisely controlled to gain an optimal focus area and minimize fluctuation due to the human factor. To approach this a small plexiglass probe was designed only to accept air/gas pressure to control the liquid surface. The depth in the liquid is calculated from data from an ultrasonic distance sensor placed outside the probe, seen Fig. 9. All errors due to offset from the middle of the probe to the sensor and orientation of the probe is corrected by trigonometry functions of the orientation angles supplied by the IMU (Inertial Measurement Unit) seen at the top of the probe. By using the real depth of the tip of the probe the pressure at the tip is calculated. The pressure is then controlled to be the same inside the probe as at the tip so that the liquid surface inside the probe, or at the tip, will be almost constant to eliminate fluctuation. Drawings of the plexiglass probe can be seen in Appendix A.

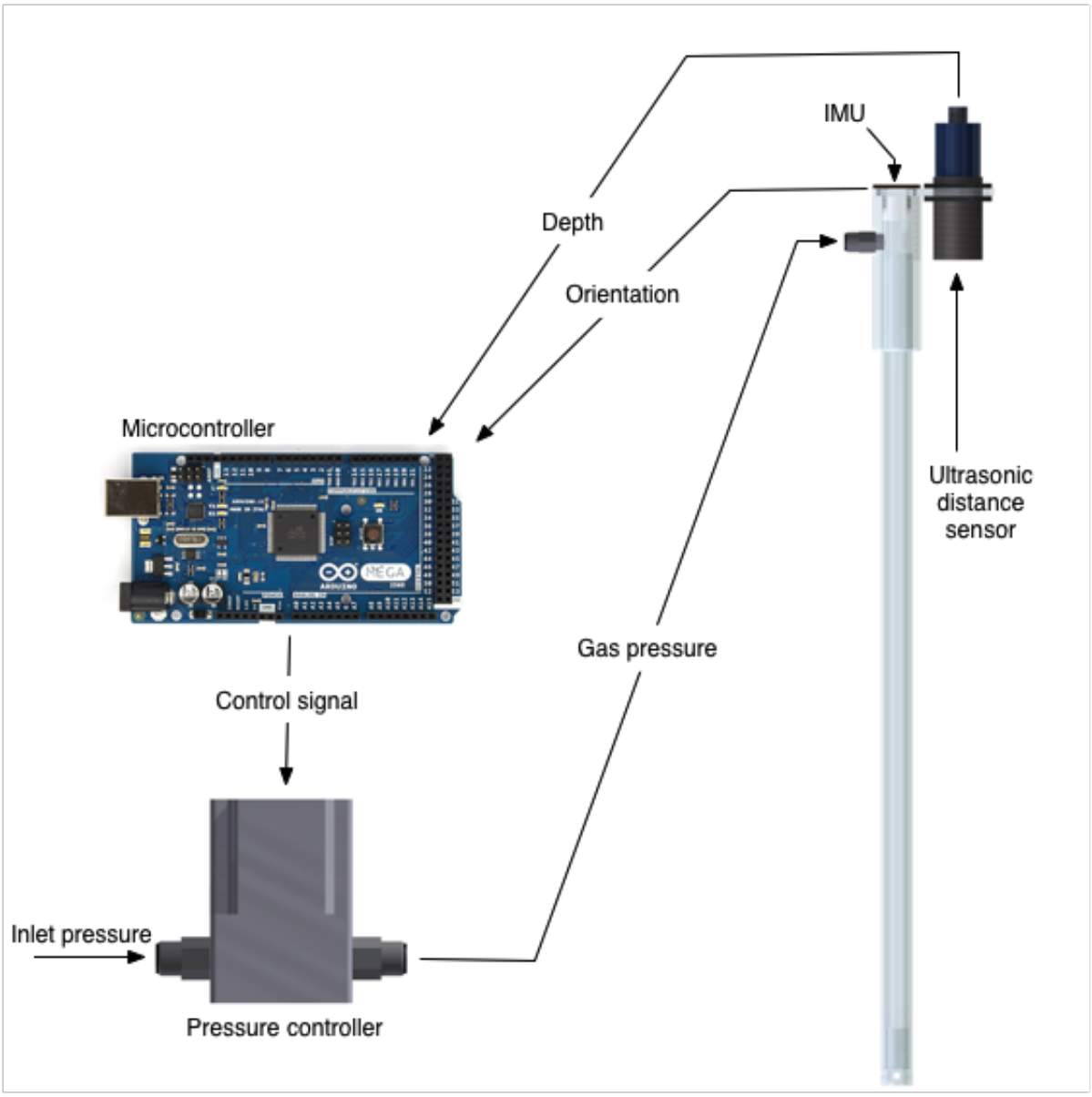

Fig. 9. Pressure control setup.

4.1 Ultrasonic Distance Sensor

An ultrasonic distance sensor converts electric energy into a sound wave at a frequency in the ultrasonic range or above 18 kHz, then the sensor evaluates the echo of the sound wave. By using the speed of sound as a constant the distance can be calculated, see (14). The calculated distance is actually the distance times two because the sound wave needs to travel to the object and back. Ultrasonic sensors are used in other appliances as well, e.g. measuring wind speed and speed through air where the distance is constant. Ultrasonic sensors have a great capability of measuring distances to reflective and clear materials, fog or dirt in the air have little effect on the accuracy. The main concern for ultrasonic sensors is the shape of the surface being measured because the soundwave cannot be deflected in another direction. The sensor chosen for this was the UM30 213113 from SICK, with a working range of 200mm - 1300mm being optimal for use with the actual probe.

$$2D = c\Delta T \tag{14}$$

D : *Distance,* c : *Speed of Sound,* ΔT : *Time Interval*

General technical data	
Operating distance (max scanning distance)	200 ... 1300 mm (2000)
Response time	110 ms
Switching frequency	6 Hz
Hysteresis	20 mm
Ultrasonic frequency	Approx. 200 kHz
Resolution	0.18 mm
Reproducibility	$\pm$ 0.15 %
Accuracy	$\leq$ 2 %
Supply voltage V_S	9-30 V DC
Output	4 ... 20 mA
Residual ripple	$\pm$ 10 %
Current consumption	$\leq$ 80 mA
Time delay before availability	$\leq$ 300 ms
Connection type	M12, 5-pin
Enclosure rating	IP 67
Ambient temperature (Operation)	-25°C ... +70°C
Ambient temperature (Storage)	-40°C ... +85°C
Material (Housing)	Nickel-plated brass, PBT, TPU
Material (Ultrasonic transducer)	Polyurethane foam, glass epoxy resin
Weight	150 g

Table 4. SICK UM30 technical data [17].

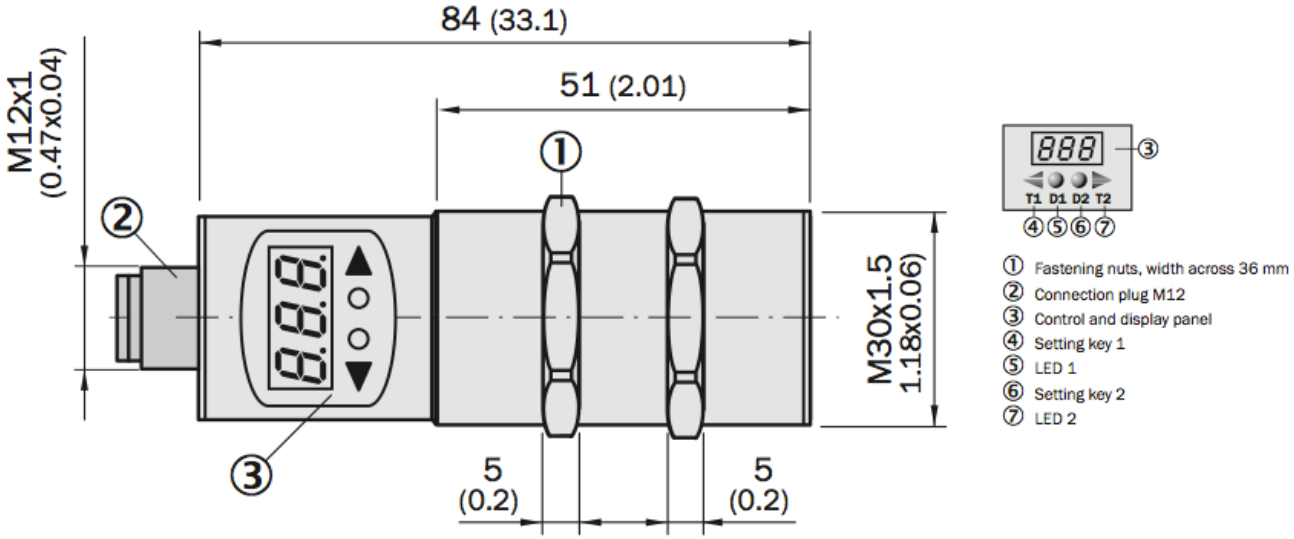

Fig. 10. SICK UM30 dimensions [17].

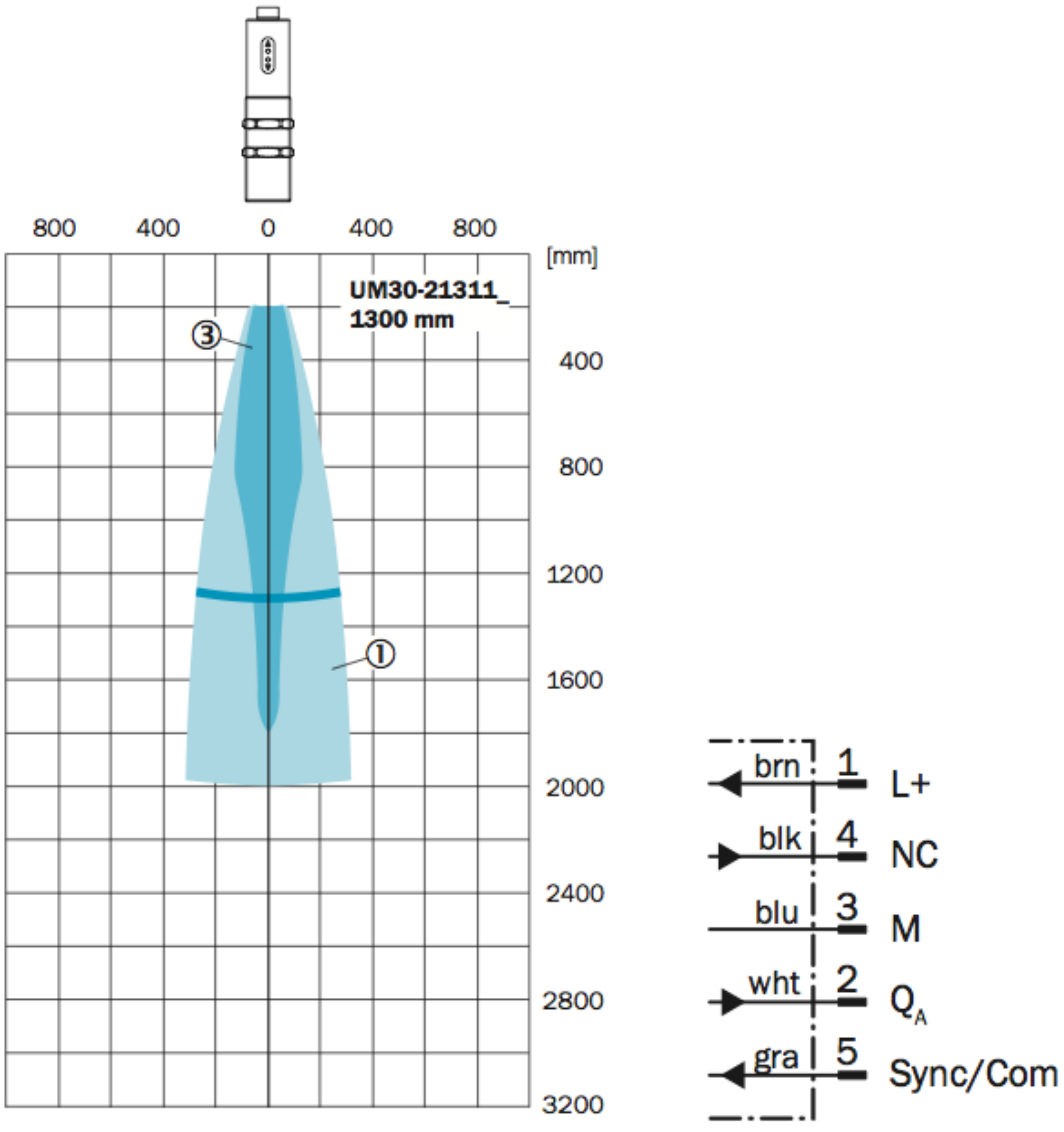

(a) Range.

(b) Connections.

Fig. 11. SICK UM30 [17].

4.2 Inertial Measurement Unit

There are several advantages of being able to know the orientation of the probe. When the probe is tilted at an angle the measured distance from the ultrasonic sensor will either be wrong due to the fact that the surface is not perpendicular enough for the sound wave to echo back to the sensor or the fact that the sensor is offset from the probe so the real distance to the surface is a function of the orientation. The depth being the distance from the sensor to the tip minus the measured distance is also distorted by the orientation. To get the real depth, measurements of the orientation are needed for calculations and as well for detecting when the probe is within a range so the distance sensor captures the echo. Another benefit will be using the orientation for safety measures, e.g. making the equipment unable to discharge when the probe is not facing downward.

An IMU or inertial measurement unit is used from SparkFun electronics (9 degrees of freedom - Razor IMU SEN-10736). A typical IMU is a fusion between three triple axis sensors: a gyroscope, accelerometer and a magnetometer. The magnetometer measures changes to the magnetic field. The accelerometer measures acceleration in all three directions and therefore measures the direction of the gravity acceleration vector and then the gyroscope measuring angular velocity around all three axes. By fusing all these sensors together it is possible to get relative angles to the magnetic field and gravitation. This sensor is actually a microcontroller with additional sensors therefore some coding was needed for it to work, as it should.

All sensors are prone to be effected by disturbances. A big issue with using magnetometers is that the earth's magnetic field is not the only thing affecting the magnetometer. All around us magnetic fields are generated by electrical components or ferocious metals and all affect the measured angle by a magnetometer.

Because there is a massive amount of magnetic field near the pots in aluminum smelters, due to the fact that around 200 kA current is running through the electrolyte and aluminum, it is very likely that there is no way to use the IMU in this sense, that is calculating the depth error due to orientation. But it will be possible to ignore the magnetometer and use the gravity acceleration vector to calculate if the probe is within the range for the distance sensor and also for safety measures.

Hard iron errors are produced when a constant magnetic field is added to the earth's field. This would happen if a ferocious metal would be near the magnetometer and rotate with the IMU. When this is the case a constant offset is applied to the measurements. The affect this has is sometimes not much but if the offset is enough to offset the measured circle into one or two quadrants the error is severe, as seen in Fig. 12. The measured angle when this is the offset can only be in the second quadrant.

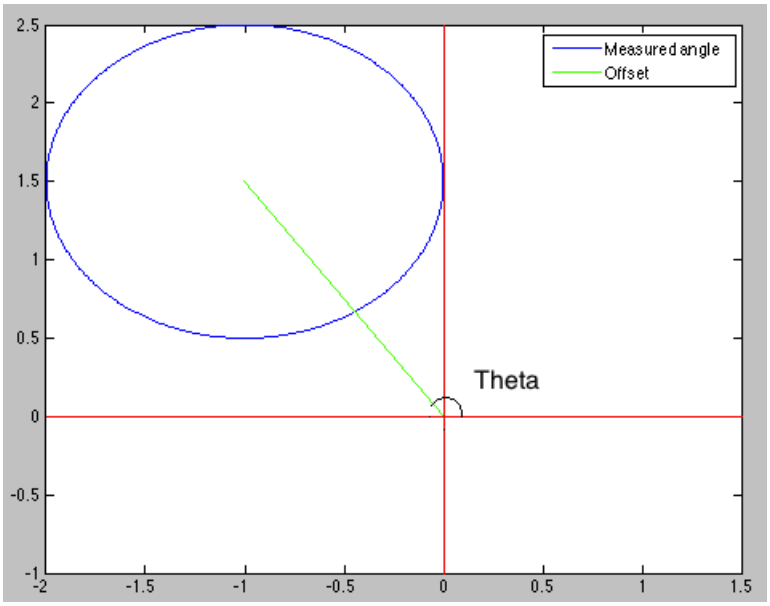

Fig. 12. Hard iron error.

To compensate for this error you need to measure the maximum and minimum value for each axis and calculate the average value of the magnetization. By withdrawing this value you compensate the offset so that the center of the measured circle is at (0,0).

$$B = Hx + b \tag{15}$$

$$B_{min} = -Hx + b \tag{16}$$

$$B_{max} = Hx + b \tag{17}$$

$$B_{ave} = \frac{Hx + b + (-Hx + b)}{2} = b \tag{18}$$

Soft iron errors are much more complex to compensate for. Soft iron errors are the result of distortion of the magnetic field instead of just an additive, so instead of offsetting the measurement it distorts the shape of the circle to an ellipse, as seen in Fig. 13 or ellipsoid in three dimensions. The effect this has in the measured angle is that when at constant rotational velocity the measured angle will have some angular acceleration and the measured angle will not be correct. As seen in Fig. 13, the green line is the angle that should be measured at 45° but instead the measured angle is as seen in cyan. In reality the ellipse can also be tilted at an angle.

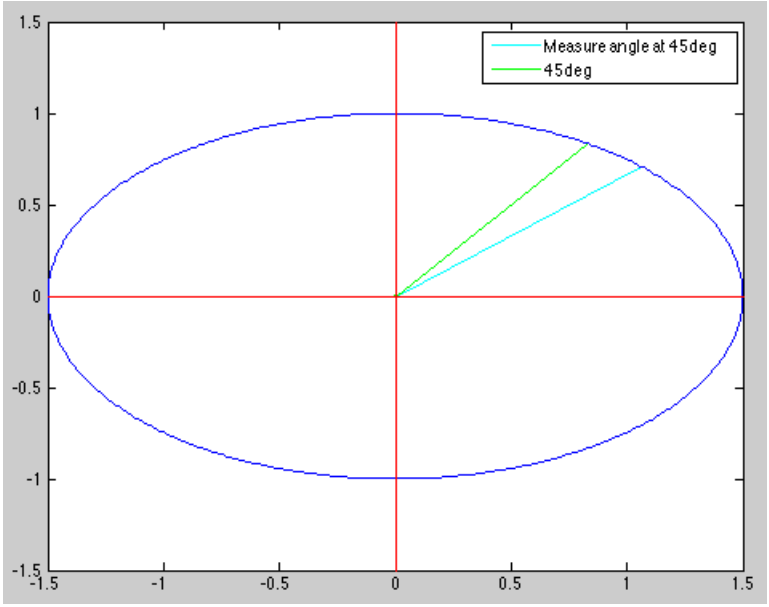

Fig. 13. Soft iron errors.

Software recommended by SparkFun was used for soft iron calibration [18]. This is an AHRS or attitude and heading reference system, which actually takes care of calibrating all the sensors but was mainly used to calibrate the magnetometer. To calibrate the magnetometer a Arduino code needs to be uploaded to the Razor IMU and a serial connection opened with Processing. Then you need to rotate the IMU within the shell that it will be in during operation. You need to rotate the shell, or in this case the probe, around every axes and try to get every possible angle. The serial connection with Processing will display the calibration as in Fig. 14 and you need to fill the ellipsoid with the measurements. When that is finished the AHRS code calculates the offset vector b and compensates for the soft iron errors with the disturbance matrix H in (15).

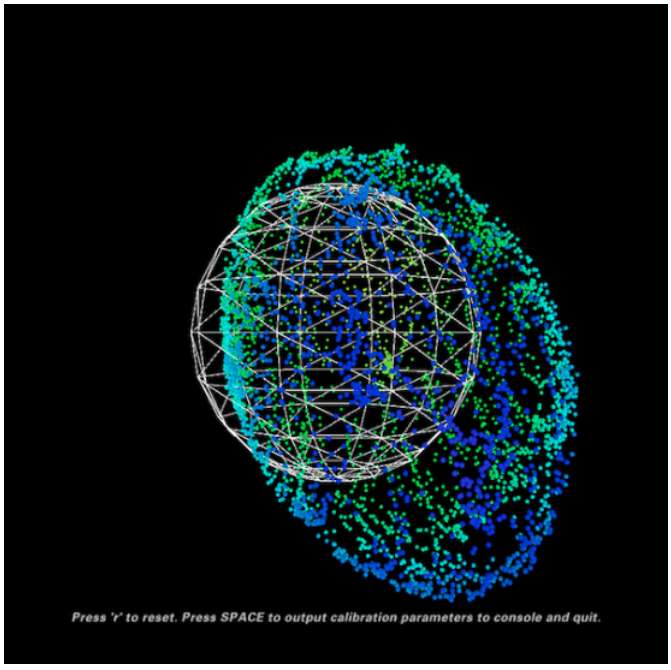

Fig. 14. Calibration of the magnetometer using AHRS code [18].

Calibrating the accelerometer is similar to the calibration of soft iron errors. By pointing the positive side of an axis on the sensor down a maximum value of acceleration can be gathered on that axis. While in that position, tilt the IMU a little bit until a maximum value is obtained. It is important to make no sudden movements, if movements accelerate above one g the calibration will fail. When that is done do the same for the negative of the same axis and take the mean value of that and withdraw from the measured acceleration around that axis. The same should be done for all axes. You also need to calibrate the sensitivity of the sensor for acceleration by taking the average output of the sensor for a positive g and a negative and the mean value of these two values is the sensitivity at one g.

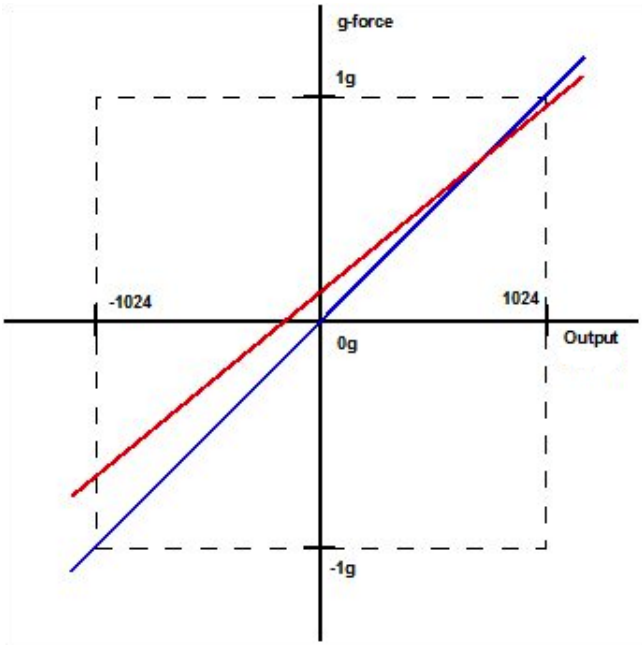

Fig. 15. Ideal accelerometer output versus an un-calibrated sensor [19].

$$g = sensitivity * output - offset \tag{19}$$

4.2.1 IMU Calculations

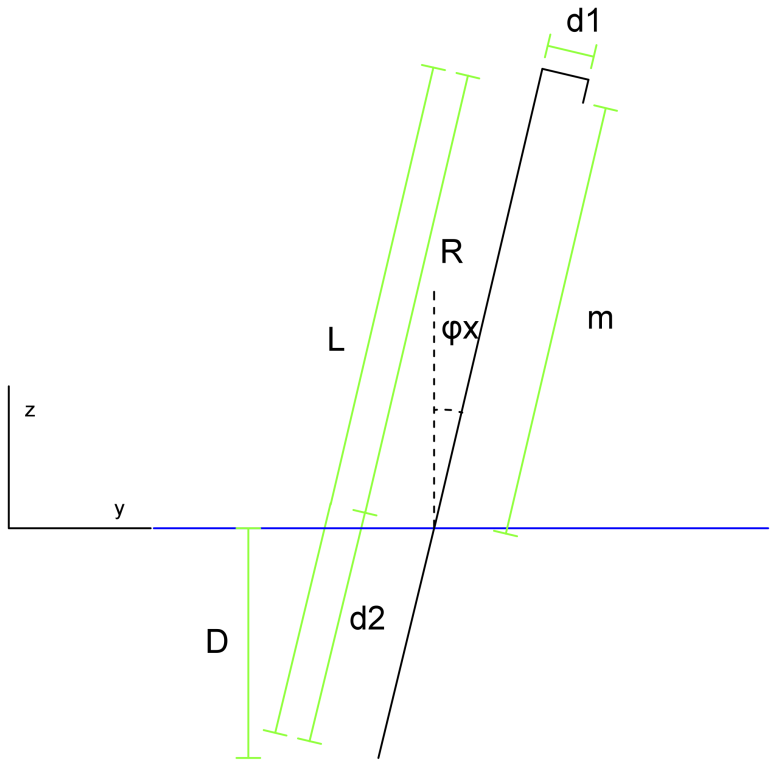

Fig. 16. Schematic for IMU calculations.

$$R = m - d_1 \tan(\phi_x) \tag{20}$$

R : *Distance from sensor to surface in line with the probe,* m : *Measured distance from sensor to surface,* d_1 : *Sensor offset,* ϕ_x : *Orientation of the probe around x-axis*

$$d_2 = L - R \tag{21}$$

d_2 : *Length of probe submerged in liquid,* L : *Length of probe from sensor to tip*

$$d_{xy} = \sqrt{(\sin(\phi_x))^2 + (\sin(\phi_y))^2} \tag{22}$$

d_{xy} : *Surjection of the surfacing part of the probe in xy plane,* ϕ_x *and* ϕ_y : *Orientation of the probe around x- and y-axis*

$$\phi_{xy} = \tan^{-1}(\frac{d_z}{d_{xy}}) = \tan^{-1}(\frac{\cos(\phi_x)\cos(\phi_y)}{\sqrt{(\sin(\phi_x))^2 + (\sin(\phi_y))^2}}) \tag{23}$$

ϕ_{xy} : *Orientation of the probe relative to the z-axis,* d_z : *Surjection of the surfacing part of the probe on the z-axis*

$$D = d_2 \sin(\phi_{xy}) = \overbrace{[L - (m - d_1 \tan(\phi_x))]}^{d_2} \sin(\tan^{-1}(\frac{\cos(\phi_x)\cos(\phi_y)}{\sqrt{(\sin(\phi_x))^2 + (\sin(\phi_y))^2}})) \tag{24}$$

D : *Depth of the tip of the probe*

4.2.2 IMU Code

The code used on the IMU was developed by Peter Bartz [18] but with some modifications. The communication between the Arduino and the IMU is serial, which means that all the information from the IMU comes in a long character array and reading data from the array is not easy so changes were made to the main file (Razor_AHRS.ino) and the output file (Output.ino). These modifications were made to output only the roll angle when needed and only the pitch angle when needed. The changes to the main file were made so that when the IMU reads a command to output the roll angle it calls the roll function in the output file and vice versa.

4.3 Pressure Controller

4.3.1 SMC ITV1030

An electronic pneumatic regulator from SMC pneumatics was chosen to control the air/gas. The range of the ITV1030 can be configured in several ways, the lower limit can be configured from -20% F.S. to 90% F.S. and the higher from 10% F.S. to 120% F.S. This does not mean that it can control pressure in that range, but that it only affects the slope and offset of the input signal and therefore the resolution of the output.

As seen in Table 5 the minimum set pressure is 0.05 bar, which is equivalent to around 500 mm in water and 230 mm in molten aluminum. This makes the ITV1030 not acceptable for application but was used in development of the pressure control system. The only difference in operation was that testing was done at a higher pressure range.

General technical data	
Model	SMC ITV1030-04F2N3
Minimum supply pressure	+1.0 bar
Maximum supply pressure	+10.0 bar
Set pressure range	+0.05 ... +5.0 bar (gage)
Supply voltage	24 VDC $\pm$ 10%
Current consumption	0.12 A or less
Input signal	Current type 4 ... 20 mA (sink type)
Input impedance	250Ωor less
Output signal	Current type 4 ... 20 mA (sink type)
Linearity	Within $\pm$1% F.S.
Hysteresis	Within 0.5% F.S.
Repeatability	Within $\pm$0.5% F.S.
Sensitivity	Within 0.2% F.S.
Temperature characteristics	$\pm$0.12% F.S./$^{\circ}C$
Enclosure	Equivalent to IP65

Table 5. SMC ITV1030-04F2N3.

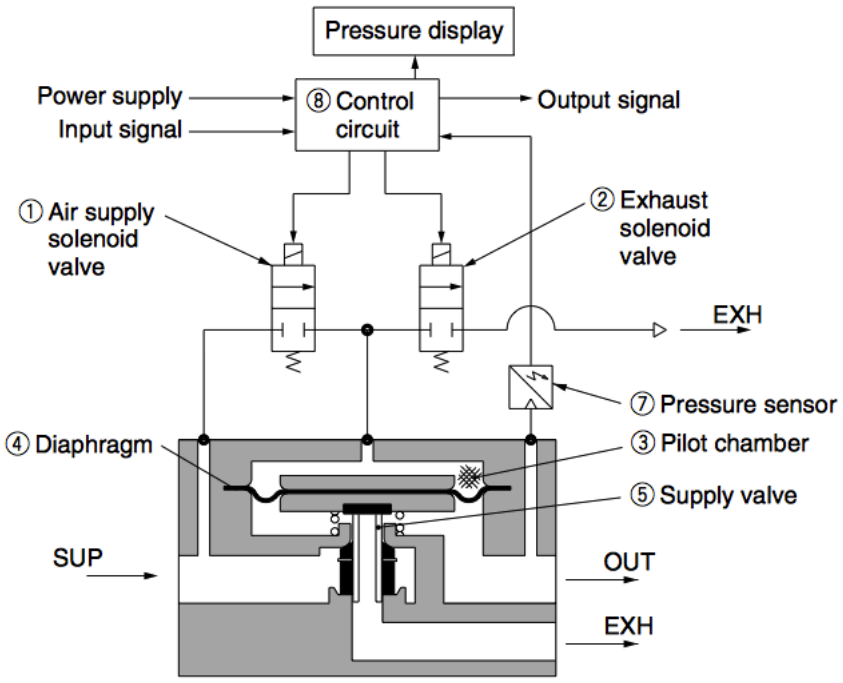

Fig. 17. ITV1030 schematic [20].

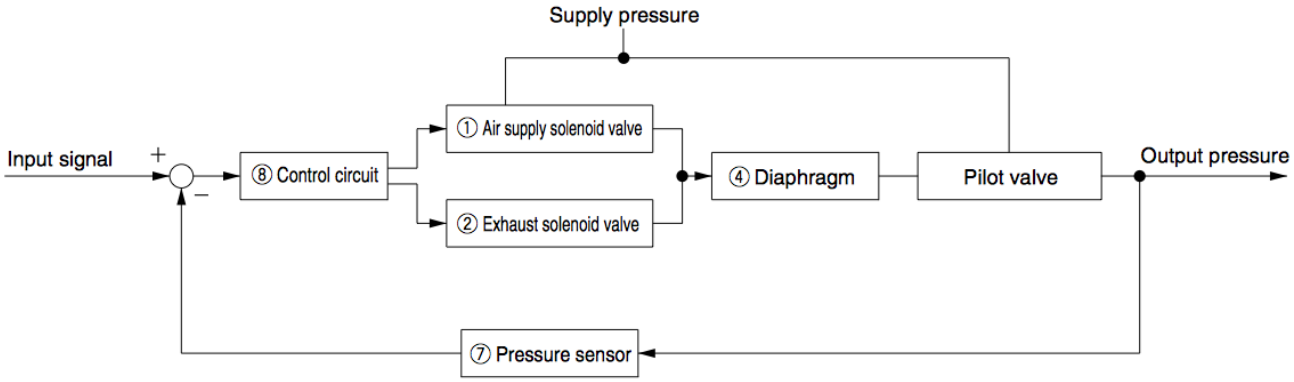

Fig. 18. ITV1030 control block diagram [20].

4.3.2 Proportion Air QPV

As mentioned here in section 4.3.1 the ITV1030 can only control pressure in the range 0.05-5.00 bar, which is not acceptable in this application because it is essential to control the pressure at 0-400 mm in aluminum/cryolite, which is around 0-0.1 bar (gage). A new pressure controller has been ordered from Proportion Air, a French company that specializes in electronic pressure regulators. The QPV was recommended by the technical staff for this application. Table 6 shows that all control parameters are the same as the SMC ITV1030. The only changes should be to the software part where the output scale is different but this is easy to change.

General technical data	
Model	Proportion Air QPV1TBNICZP200MBGDXL
Minimum supply pressure	Full vacuum
Maximum supply pressure	+1.4 bar
Set pressure range	0 ... +0.2 bar
Supply voltage	+15 ... +24 VDC
Current consumption	+100 ... + 350 mADC
Input signal	Current type 4 ... 20 mA (sink type)
Input Impedance	100Ω
Output signal	Current type 4 ... 20 mA (sink type)
Hysteresis	±0.02% F.S.
Repeatability	±0.02% F.S. (typical)
Resolution	±0.2% F.S. ... ±0.005% F.S.
Accuracy	±0.2% F.S. ... ±0.1% F.S.
Enclosure	NEMA 4/IP65

Table 6. Proportion Air QPV-1.

4.4 Microcontroller

It was decided to use a microcontroller instead of a PLC computer for prototyping. The advantages of using a microcontroller is that they are cheap, easy to program and have enough inputs and outputs to manage this type of system, with some exceptions discussed later. The microcontroller that was chosen is the Arduino Mega 2560, which costs around $50.

General technical data	
Microcontroller	ATmega 2560
Operation voltage	5 V
Input voltage (recommended)	7 ... 12 V
Input voltage (limits)	6 ... 20 V
Digital I/O pins	54 (15 PWM)
PWM resolution	8 bit
Analog input pins	16
Analog input resolution	10 bit
DC current per I/O pin	40 mA
DC current for 3.3V pin	50 mA
Flash memory	256 KB (8KB used by bootloader)
SRAM	8 KB
EEPROM	4 KB
CLock speed	16 MHz

Table 7. Arduino Mega 2560.

As said before there are some issues that needed fixing to make the ATmega 2560 work for the system. First of all it is that most analog communication with sensors or other electronic devices use current type I/O, that being 0-20 mA or more common 4-20 mA. The advantage of this type of communication is that voltage drops with the length of the wire due to the resistance of the wire but the current is constant. The analog inputs and outputs of the ATmega2560 are voltage type 0-5 V but the SICK UM30 was chosen with a current type output (4-20 mA) for further use in the future and the SMC ITV1030 pressure controller is also a current type (4-20 mA). The easiest way to read data from a current type sensor with a voltage type input is letting the current flow through a resistor and by that generating a voltage between the output of the sensor and the ground. To control a constant current with a voltage type output, a voltage to current converter was needed. Industrial transducers for this kind of conversion go for about $600 but the integrated circuit you see here in section 4.4.1 costs about $5 but is instead much harder to implement.

4.4.1 Texas Instruments XTR110

The TI XTR110 is a precision voltage to current converter designed to convert voltage to current signals, see datasheet in Appendix B. Available inputs being in the range of 0-10 V and outputs of 0-25 mA as seen in Table 8. The output being a function of a reference voltage, input voltage and the total impedance seen by the emitter of the internal NPN transistor as seen in (25). In Table 8 you can see how to connect the pins for different configurations and the circuit seen in Fig. 19 shows how the configuration for a

conversion of 0-5 V to 4-20 mA signal looks like. An external transistor is required as shown in Fig. 19, recommended by TI is a P-channel enhancement mosfet transistor with a voltage rating equal or greater than the maximum power supply voltage. The transistor chosen for the design was a FQP17P06 P-channel QFET enhancement mosfet from Fairchild Semiconductors, see datasheet in Appendix C.

$$I_O = \frac{10(\frac{V_{REFIN}}{16} + \frac{V_{IN1}}{4} + \frac{V_{IN2}}{2})}{R_{SPAN}} \tag{25}$$

R_{SPAN} is the total impedance seen at the emitter of the internal NPN transistor [21]

Input range (V)	Output range (mA)	Pin 3	Pin 4	Pin 5	Pin 9	Pin 10
0-10	0-20	Com	Input	Com	Com	Com
2-10	4-20	Com	Input	Com	Com	Com
0-10	4-20	+10V Ref	Input	Com	Com	Open
0-10	5-25	+10V Ref	Input	Com	Com	Com
0-5	0-20	Com	Com	Input	Com	Com
1-5	4-20	Com	Com	Input	Com	Com
0-5	4-20	+10V Ref	Com	Input	Com	Open
0-5	5-25	+10V Ref	Com	Input	Com	Com

Table 8. TI XTR110 I/O configuration [21].

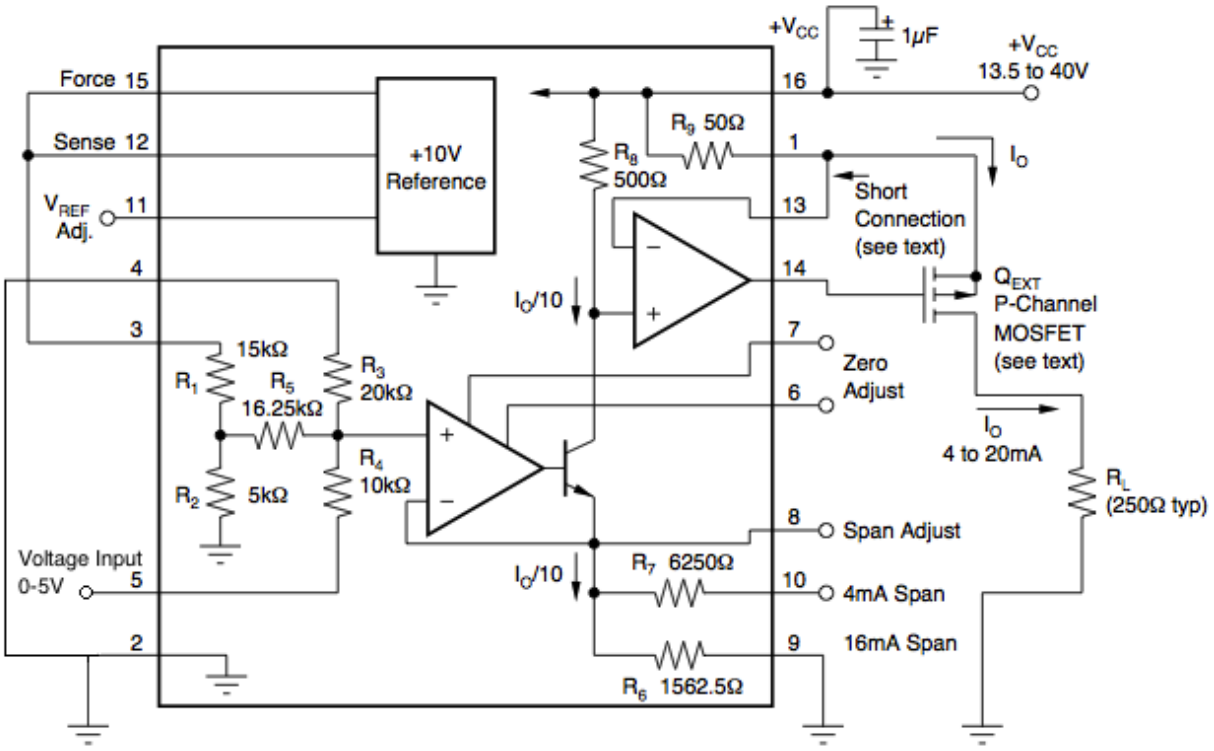

Fig. 19. TI XTR110 basic circuit connection, 0-5V to 4-20mA.

4.4.2 Arduino Code

The Arduino code is rather self-explanatory, although some exceptions need explaining, see code in Appendix D. The serial baud rate is set at 57600 because the baud rate of the imu is running 57600.

The pwm output pins on the Mega 2560 are configured with an 8-bit resolution, which means that 0-5 V in 256 increments can be controlled. This and the fact that the pressure controller can be configured with an output of 0-0.5 bars means that the increments in pressure are around 0.002 bars, when 0.002 bars are equivalent to the pressure at 20 mm depth in water the accuracy of all the other measuring equipment are worthless.

Pwm signal or pulse width modulation is a digital square wave at a constant frequency for a variable time duration between 0-100%. By doing this a digital output with a fixed voltage can be filtered into an analog value. The ATmega2560 uses several timers to control these pwm signals and by going through the datasheet [22] for the ATmega 2560 chip you see that for example timer one controls pwm pin 11, 12 and 13, this timer is actually a 16-bit timer but the analog write function is configured for an 8-bit signal. By manipulating the timer registers directly, it is possible to change the resolution. The code used for this is a variation of several different designs found on the Internet, see the code in Appendix E. By adding this code to the void setup of the Arduino code you have changed the resolution of pin 11 to 10-bits giving increments of 1024 and therefore being able to control the pressure four times better than with the regular 8-bit resolution, resulting in a pressure change every 5 mm in water and around every 2 mm in molten aluminum.

4.5 Electrical

All the electrical work was designed before work on the prototype started and was tweaked and parts redesigned in the prototyping period. All the prototype work was done on a breadboard as seen in Fig. 20. The potentiometer is used for linear calibrations and the red led is used to give feedback when developing code, the schematics can be seen in Appendix F.

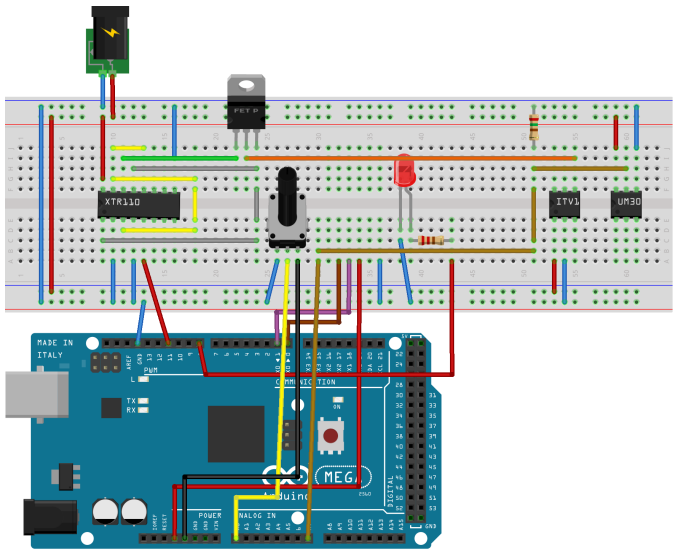

Fig. 20. Breadboard prototype electrical connections.

4.5.1 PCB Design

A PCB board was designed in EAGLE CAD to connect directly to the Arduino Mega as a shield. The PCB was made with a MEGA Electronics Rota-Spray etching machine and the process is listed below.

Etching process

1. Print top and bottom layer on a transparent film using a laser printer. Top layer must be mirrored.
2. Glue the transparent film together as a pocket with the printed side inward. Make sure they are perfectly concentric.
3. Only non-UV light allowed.
4. Take the protective film of the PCB board and place in the film pocket.
5. Expose each side of the PCB board inside the pocket to UV light for four minutes.
6. Take the PCB board out of the pocket and place in developing liquid at 20-25°C.
7. Rinse in water and turn on regular light.
8. Etch for 15 minutes at 40-45°C.
9. Rinse again.

The PCB was designed so that all the male pins going to the Arduino Mega are soldered at the top layer and all screw terminals are soldered at the bottom layer, see Fig. 21, see Appendix G and H for printable versions (only in pdf) to remake the shield.

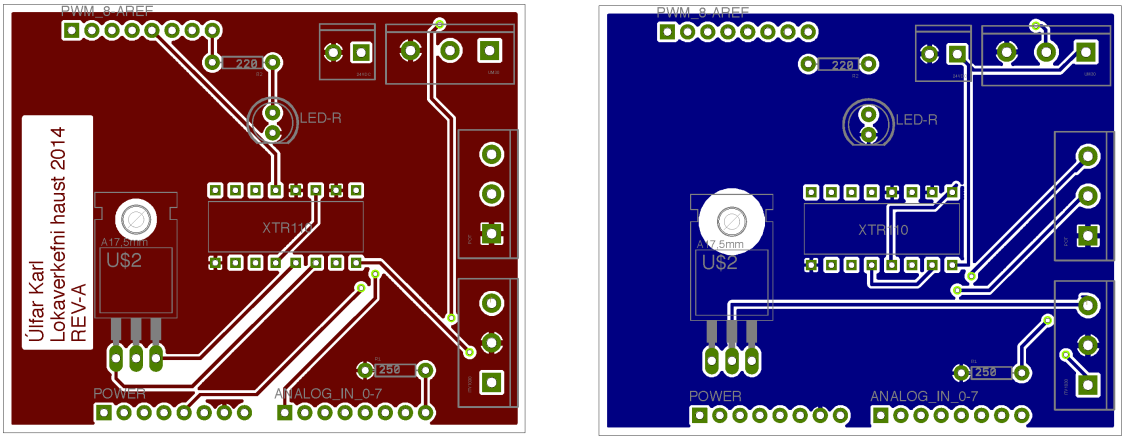

(a) Top layer

(b) Bottom layer

Fig. 21. PCB layers.

4.6 Resolution

4.6.1 SICK UM30

The SICK UM30 has a resolution of 0.18 mm [17] but this is not the resolution the software sees. The UM30 has a range of 200-1200 mm and a current type 4-20 mA signal but the fact that the microcontroller has only voltage type analog inputs, the current is led to ground through a 250 Ω resistor, which gives us an input to the microcontroller of 1-5 V. The analog inputs on the microcontroller are 10-bit so the resolution is 1.221 mm. This translates to around 0.1 mbar in water at 20$^{\circ}C$ and 0.3 mbar in aluminum at 960$^{\circ}C$.

$$[H]r = \frac{UM30_{range}}{bit} = \frac{1200 - 200}{round(1024 - \frac{1024}{5})} \tag{26}$$

4.6.2 SMC ITV1030

Unfortunately the ITV1030 datasheet does not provide information about the resolution of the pressure but the analog signal from the microcontroller is a 10-bit signal and the smallest pressure range that the ITV1030 can be configured to is 0-0.5 bar so the resolution is around 0.5 mbar.

4.7 Pressure Drop in Pipes

The pressure drop in the pipes is insignificant when the system is stable and there is no flow rate but has some effect when the system is purging gas. It is hard to measure very low flow rates so for these calculations the assumption is made that the bubbles released from the system in liquid have a constant diameter of 10 mm (found out by testing the system) and have a variable frequency from one to ten per second, depending on the stability of the system. The pressure drop is plotted in Fig. 22 where the inside diameter of the pipe is 4 mm and in Fig. 23 where the diameter is 6 mm. The pressure drop is about five times less with an inside diameter of 6 mm. All assumptions and values for a frequency of five can be seen in Table 9.

Symbol	Description	Value	
d_p	Inside diameter of pipe	4 mm	6 mm
L_p	Length of pipe	4 m	
ΔZ	Height change from controller to probe	zero	
d_b	Diameter of bubble	10 mm	
f_b	Frequency of bubbles	5 [1/s] (variable)	
ρ_{air}	Density of air (1atm)	1.2 $\frac{kg}{m^3}$[23]	
μ	Absolute viscosity of air (20°C)	1.8E-5 $\frac{Ns}{m^2}$[23]	
A	Cross section area of pipe	12.57 mm^2	
Q	Flow rate of air in pipe	2618 $\frac{mm^3}{s}$	
v	Velocity of air in pipe	208 $\frac{mm}{s}$	93 $\frac{mm}{s}$
Re	Reynolds number	55.5	37
f	Frictional factor	1.15	1.73
h_f	Head loss in pipe	2.54 m	0.50 m
Δp	Pressure drop over pipe	30.00 mbar	5.92 mbar

Table 9. Assumptions and values from pressure drop calculations.

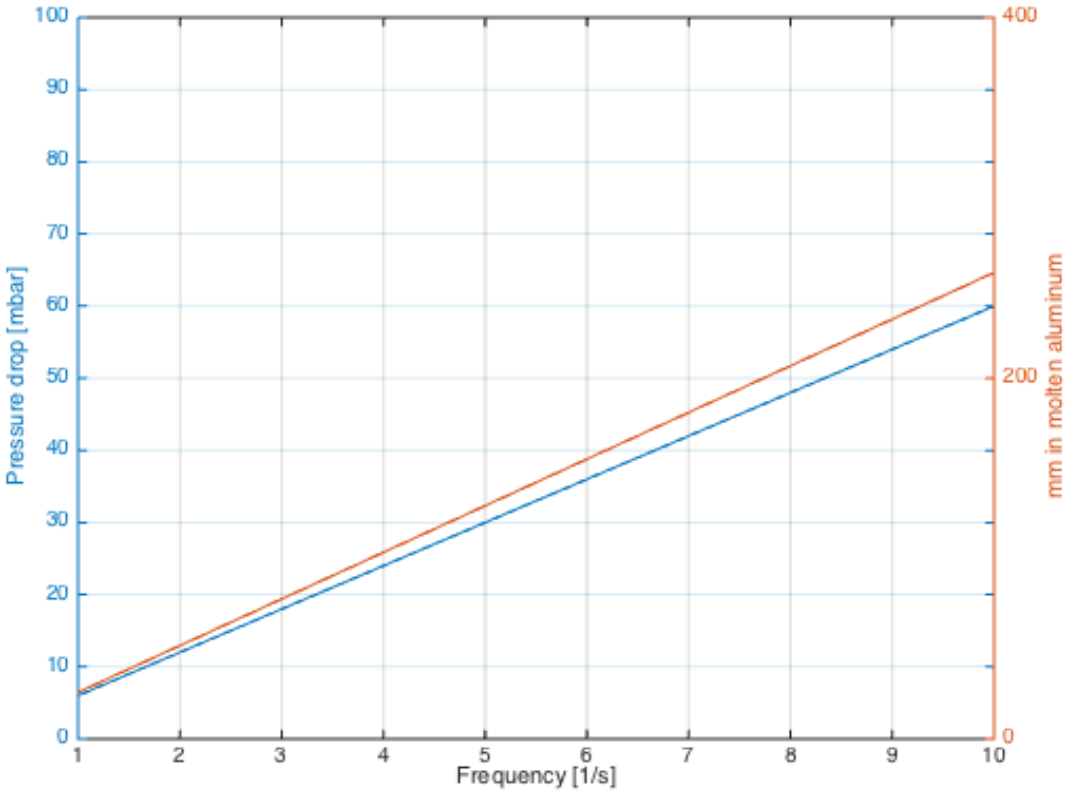

Fig. 22. Pressure drop as a function of bubble frequency, inside diameter of pipe 4 mm.

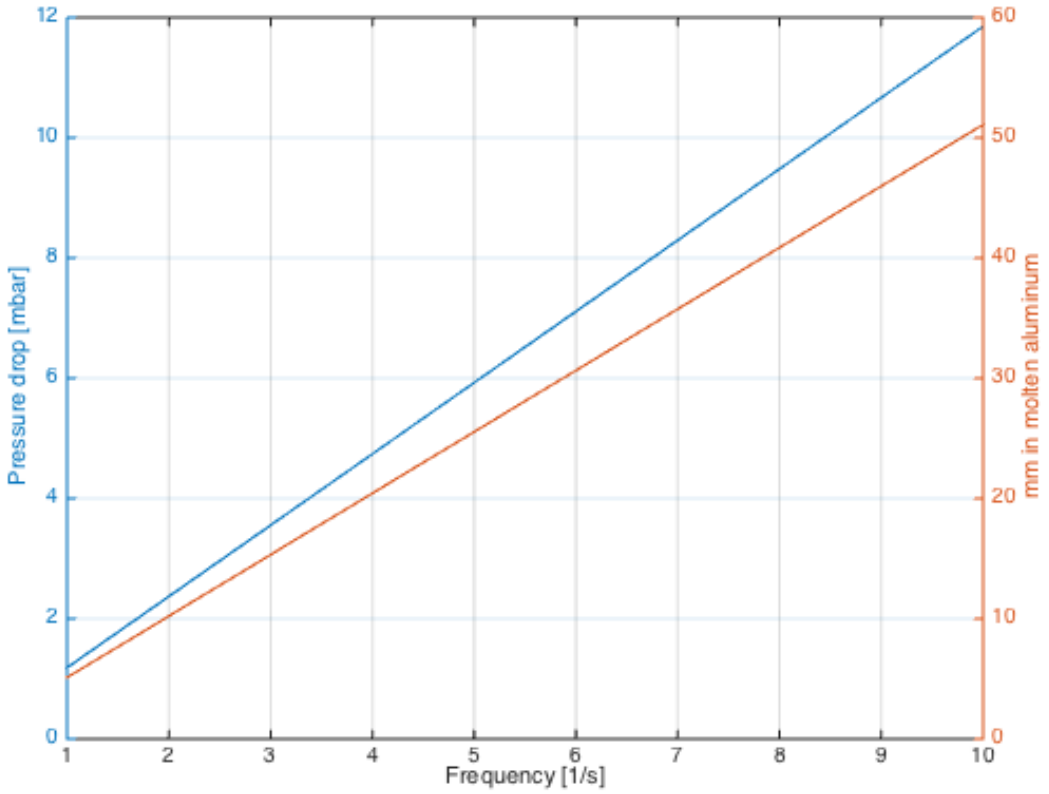

Fig. 23. Pressure drop as a function of bubble frequency, inside diameter of pipe 6 mm.

$$A = \frac{d_p^2 \pi}{4} \tag{27}$$

$$Q = fV = f\frac{1}{6}\pi d_b^3 \tag{28}$$

$$v = \frac{Q}{A} \tag{29}$$

$$Re = \frac{\rho_{air} v d_p}{\mu} \tag{30}$$

The flow is laminar so by the Moody graph in Fig. 24 this is the friction factor

$$f = \frac{64}{Re} \tag{31}$$

$$h_f = f\frac{L_p}{d_p}\frac{v^2}{2g} \tag{32}$$

$$\Delta p = \rho g h_f \tag{33}$$

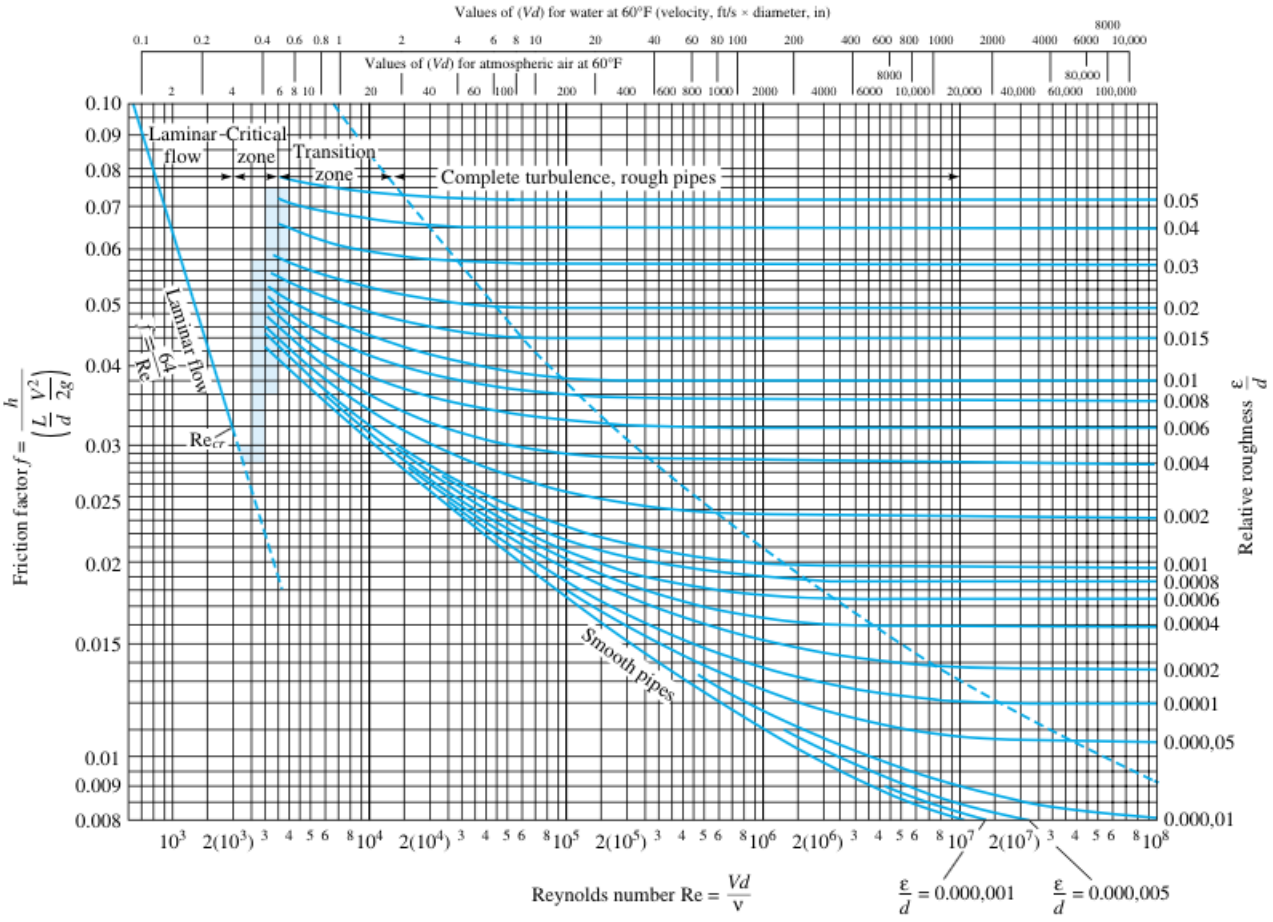

Fig. 24. Moody graph [23].

5 Probe Design

The main focus of this first prototype is to test the concept in a laboratory setup without losing a large part of the light emitting from the plasma to the surroundings. The laser would be transferred through an optical fiber connected to one end of the probe and focused with a 50 mm focusing lens with a focal length of 500 mm. The end of the probe should be designed so it could be submerged in liquid and also so that a solid sample could be placed at the end for testing so all design parameters from the pressure system design in section 4 should be considered. The probe should withstand the heat of molten aluminum. The focus was not set on addressing the corrosion of the bath material at this point but the design was kept as modular as possible so that it could be addressed with little effort.

5.1 Materials

The material chosen for the probe is 304 austenitic stainless steel. The solidus line of 304 stainless steel is at 1400$^{\circ}C$, according to ASM Specialty Handbook of Stainless Steels [24], so it is well within the range of the solidus line of aluminum which is around 660$^{\circ}C$ depending on additives [25]. Although this prototype should not be tested in a smelter, so it would not experience the corrosive environment of the electrolyte. The 304 stainless steel was also chosen because of its great corrosion resistance [26], relative low cost and good machinability compared to other austenitic stainless steels. All the stainless-steel will be electrically polarized to make a chrome film on the material. This will help the collimator on the optical fiber capture more of the emitting light from the plasma.

When it comes to submerging the probe into the molten cryolite the stainless steel will not resist corroding as seen in section 3.3. The material used to shield the probe should have low solubility in cryolite and molten aluminum, high oxidation resistance, be mechanically robust, and be easy to fabricate and join. The material that will be tested at that point is alumina (Al_2O_3). The solidus temperature is around 2040$^{\circ}C$ and has an average flexural strength of 200-500 MPa [27]. Although the aluminum smelting process is designed to melt alumina, a solid piece of alumina should degrade slower than any metal and should not leak to the molten material and spoil the sample.

5.2 Design

The assembly of the prototype, has a ceramic hull to be able to submerge the probe into the electrolyte, but the probe was also designed with this part in three pieces to be able to make it out of stainless steel for the first prototype, see Fig. 25 and detailed drawings in Appendix I. This first design is also a little smaller than the actual probe will have to be, the length of the entire probe is just over one meter but to lengthen the probe the only part that needs changing is the pipe between the optical fiber connector and the lens housing. This part can also be modified to house a collimating lens to extend the diameter of the laser beam, see a part list in Fig. 26 and in sheet 3 in appendix I.

The ceramic material absorbs more light than stainless-steel so the the steel pipe, marked 9 in Fig. 26, makes sure that more of the emitting light will pass to the collimator of the optical fiber. This way the gas is also insulated from the hull which is in contact with the hot material.

The bracket for the distance sensor seen in Fig. 25 and 26 is only a mock-up. When the probe is ready tests will be done with the distance sensor to have the offset of the sensor as little as possible.

If we look back on section 3.4 we see that by the recommended weight limit for equipment operated with two hands is around 7.6 kg. If the probe is lengthened to 1.5 m, which was the required length also addressed in section 3.4, and all parts are made from stainless-steel, the weight of the entire probe is around 5.6 kg. This should be well within range when certain parts are made from ceramic with about 50% less density.

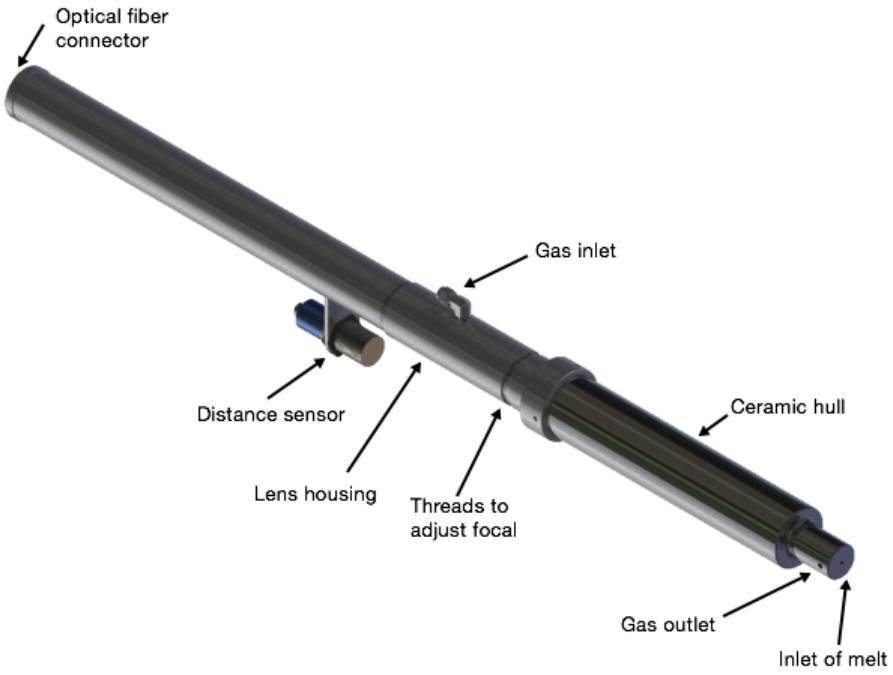

Fig. 25. Overview of prototype.

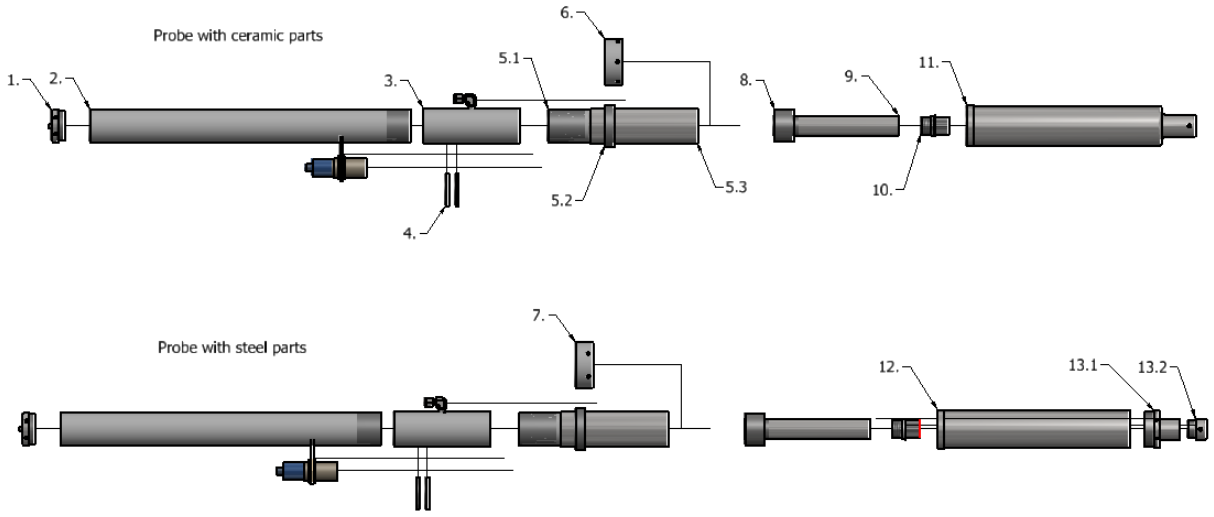

Fig. 26. Partlist.

5.3 Optical Fiber Connector

A high power multi-mode optical fiber from OZ-Optics, datasheet can be seen in [28], will be used to transfer the laser beam from the laser to the probe and the emitting light back to the spectrometer. This optical fiber comes with a standard SMA-905 connector, dimensions seen in 27, with a 1/4"-36 UNS-2B threaded nut. The connector on the probe was designed with these specifications, see detailed drawings in appendix I.

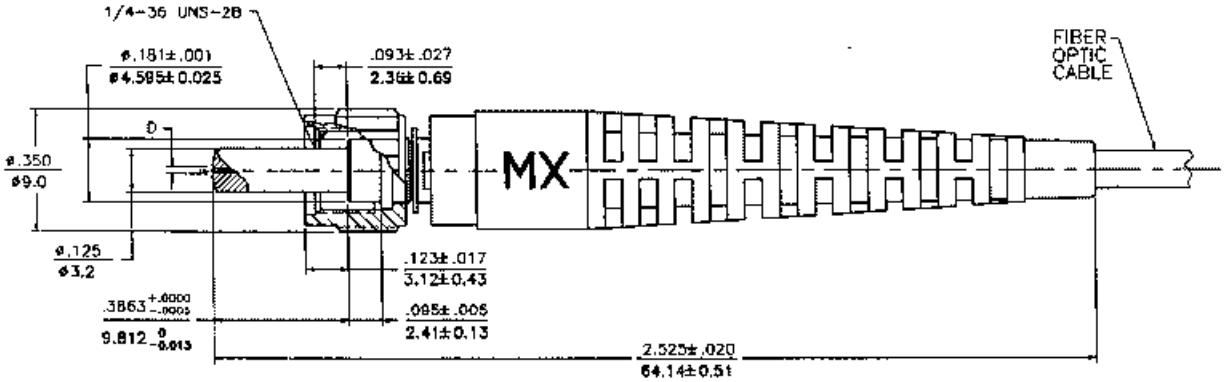

Fig. 27. SMA 905 dimension.

5.4 Lens and Focus Adjusting

The focus lens is fitted inside part 3 in Fig. 28 with an inside diameter of 50.5 mm and is fastened with two custom nuts (part 4. in Fig. 28). The probe was designed so that the focal point could be adjusted at least 50 mm or from a theoretical zero diameter of the laser beam to a diameter of 1 mm with the current setup but if the beam is collimated before the focusing lens this diameter can get bigger. This is done by screwing the focus adjuster (part 5 in Fig. 28) outward and adjusting the position of the lens. The pitch of the threads is 1.5 mm so each revolution results in 1.5 mm focus point change. The focus point can be seen in Fig. 29, which is the position of the molten material at steady-state, according to the results seen in section 6.5.1.

For the first prototype the ceramic hull was made from stainless steel as mentioned before. This was done in three parts so it would be possible to make the most of it from a pipe instead of a solid cylinder and in order to change the tip type you would only need to make part 13.2 in Fig. 29 again. Part 10 in Fig. 29 will also be made from ceramic, this part will be tested and configured so that most of the emitting light can travel back to the optical fiber and keep the molten material from going further up inside the probe.

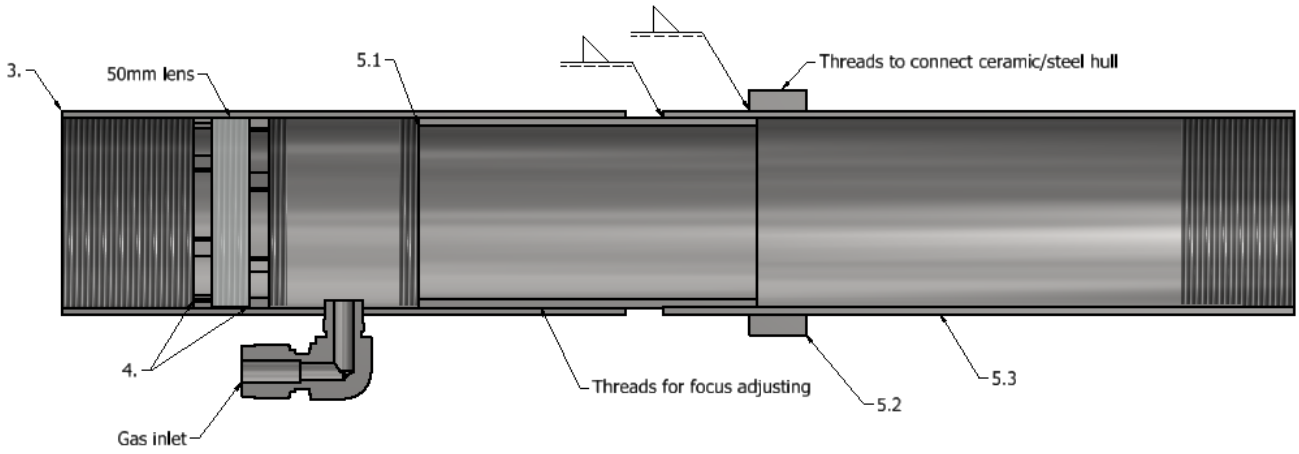

Fig. 28. Lens house and focus adjuster.

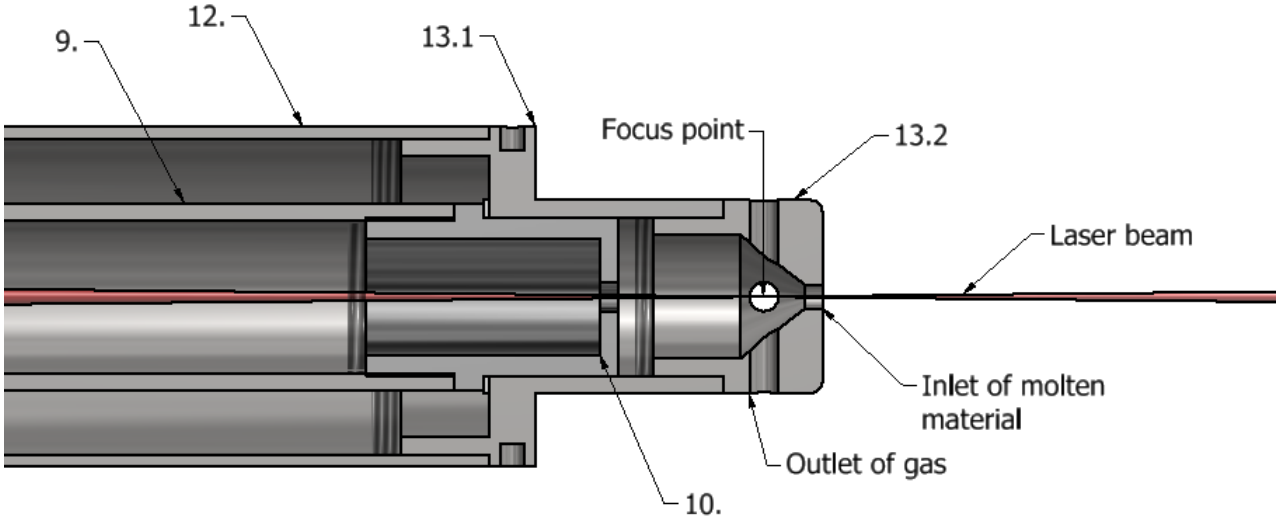

Fig. 29. Focus point of laser beam.

5.5 Weldings

Two connections of the probe are welded, see sheet 8 in drawing sheets in Appendix I. The weldings are designed by the CK Worldwide Technical Specifications for Tig Welding [29]. This is a fillet joint type with metal gauge of around 1.75 mm and the material is 304 stainless steel. Specifications for a 1.6 mm fillet welding can be seen in Table 10.

					Sheild Gas				
Metal gauge	Joint type	Tungsten size	Fillet rod size	Cup size	Type	Flow	Pressure	Amperes	Travel speed
1.6 mm	Fillet	1.6 mm	1.6 mm	4, 5, 6	Argon	5.5 l/min	20 psi	90-100	256 mm/min

Table 10. Welding specifications.

6 Experiments

The system would not be tested at this point with results from a spectroscopy because the overall design is in its early stages of development. Now the spectroscopy part of the project is a setup at the *Innovation Center Iceland* at Árleynir 2-8, 112 Reykjavík, Iceland. Because of this it was decided to gain as much control over the way the pressure system behaves with different setups and inputs so when the time comes to test the overall design by shooting at liquid samples, through a working prototype of the probe, it would take as little time as possible to adjust the system to get the results aimed for. To accomplish this, three different approaches discussed in the following sections 6.3, 6.4, 6.5 were taken.

For these first tests of the behavior of the system water was chosen as a medium. Although water has less than half the density of molten aluminum the only thing that changes for the response of the system is the slope of the pressure as a function of depth. The depth of the aluminum in the pot varies from 10-20 cm so the maximum depth is around 30 cm in a medium with density equal to molten aluminum or bath which is a little less. This translates to about 0-70 cm in water at 20$^{\circ}C$. Because the working range of ITV1030 is only from 0.05 bar or around 50 cm in water, all experiments were done at 70 cm and below. The viscosity of molten aluminum at 960$^{\circ}C$ is very low, as seen in Table 11, actually a little lower than the viscosity of water but the difference is very small.

	Density [$\frac{kg}{m^3}$]	**Viscosity [$\frac{mNs}{m^2}$]**
Water at 20$^{\circ}C$	998 [23]	1.003 [23]
Aluminum at 960$^{\circ}C$	2365 [4]	0.746 [30]

Table 11. Comparison of molten aluminum and water properties.

$$\eta = 0.1492exp(\frac{1984.5}{T}) \tag{34}$$

η : *Dynamic viscosity of molten aluminum,* T : *Temperature in kelvin [30]*

6.1 Data

The fact that it is hard to get numerical data from testing the system, makes it hard to determine how well it is responding. To do this, videos and still pictures were taken of the tip of the probe to see how it behaves. The videos were taken at 120 fps and played back four times slower than real time giving us 30 fps in playback. All still pictures were taken with a burst function, which gave 10 fps. The author and instructor made all interpretations of the data.

6.2 Tip Types

Several tip types were tested but the ones that came out best and were used in the following experiments can be seen in Fig. 30 and detailed drawings in Appendix A. Tip type one was mainly used to try to capture an air bubble inside the bore at the end and keeping the flow rate as low as possible. Tip type two was used to get liquid up through the hole at the end of the tip and let gas purge out the sides keeping the liquid surface at the same level as the output holes.

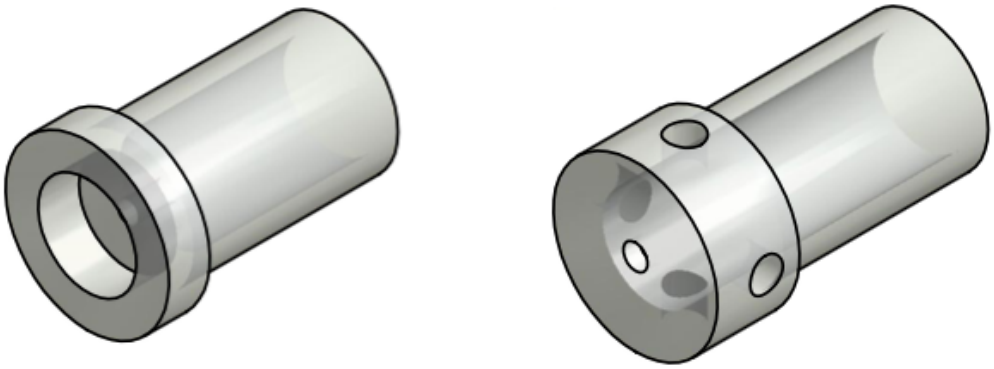

(a) Type 1. (b) Type 2.

Fig. 30. Tip types.

6.3 Constant Pressure

The first and simplest approach was to adjust the inlet pressure of the probe to some constant and by this always purge gas out of the tip of the probe. This would theoretically always keep the molten surface right outside the tip of the probe and prevent the material to enter the probe at the same time. This constant pressure would have to be greater than the pressure at the greatest submerging level in the liquid. The disadvantage is that the pressure at the tip is changing with the depth so by that the flow rate should change and the frequency of air/gas bubbles from the tip should increase.

The goal of this experiment was to see how the pressure difference at the tip affects the flow rate of air and the deviation from the desired position of the water.

6.3.1 Results

The system was adjusted so that the system would be stable at 85 cm depth. The deviation is around 9 mm at 85 cm depth put when the probe was lifted to 70 cm depth the inlet pressure is too great and the maximum distance from tip to liquid surface captured, is around 10-12 mm and the frequency of the air bubbles is around ten bubbles per second while the frequency at 85 cm depth was around one per second.

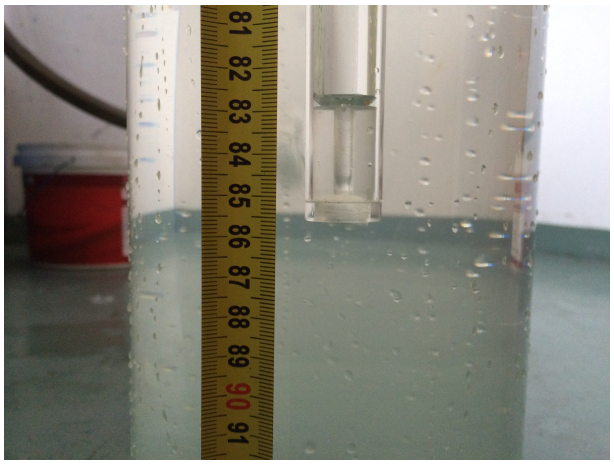

(a) No air bubble.

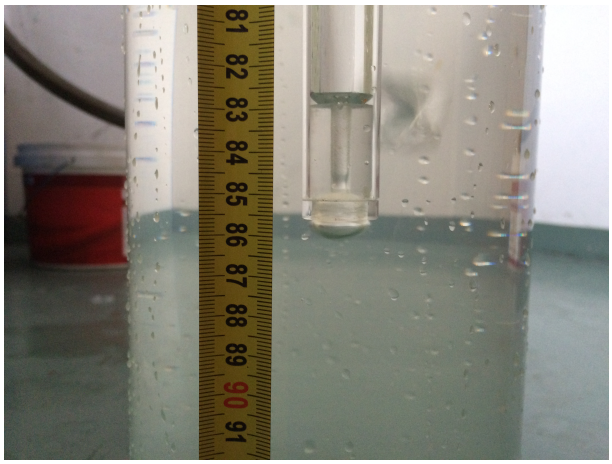

(b) Maximum bubble size.

Fig. 31. Constant pressure at 85 cm depth (tip type 1).

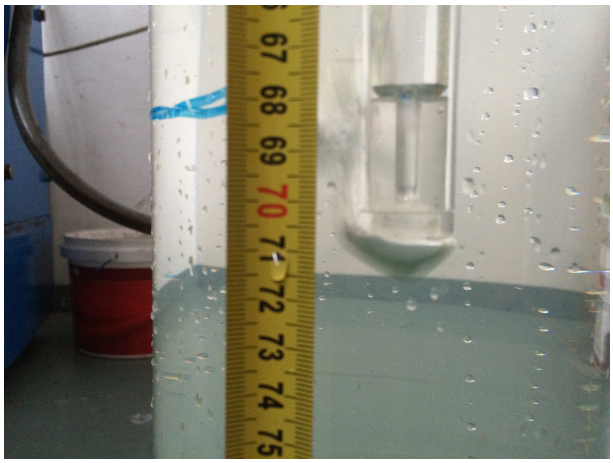

Fig. 32. Constant pressure at 70 cm depth (tip type 1).

6.4 Under Pressure

This approach was to see if it is possible to keep the water sucked inside the probe and kept at a fixed distance from the tip. If this would be possible, the flow rate of gas would be zero at steady state. The pressure is a function of the depth but is configured a little lower than actual pressure at the tip.

6.4.1 Results

This method proved not to be acceptable because the deviation is around 30 mm, see Fig. 33. The surface inside the probe oscillated with a frequency around 1/s and is probably a result of pressure delay inside the tubes and other factors.

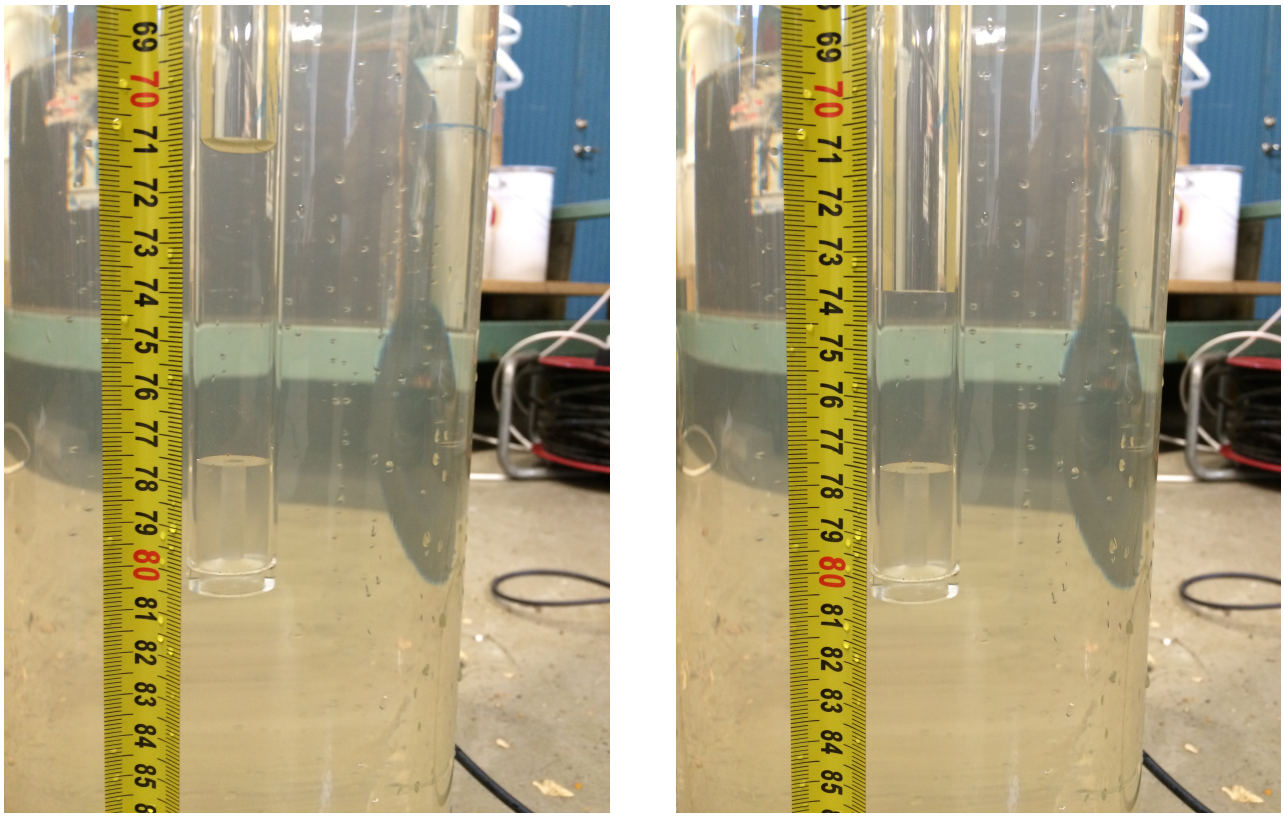

(a) Level at 71 cm.

(b) Level at 74 cm.

Fig. 33. Under pressure at 70 cm depth (tip type 1).

6.5 Tip Pressure as a Function of Depth

The main focus of this method was on this approach. The pressure is set to the pressure at the tip of the probe and was tested with two different tip types.

6.5.1 Results

The systems response with type one and the maximum deviation of the surface is around 10 mm, see Fig. 34 and 35.

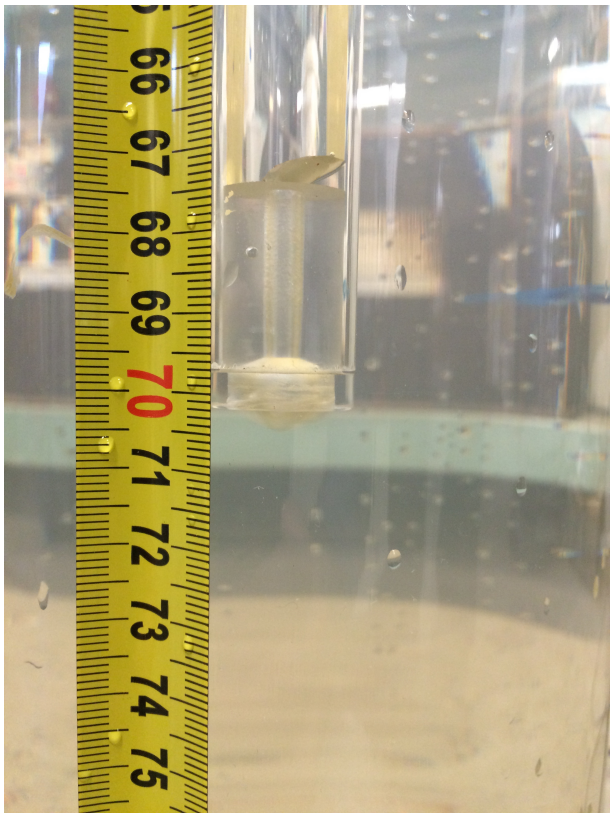

(a) No air bubble.

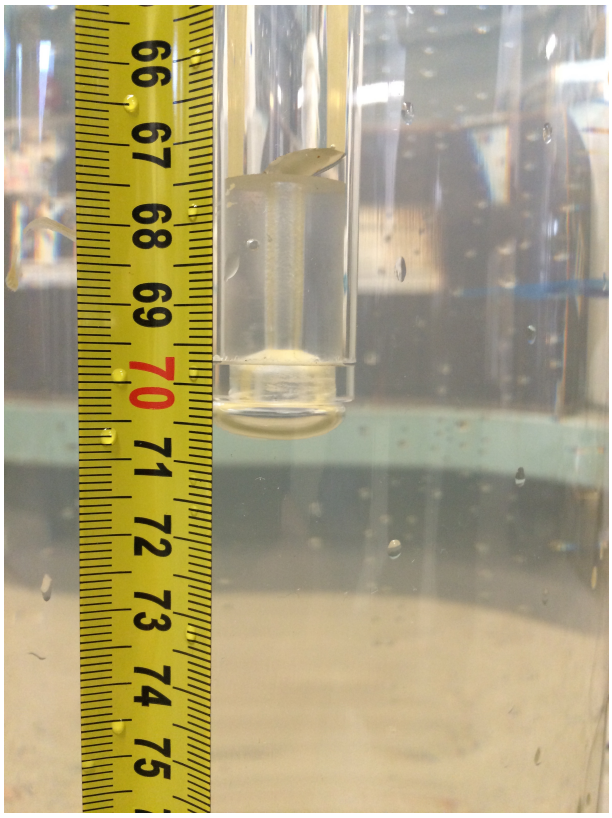

(b) Maximum air bubble size.

Fig. 34. Tip pressure at 70 cm depth (tip type 1).

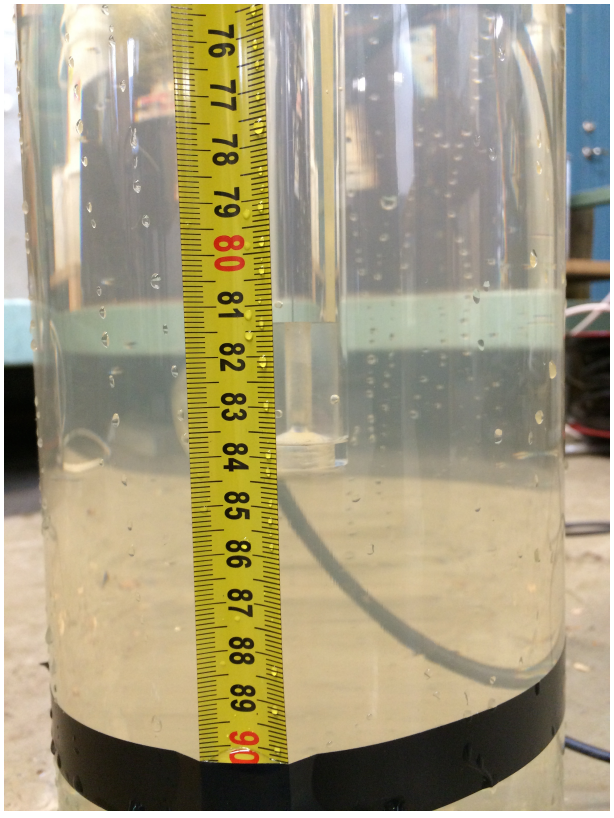

(a) No air bubble.

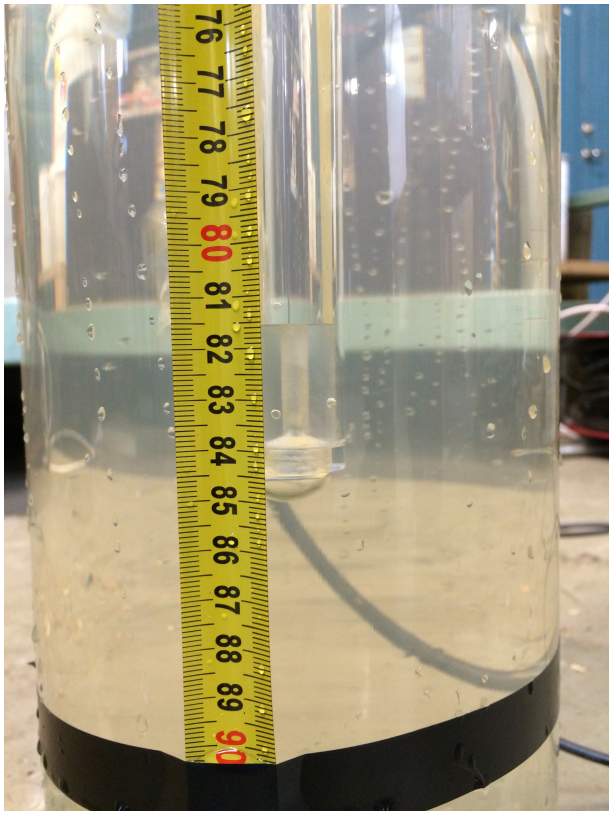

(b) Maximum bubble size.

Fig. 35. Tip pressure at 85 cm depth (tip type 1).

By watching a slow motion video of the experiment it can be seen that the deviation with a tip type two is insignificant, around 2 mm, see Fig. 36. The surface of the water inside the tip is around the center of the four outlet holes on the side of the tip. The black lines mark the surface inside the tip. 50 pictures were taken in a 5 second and there was no change in the level.

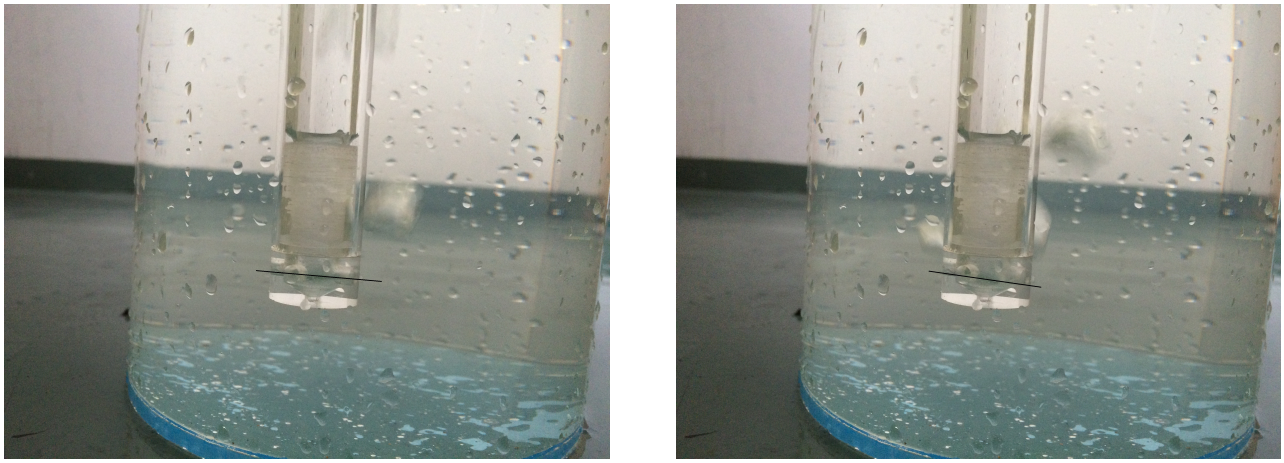

(a) (b)

Fig. 36. Tip pressure at 90 cm depth (tip type 2).

7 Conclusion

When I started this project the objective was to design, build and test a prototype of a probe. It looked like it would be a purely mechanical design of a probe that would be connected to an optical fiber and house some lenses. But soon I discovered that some issues needed to be figured out before the design of the actual probe would start. First off to gain good conditions for measurements and repeatability the surface of the melt needs to be stable at a fixed distance from the focusing lens. This would have to work at all depths. Also the inside of the probe, i.e. the lens, needs to be protected from the hot and corrosive material, no matter how the operator would thrust the probe into the molten matter. I came to the conclusion that in order to achieve this I would need to design a pressure control system. Because of my background being mainly mechanical I needed to go out of my comfort zone into electrical and coding work, which I was glad to do because I am really interested in autonomation. There is not an emphasis on electronics or computer science in my studies for the bachelor's degree but I have had some experience in those fields through interdisciplinary projects where I also tried to step outside of my comfort zone.

It has been demonstrated that by controlling the inlet pressure to the probe it is possible to control the liquid surface inside a probe that is being submerged into liquid. By having the pressure a function of traveling speed, the system also makes sure that no excess liquid goes up into the probe if an operator thrust the probe down. Tests have shown that tip type two or a variation of that type of outlet works well to control the surface inside the tip. The tip of the steel probe was designed according to the tip made from plexiglass but was modified to let the melt leak out as soon as the probe would be surfaced. The only thing that needs modification is the actual tip on the steel probe if we wish to modify the outlet. There is also a big advantage of having the melt inside the probe, which is to be able to capture more of the emitting plasma from the matter.

The next step now is to test the probe. The first tests will include analysing solid samples of aluminum in a laboratory setup. This will allow us to make the adjustments needed to get good signal readings. Next up there will be tests on molten aluminum melted in a laboratory furnace. In these tests the pressure system will be tested and configured further for optimal signal readings.

The people behind this project are hopeful that a working prototype of the equipment will be tested in an aluminum smelter in the following year.

The author wishes to thank DTE for the co-operation in the project and Indriði Sævar Ríkharðsson for introducing me with the people of DTE and Bryndís Marteinsdóttir for proofreading and Carmen Maja Valencia his significant other.

References

[1] P. Entner, “Principles of the hall-héroult process.” [Online]. Available: http://www.peter-entner.com/E/Theory/PrincHH/PrincHH.aspx [Accessed Nov. 4, 2014].

[2] P. Entner, “Components of the cell voltage.” [Online]. Available: http://www.peter-entner.com/e/theory/cellvolt/cellvolt-1.aspx [Accessed Nov. 4, 2014].

[3] W. D. Callister and D. G. Rethwisch, Eds., *Material Science and Engineering*, Wiley, 2011.

[4] J. R. Davis, Ed., *Handbook: Aluminum and Aluminum Alloys*, ASM International, 1993, ch. Properties of Aluminum and Aluminum Alloys, p. 642.

[5] M. MALINOVSKÝ, M. PAUČÍROVÁ, and K. MATIAŠOVSKÝ, “Liquidus curve and density of the molten system $li_3alf_6 - na_3alf_6$,” *Chemical Papers*, vol. 23, no. 11696, pp. 27–34, Jul. 1969.

[6] S. J. Lindsay, Ed., *Light Metals 2011*, Wiley, 2011, ch. Alcoa Starprobe, pp. 483–489.

[7] D. M. Dupuis, “Bath ratio and temperature control enhancement in the potroom,” *Light Metal Age*, 2013.

[8] P. Bouchard, “The starprobe,” STAS Inc., Tech. Rep.

[9] H. min Kan and Z. wen Wang, “Liquidus temperature of molten cryolite-based aluminum electrolyte,” *The Electrochemical Society*, 2007.

[10] P. Entner, “Liquidus temperature.” [Online]. Available: http://www.peter-entner.com/e/theory/ElProp/LiquTemp.aspx [Accessed Nov. 4, 2014].

[11] P. Entner, “Systems nacry - alf3 and naf - alf3.” [Online]. Available: http://www.peter-entner.com/e/theory/ElProp/ElProp-1.aspx [Accessed Nov. 4, 2014].

[12] G. E. Totten and D. S. MacKenzie, Eds., *Handbook of Aluminum: Alloy Production and Materials Manufacturing*, CRC Press, 2003, vol. 2.

[13] Balco, “Aluminium production technology.” [Online]. Available: http://www.balcoindia.com/operation/pdf/aluminium-production-process.pdf [Accessed Des. 2, 2014].

[14] A. K. Rai, F.-Y. Yueh, and J. P. Singh, “Laser-induced breakdown spectroscopy of molten aluminum alloy,” *APPLIED OPTICS*, vol. 42, no. 12, pp. 2078–2084, Apr. 2003.

[15] Efunda, “Corrosion fundamentals.” [Online]. Available: http://www.efunda.com/materials/corrosion/corrosion_basics.cfm [Accessed Nov. 18, 2014].

[16] T. R. Waters, V. Putz-Anderson, and A. Garg, *Applications manual for the revised NIOSH lifting equation*, U.S. Department of Health And Human Services, Jan. 1994.

[17] SICK, “Um30-2,” datasheet, Apr. 2009.

[18] P. Bartz, “Razor 9dof ahrs.” [Online]. Available: https://github.com/ptrbrtz/razor-9dof-ahrs/wiki/Tutorial [Accessed Nov. 12, 2014].

[19] GCDC, “Calibration instructionstitle.” [Online]. Available: http://www.gcdataconcepts.com/calibration.html [Accessed Nov. 2, 2014].

[20] SMC, “Electro-pneumatic regulator itv1000/2000/3000,” datasheet.

[21] T. Instruments, “Xtr110 precision voltage-to-current converter/transmitter,” datasheet, Sep. 2009.

[22] Atmel, “Atmel atmega640/v-1280/v-1281/v-2560/v-2561/v,” datasheet, February 2014.

[23] F. M. White, Ed., *Fluid Mechanics*, McGraw-Hill, 2011.

[24] J. R. Davis, Ed., *Stainless Steels*, ASM International, 1994.

[25] ——, *Aluminum and Aluminum Alloys*, ASM, 1993.

[26] B. D. Craig and D. S. Anderson, Eds., *Handbook of Corrosion Data*, ASM International, 1994.

[27] P. Auerkari, “Mechanical and physical properties of eng alumina ceramics,” Technical Research Centre of Finland, Tech. Rep., 1996.

[28] OZ-Optics, “High power fiber optics patchcords,” datasheet, Sep. 2014.

[29] “Technical specifications for tig welding,” CK Worldwide, Tech. Rep., 2008.

[30] J. E. Hatch, Ed., *Properties and Physical Metallurgy*, ASM, 1984, ch. Properties of Pure Aluminum, p. 16.

A Plexiprobe Drawings

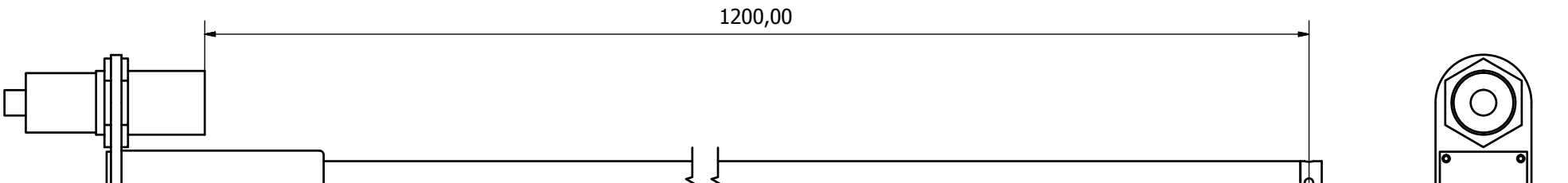

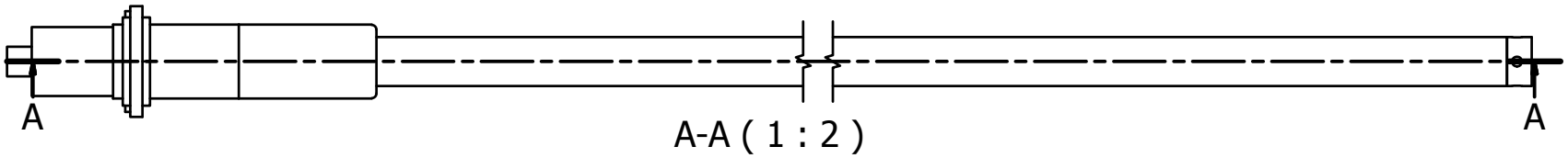

A-A (1 : 2)

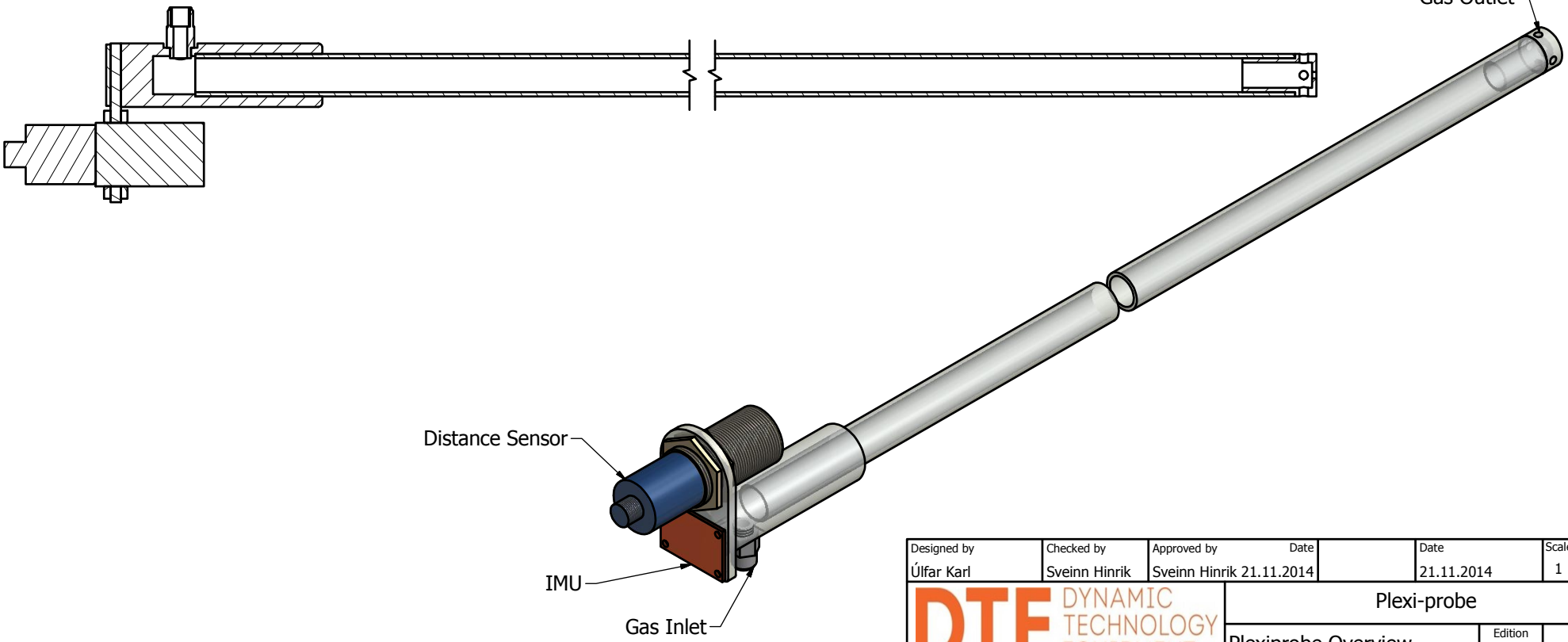

Designed by	Checked by	Approved by	Date		Date	Scale
Úlfar Karl	Sveinn Hinrik	Sveinn Hinrik	21.11.2014		21.11.2014	1 : 2

DTE DYNAMIC TECHNOLOGY EQUIPMENT

Plexi-probe

Plexiprobe Overview

Edition

Sheet 1 / 5

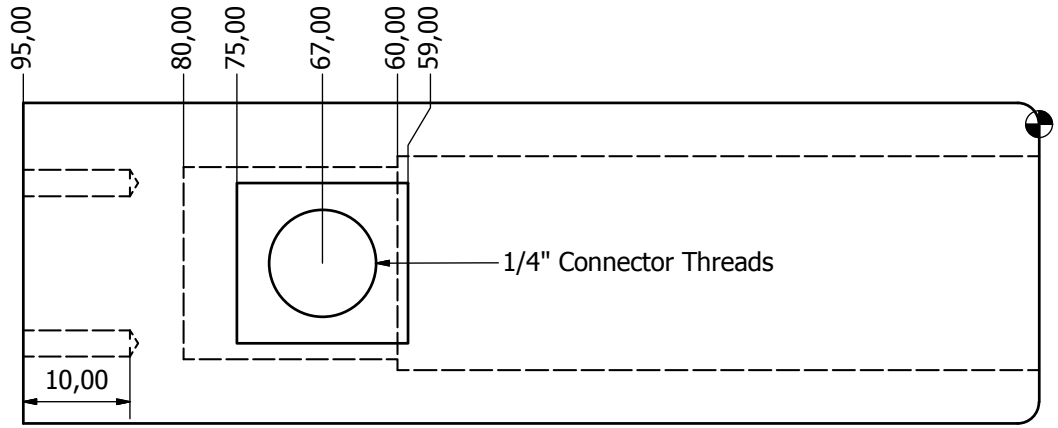

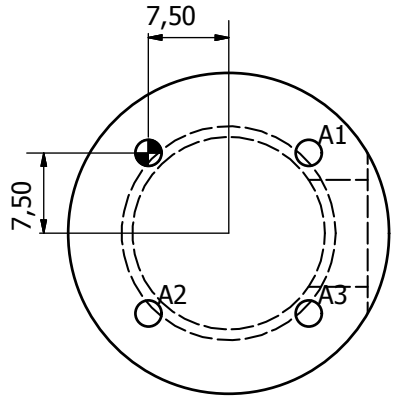

HOLE TABLE			
HOLE	XDIM	YDIM	DESCRIPTION
A1	15,00	0,00	M3x0.5 - 6H
A2	0,00	-15,00	M3x0.5 - 6H
A3	15,00	-15,00	M3x0.5 - 6H

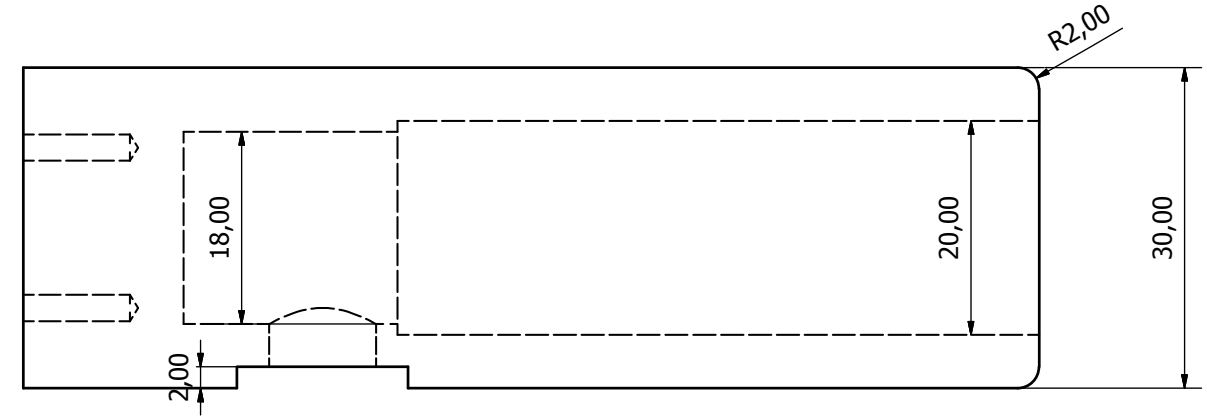

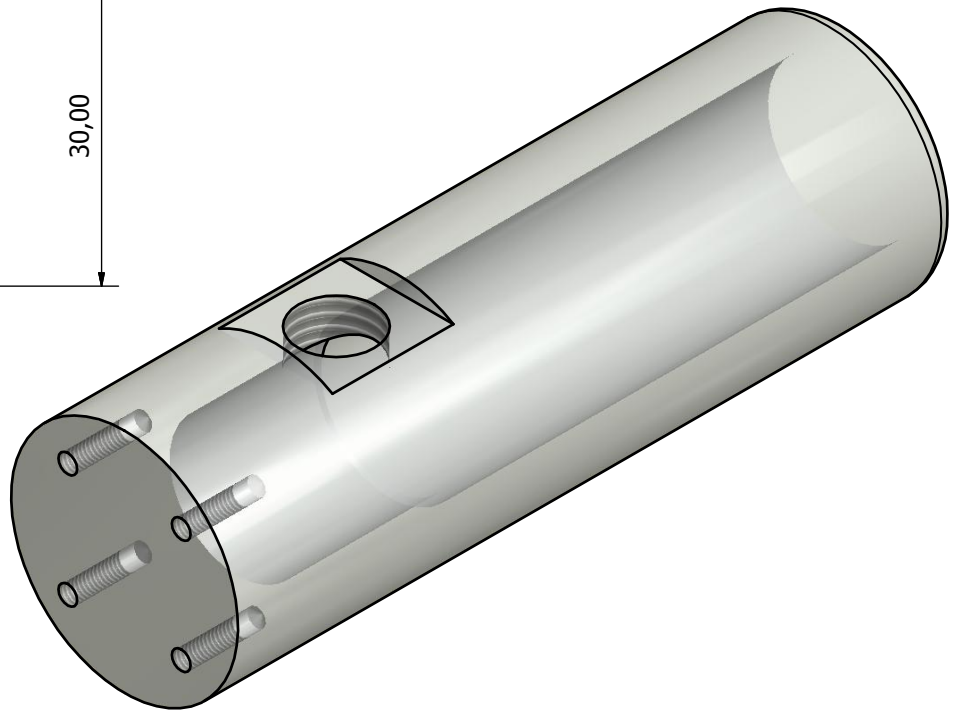

Designed by	Checked by	Approved by	Date		Date	Scale
Úlfar Karl	Sveinn Hinrik	Sveinn Hinrik	21.11.2014		21.11.2014	2 : 0

DTE DYNAMIC TECHNOLOGY EQUIPMENT

Plexi-probe

Inlet Pipe

Edition

Sheet 2 / 5

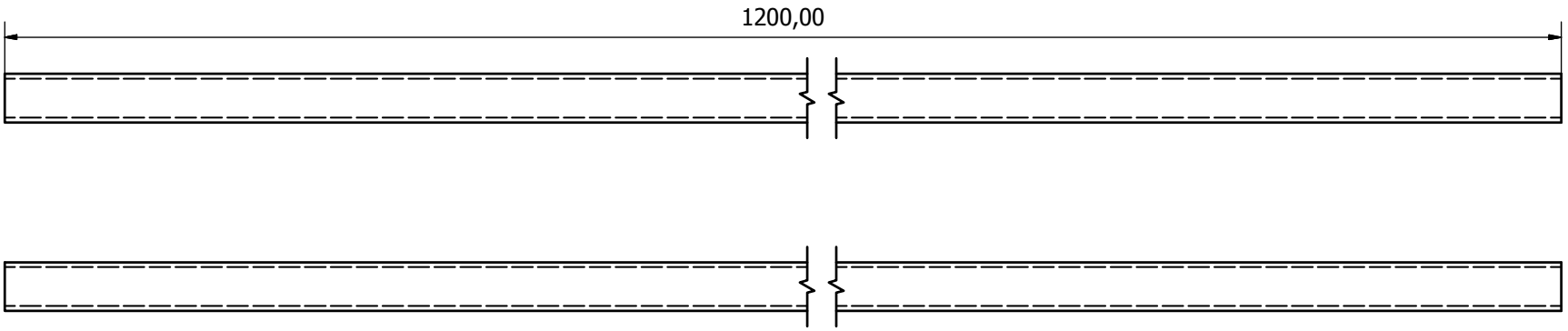

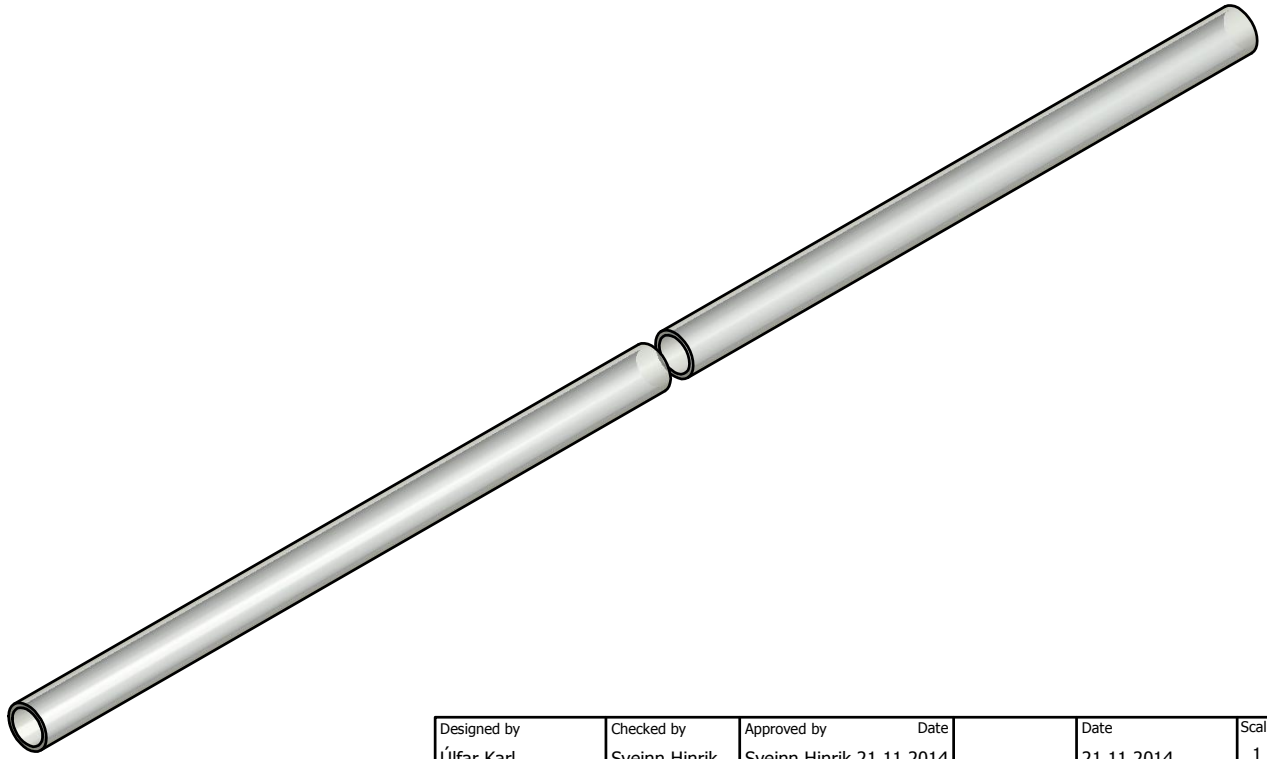

Designed by	Checked by	Approved by	Date		Date	Scale
Úlfar Karl	Sveinn Hinrik	Sveinn Hinrik	21.11.2014		21.11.2014	1 : 2

DTE DYNAMIC TECHNOLOGY EQUIPMENT

Plexi-probe		
Pipe	Edition	Sheet 3 / 5

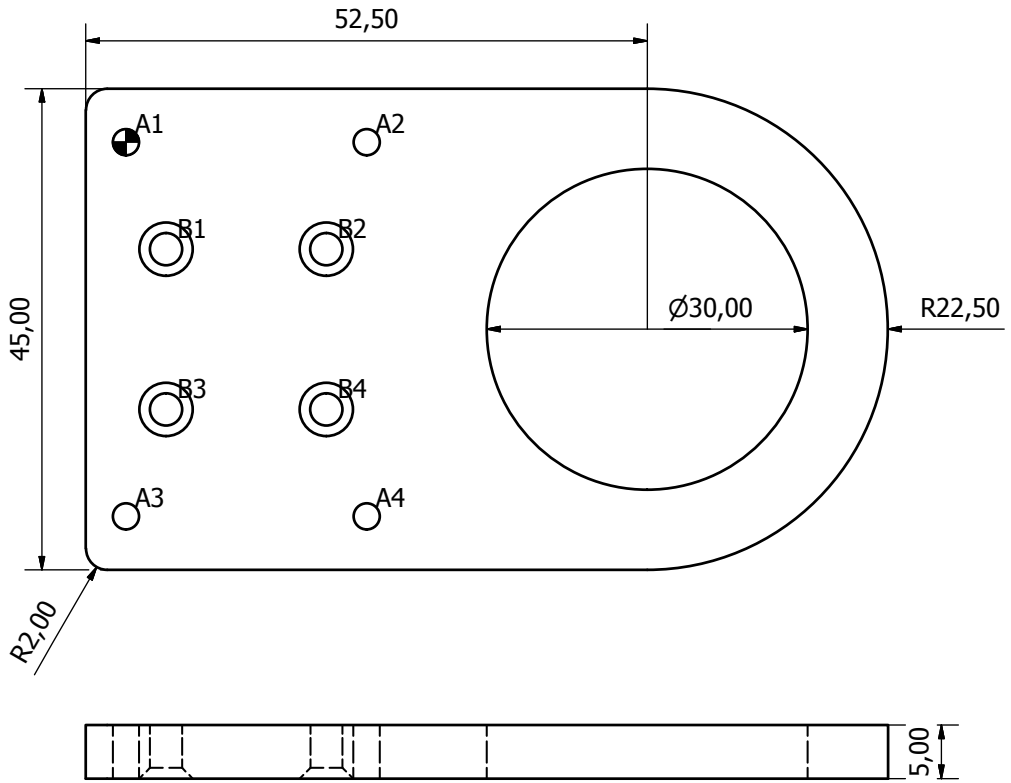

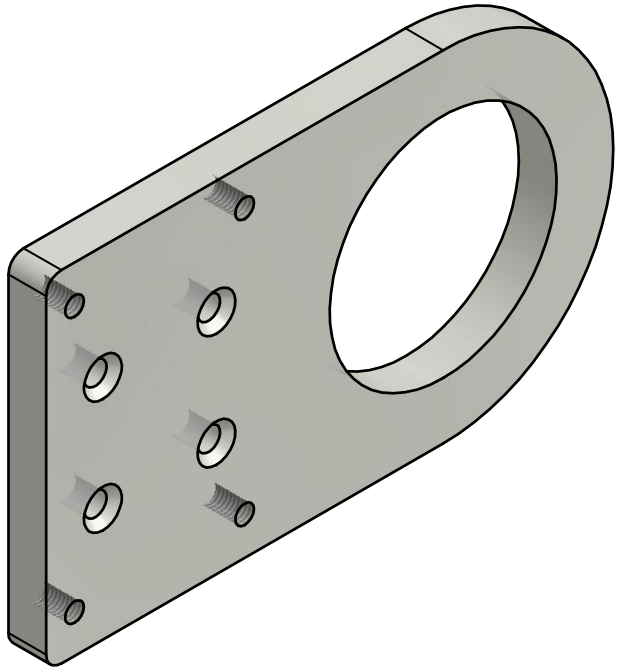

HOLE TABLE			
HOLE	XDIM	YDIM	DESCRIPTION
A1	0,00	0,00	M3x0.5 - 6H
A2	22,50	0,00	M3x0.5 - 6H
A3	0,00	-35,00	M3x0.5 - 6H
A4	22,50	-35,00	M3x0.5 - 6H
B1	3,75	-10,00	Ø3,00 THRU ⌵ Ø5,00 X 90,00°
B2	18,75	-10,00	Ø3,00 THRU ⌵ Ø5,00 X 90,00°
B3	3,75	-25,00	Ø3,00 THRU ⌵ Ø5,00 X 90,00°
B4	18,75	-25,00	Ø3,00 THRU ⌵ Ø5,00 X 90,00°

Designed by	Checked by	Approved by	Date		Date	Scale
Úlfar Karl	Sveinn Hinrik	Sveinn Hinrik	21.11.2014		21.11.2014	2 : 0

DTE DYNAMIC TECHNOLOGY EQUIPMENT

Plexi-probe

Sensor Bracket

Edition

Sheet 4 / 5

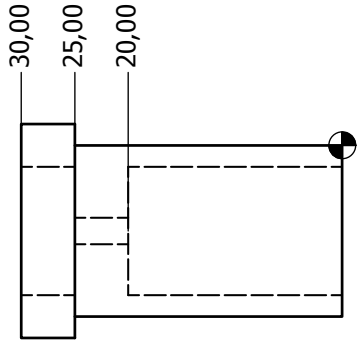

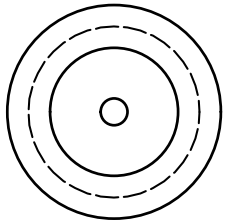

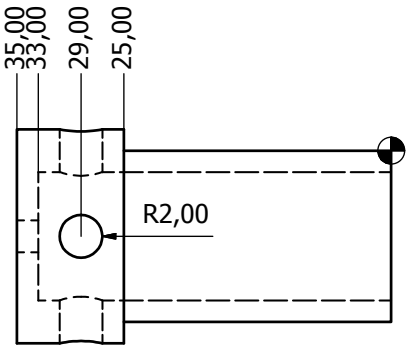

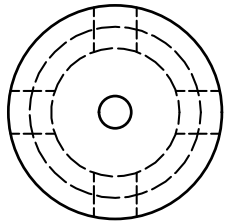

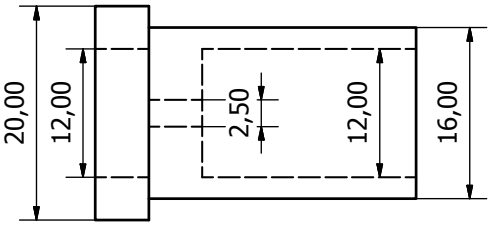

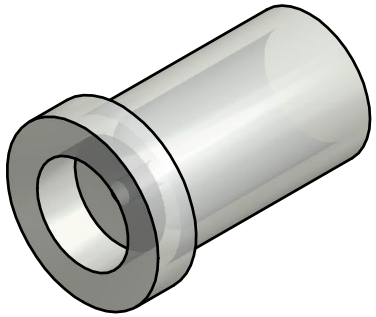

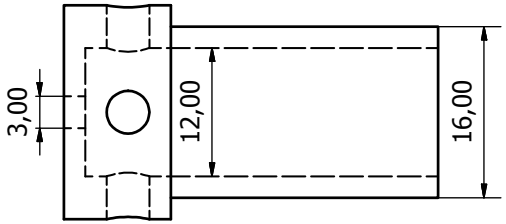

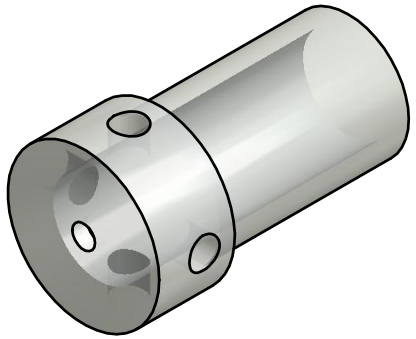

Designed by	Checked by	Approved by	Date		Date	Scale
Úlfar Karl	Sveinn Hinrik	Sveinn Hinrik	21.11.2014		21.11.2014	2 : 0

DTE DYNAMIC TECHNOLOGY EQUIPMENT

Plexi-probe

Tip Types

Edition

Sheet 5 / 5

B Texas Instruments XTR110

SBOS141C – JANUARY 1984 – REVISED SEPTEMBER 2009

PRECISION VOLTAGE-TO-CURRENT CONVERTER/TRANSMITTER

FEATURES

- 4mA TO 20mA TRANSMITTER
- SELECTABLE INPUT/OUTPUT RANGES:
  0V to +5V, 0V to +10V Inputs
  0mA to 20mA, 5mA to 25mA Outputs
  Other Ranges
- 0.005% MAX NONLINEARITY, 14 BIT
- PRECISION +10V REFERENCE OUTPUT
- SINGLE-SUPPLY OPERATION
- WIDE SUPPLY RANGE: 13.5V to 40V

APPLICATIONS

- INDUSTRIAL PROCESS CONTROL
- PRESSURE/TEMPERATURE TRANSMITTERS
- CURRENT-MODE BRIDGE EXCITATION
- GROUNDED TRANSDUCER CIRCUITS
- CURRENT SOURCE REFERENCE FOR DATA ACQUISITION
- PROGRAMMABLE CURRENT SOURCE FOR TEST EQUIPMENT
- POWER PLANT/ENERGY SYSTEM MONITORING

DESCRIPTION

The XTR110 is a precision voltage-to-current converter designed for analog signal transmission. It accepts inputs of 0 to 5V or 0 to 10V and can be connected for outputs of 4mA to 20mA, 0mA to 20mA, 5mA to 25mA, and many other commonly used ranges.

A precision on-chip metal film resistor network provides input scaling and current offsetting. An internal 10V voltage reference can be used to drive external circuitry.

The XTR110 is available in 16-pin plastic DIP, ceramic DIP and SOL-16 surface-mount packages. Commercial and industrial temperature range models are available.

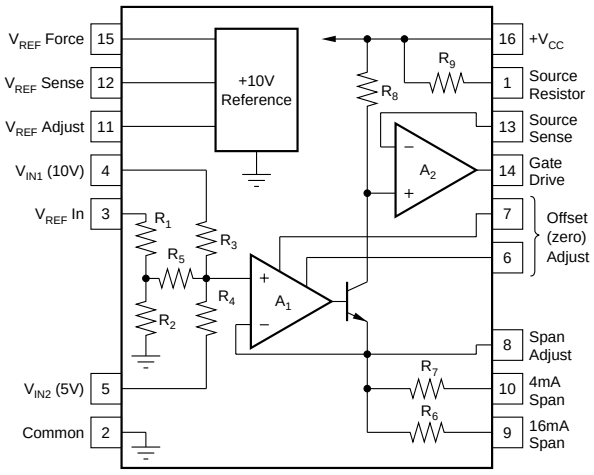

Please be aware that an important notice concerning availability, standard warranty, and use in critical applications of Texas Instruments semiconductor products and disclaimers thereto appears at the end of this data sheet.

All trademarks are the property of their respective owners.

PRODUCTION DATA information is current as of publication date. Products conform to specifications per the terms of Texas Instruments standard warranty. Production processing does not necessarily include testing of all parameters.

Copyright © 1984-2009, Texas Instruments Incorporated

ABSOLUTE MAXIMUM RATINGS(1)

Power Supply, $+V_{CC}$	40V
Input Voltage, V_{IN1}, V_{IN2}, $V_{REF\ IN}$	$+V_{CC}$
See text regarding safe negative input voltage range.	
Storage Temperature Range: A, B	–55°C to +125°C
K, U	–40°C to +85°C
Output Short-Circuit Duration, Gate Drive and V_{REF} Force	Continuous to common and $+V_{CC}$
Output Current Using Internal 50Ω Resistor	40mA

NOTE: (1) Stresses above these ratings may cause permanent damage. Exposure to absolute maximum conditions for extended periods may degrade device reliability.

ELECTROSTATIC DISCHARGE SENSITIVITY

This integrated circuit can be damaged by ESD. Texas Instruments recommends that all integrated circuits be handled with appropriate precautions. Failure to observe proper handling and installation procedures can cause damage.

ESD damage can range from subtle performance degradation to complete device failure. Precision integrated circuits may be more susceptible to damage because very small parametric changes could cause the device not to meet its published specifications.

PACKAGE/ORDERING INFORMATION(1)

PRODUCT	PACKAGE-LEAD	PACKAGE DESIGNATOR	TEMPERATURE RANGE
XTR110AG	DIP-16 Ceramic	JD	–40°C to +85°C
XTR110BG	DIP-16 Ceramic	JD	–40°C to +85°C
XTR110KP	DIP-16 Plastic	N	0°C to +70°C
XTR110KU	SOL-16 Surface-Mount	DW	0°C to +70°C

NOTE: (1) For the most current package and ordering information, see the Package Option Addendum at the end of this document, or see the TI website at www.ti.com.

PIN CONFIGURATION

TOP VIEW

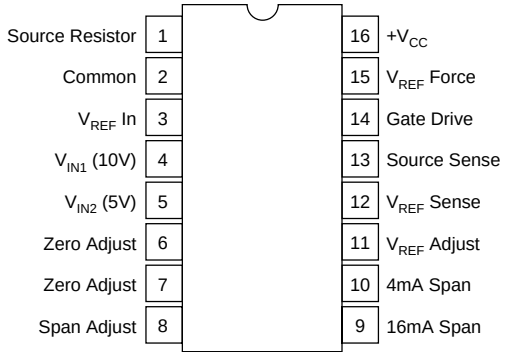

ELECTRICAL CHARACTERISTICS

At T_A = +25°C and V_{CC} = +24V and R_L = 250Ω**, unless otherwise specified.

PARAMETER	CONDITIONS	XTR110AG, KP, KU			XTR110BG			UNITS
		MIN	TYP	MAX	MIN	TYP	MAX	
TRANSMITTER								
Transfer Function			$I_O = 10\ [(V_{REF}In/16) + (V_{IN1}/4) + (V_{IN2}/2)]\ /R_{SPAN}$					
Input Range: V_{IN1}[5]	Specified Performance	0		+10	*		*	V
V_{IN2}	Specified Performance	0		+5	*		*	V
Current, I_O	Specified Performance[1]	4		20	*		*	mA
	Derated Performance[1]	0		40	*		*	mA
Nonlinearity	16mA/20mA Span[2]		0.01	0.025		0.002	0.005	% of Span
Offset Current, I_{OS}	I_O = 4mA[1]							
Initial	[1]		0.2	0.4		0.02	0.1	% of Span
vs Temperature	[1]		0.0003	0.005		*	0.003	% of Span/°C
vs Supply, V_{CC}	[1]		0.0005	0.005		*	*	% of Span/V
Span Error	I_O = 20mA							
Initial	[1]		0.3	0.6		0.05	0.2	% of Span
vs Temperature	[1]		0.0025	0.005		0.0009	0.003	% of Span/°C
vs Supply, V_{CC}	[1]		0.003	0.005		*	*	% of Span/V
Output Resistance	From Drain of FET (Q_{EXT})[3]		10×10^9			*		Ω
Input Resistance	V_{IN1}		27			*		kΩ
	V_{IN2}		22			*		kΩ
	V_{REF} In		19			*		kΩ
Dynamic Response								
Settling Time	To 0.1% of Span		15			*		µs
	To 0.01% of Span		20			*		µs
Slew Rate			1.3			*		mA/µs
VOLTAGE REFERENCE								
Output Voltage		+9.95	+10	+10.05	+9.98	*	+10.02	V
vs Temperature			35	50		15	30	ppm/°C
vs Supply, V_{CC}	Line Regulation		0.0002	0.005		*	*	%/V
vs Output Current	Load Regulation		0.0005	0.01		*	*	%/mA
vs Time			100			*		ppm/1k hrs
Trim Range		–0.100		+0.25	*		*	V
Output Current	Specified Performance	10			*			mA
POWER SUPPLY								
Input Voltage, V_{CC}		+13.5		+40	*		*	V
Quiescent Current	Excluding I_O		3	4.5		*	*	mA
TEMPERATURE RANGE								
Specification: AG, BG		–40		+85	*		*	°C
KP, KU		0		+70				°C
Operating: AG, BG		–55		+125	*		*	°C
KP, KU		–25		+85				°C

* Specifications same as AG/KP grades. ** Specifications apply to the range of R_L shown in Typical Performance Curves.

NOTES: (1) Including internal reference. (2) Span is the change in output current resulting from a full-scale change in input voltage. (3) Within compliance range limited by ($+V_{CC}$ – 2V) $+V_{DS}$ required for linear operation of the FET. (4) For V_{REF} adjustment circuit see Figure 3. (5) For extended I_{REF} drive circuit see Figure 4. (5) Unit may be damaged. See *Input Voltage Range* section.

TYPICAL PERFORMANCE CURVES

T_A = +25°C, V_{CC} = 24VDC, R_L = 250Ω, unless otherwise noted.

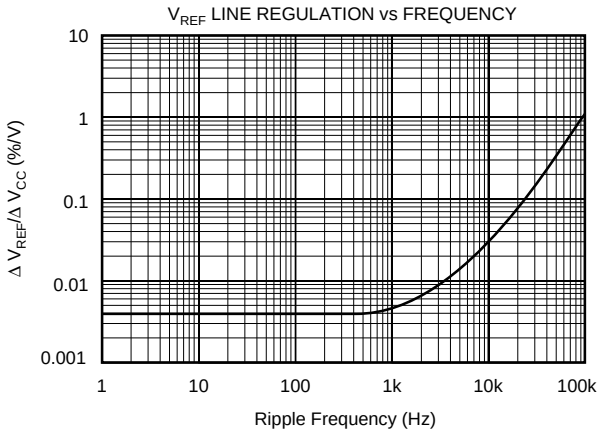

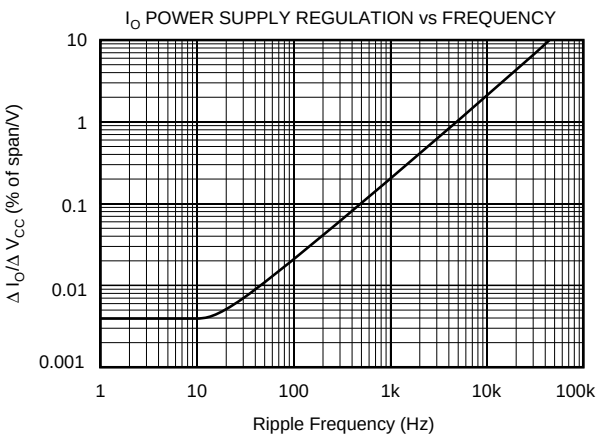

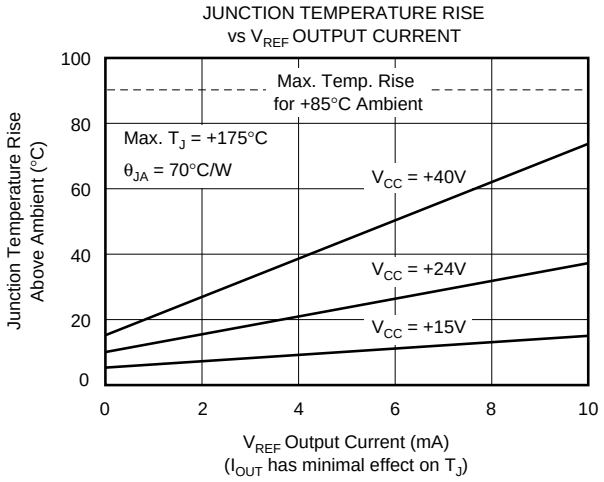

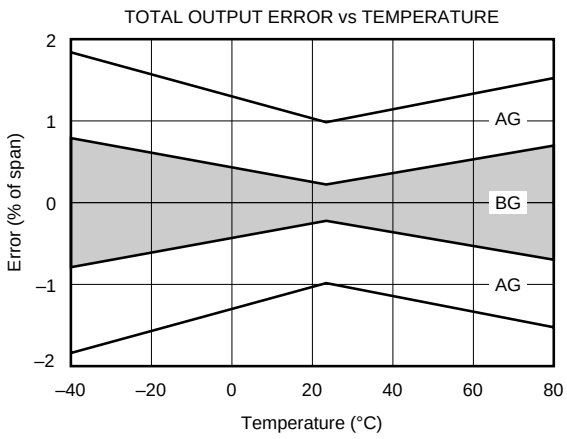

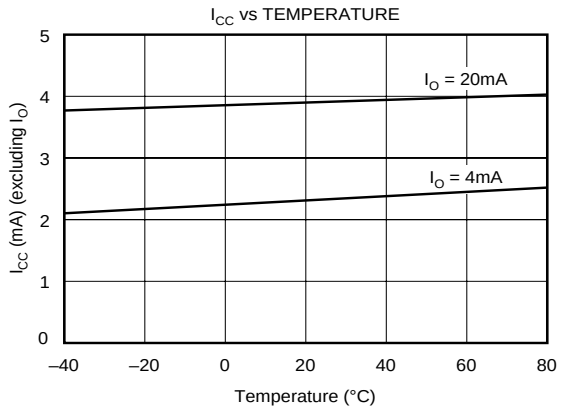

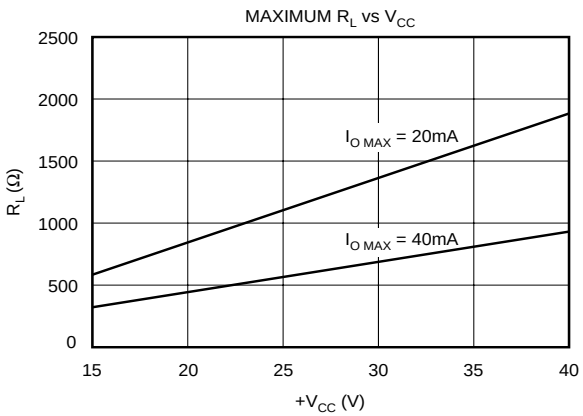

TYPICAL PERFORMANCE CURVES (Continued)

At T_A = +25°C, V_{CC} = 24VDC, R_L = 250Ω, unless otherwise noted.

SETTLING TIME WITH NEG V_{IN} STEP

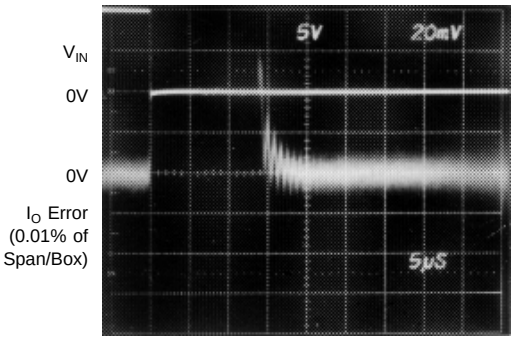

PULSE RESPONSE

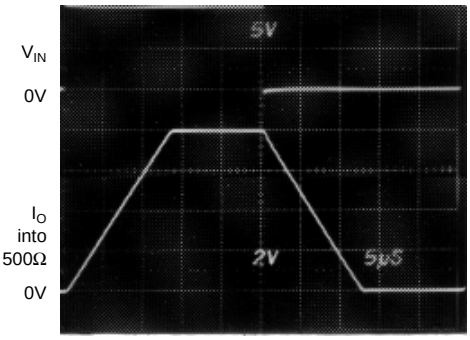

SETTLING TIME WITH POS V_{IN} STEP

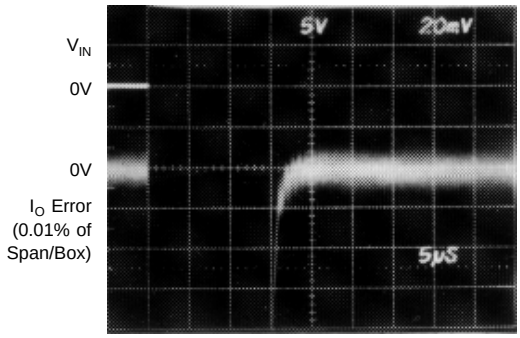

APPLICATIONS INFORMATION

Figure 1 shows the basic connections required for 0V to 10V input and 4ma to 20mA output. Other input voltage and output current ranges require changes in connections of pins 3, 4, 5, 9 and 10 as shown in the table of Figure 1.

The complete transfer function of the XTR110 is:

$$I_O = \frac{10\left[\frac{(V_{REF\ IN})}{16} + \frac{(V_{IN1})}{4} + \frac{(V_{IN2})}{2}\right]}{R_{SPAN}} \qquad (1)$$

R_{SPAN} is the total impedance seen at the emitter of the internal NPN transistor. This impedance varies depending on how pins 8, 9 and 10 are configured. Typical operating region configurations are shown in Figure 1. An external R_{SPAN} can be connected for different output current ranges as described later.

EXTERNAL TRANSISTOR

An external pass transistor, Q_{EXT}, is required as shown in Figure 1. This transistor conducts the output signal current. A P-channel MOSFET transistor is recommended. It must have a voltage rating equal or greater than the maximum power supply voltage. Various recommended types are shown in Table I.

MANUFACTURER	PART NO.	BV_{DSS}(1)	BV_{GS}(1)	PACKAGE
Ferranti	ZVP1304A	40V	20V	TO-92
	ZVP1304B	40V	20V	TO-39
	ZVP1306A	60V	20V	TO-92
	ZVP1306B	60V	20V	TO-39
International Rectifier	IRF9513	60V	20V	TO-220
Motorola	MTP8P08	80V	20V	TO-220
RCA	RFL1P08	80V	20V	TO-39
	RFT2P08	80V	20V	TO-220
Siliconix (preferred)	VP0300B	30V	40V	TO-39
	VP0300L	30V	40V	TO-92
	VP0300M	30V	40V	TO-237
	VP0808B	80V	40V	TO-39
	VP0808L	80V	40V	TO-92
	VP0808M	80V	40V	TO-237
Supertex	VP1304N2	40V	20V	TO-220
	VP1304N3	40V	20V	TO-92
	VP1306N2	60V	20V	TO-220
	VP1306N3	60V	20V	TO-92

NOTE: (1) BV_{DSS}—Drain-source breakdown voltage. BV_{GS}—Gate-source breakdown voltage.

TABLE I. Available P-Channel MOSFETs.

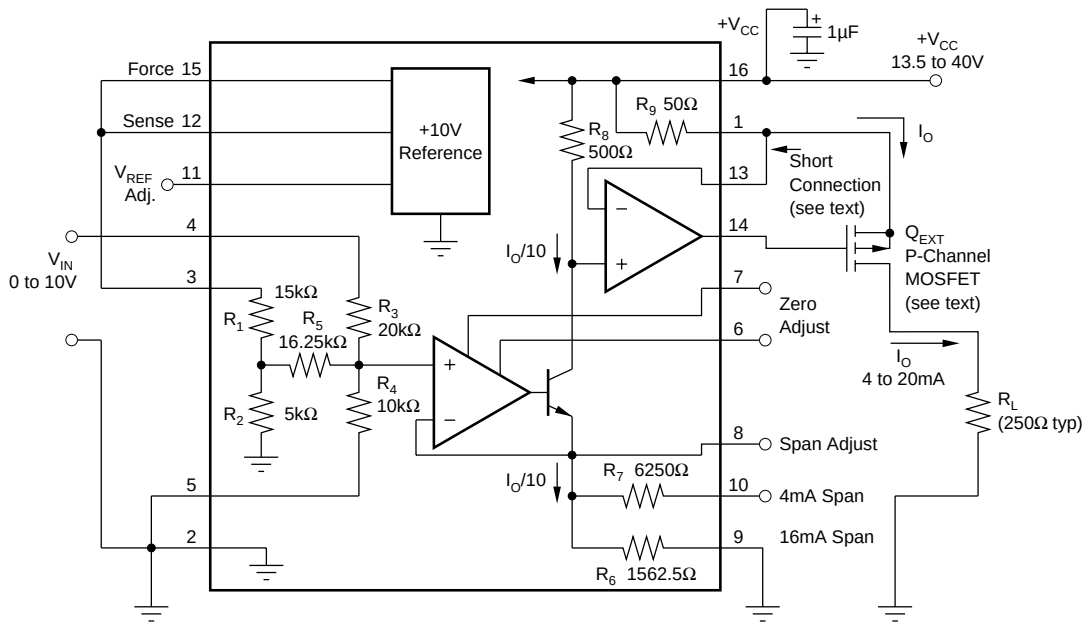

INPUT RANGE (V)	OUTPUT RANGE (mA)	PIN 3	PIN 4	PIN 5	PIN 9	PIN 10
0-10	0-20	Com	Input	Com	Com	Com
2-10	4-20	Com	Input	Com	Com	Com
0-10	4-20	+10V Ref	Input	Com	Com	Open
0-10	5-25	+10V Ref	Input	Com	Com	Com
0-5	0-20	Com	Com	Input	Com	Com
1-5	4-20	Com	Com	Input	Com	Com
0-5	4-20	+10V Ref	Com	Input	Com	Open
0-5	5-25	+10V Ref	Com	Input	Com	Com

FIGURE 1. Basic Circuit Connection.

If the supply voltage, $+V_{CC}$, exceeds the gate-to-source breakdown voltage of Q_{EXT}, and the output connection (drain of Q_{EXT}) is broken, Q_{EXT} could fail. If the gate-to-source breakdown voltage is lower than $+V_{CC}$, Q_{EXT} can be protected with a 12V zener diode connected from gate to source.

Two PNP discrete transistors (Darlington-connected) can be used for Q_{EXT}—see Figure 2. Note that an additional capacitor is required for stability. Integrated Darlington transistors are not recommended because their internal base-emitter resistors cause excessive error.

TRANSISTOR DISSIPATION

Maximum power dissipation of Q_{EXT} depends on the power supply voltage and full-scale output current. Assuming that the load resistance is low, the power dissipated by Q_{EXT} is:

$$P_{MAX} = (+V_{CC})\ I_{FS} \qquad (2)$$

The transistor type and heat sinking must be chosen according to the maximum power dissipation to prevent overheating. See Table II for general recommendations.

PACKAGE TYPE	ALLOWABLE POWER DISSIPATION
TO-92	Lowest: Use minimum supply and at +25°C.
TO-237	Acceptable: Trade-off supply and temperature.
TO-39	Good: Adequate for majority of designs.
TO-220	Excellent: For prolonged maximum stress.
TO-3	Use if hermetic package is required.

TABLE II. External Transistor Package Type and Dissipation.

INPUT VOLTAGE RANGE

The internal op amp A_1 can be damaged if its non-inverting input (an internal node) is pulled more than 0.5V below common (0V). This could occur if input pins 3, 4 or 5 were driven with an op amp whose output could swing negative under abnormal conditions. The voltage at the input of A_1 is:

$$V_{A1} = \frac{(V_{REF\ IN})}{16} + \frac{(V_{IN1})}{4} + \frac{(V_{IN2})}{2} \qquad (3)$$

This voltage should not be allowed to go more negative than –0.5V. If necessary, a clamp diode can be connected from the negative-going input to common to clamp the input voltage.

COMMON (Ground)

Careful attention should be directed toward proper connection of the common (grounds). All commons should be joined at one point as close to pin 2 of the XTR110 as possible. The exception is the I_{OUT} return. It can be returned to any point where it will not modulate the common at pin 2.

VOLTAGE REFERENCE

The reference voltage is accurately regulated at pin 12 ($V_{REF\ SENSE}$). To preserve accuracy, any load including pin 3 should be connected to this point. The circuit in Figure 3 shows adjustment of the voltage reference.

The current drive capability of the XTR110's internal reference is 10mA. This can be extended if desired by adding an external NPN transistor shown in Figure 4.

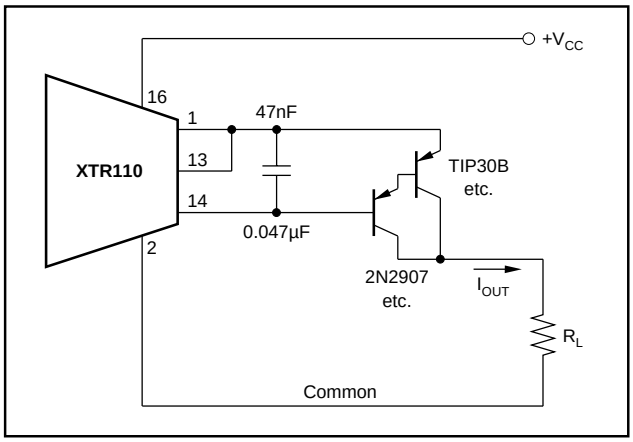

FIGURE 2. Q_{EXT} Using PNP Transistors.

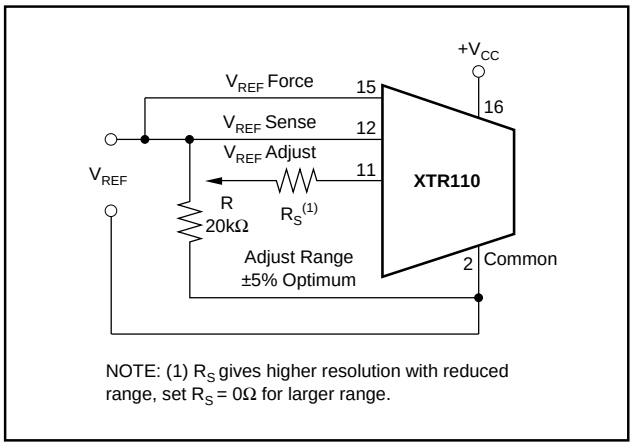

FIGURE 3. Optional Adjustment of Reference Voltage.

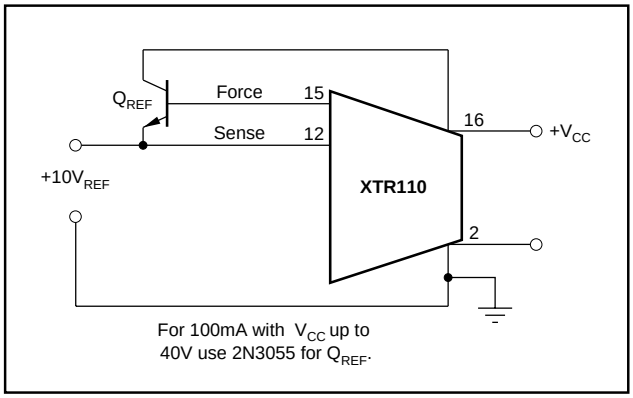

FIGURE 4. Increasing Reference Current Drive.

OFFSET (ZERO) ADJUSTMENT

The offset current can be adjusted by using the potentiometer, R_1, shown in Figure 5. Set the input voltage to zero and then adjust R_1 to give 4mA at the output. For spans starting

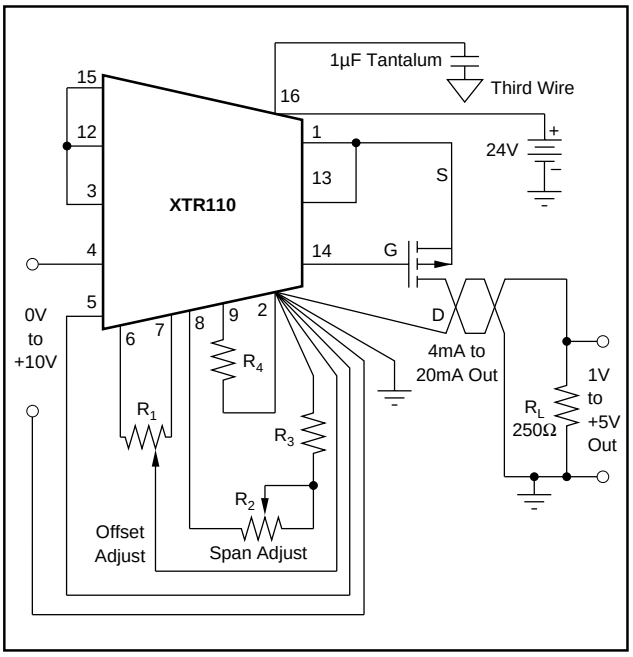

FIGURE 5. Offset and Span Adjustment Circuit for 0V to +10V Input, 4mA to 20mA Output.

at 0mA, the following special procedure is recommended: set the input to a small nonzero value and then adjust R_1 to the proper output current. When the input is zero the output will be zero. Figures 6 and 7 show graphically how offset is adjusted.

SPAN ADJUSTMENT

The span is adjusted at the full-scale output current using the potentiometer, R_2, shown in Figure 5. This adjustment is interactive with the offset adjustment, and a few iterations may be necessary. For the circuit shown, set the input voltage to +10V full scale and adjust R_2 to give 20mA full-scale output. Figures 6 and 7 show graphically how span is adjusted.

The values of R_2, R_3, and R_4 for adjusting the span are determined as follows: choose R_4 in series to slightly decrease the span; then choose R_2 and R_3 to increase the span to be adjustable about the center value.

LOW TEMPERATURE COEFFICIENT OPERATION

Although the precision resistors in the XTR110 track within 1ppm/°C, the output current depends upon the absolute temperature coefficient (TC) of any one of the resistors, R_6, R_7, R_8, and R_9. Since the absolute TC of the output current can have 20ppm/°C, maximum, the TC of the output current can have 20ppm/°C drift. For low TC operation, zero TC resistors can be substituted for either the span resistors (R_6 or R_7) or for the source resistor (R_9) but not both.

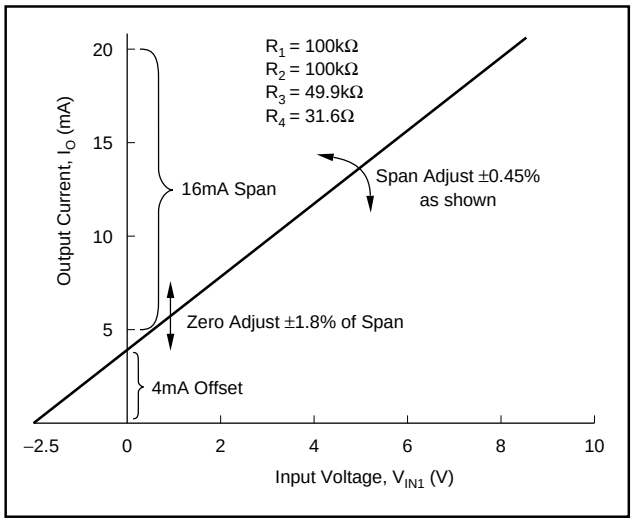

FIGURE 6. Zero and Span of 0V to +10V Input, 4mA to 20mA Output Configuration (see Figure 5).

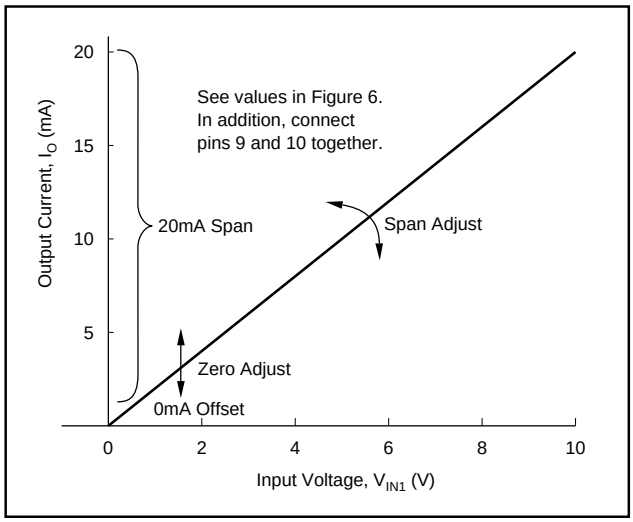

FIGURE 7. Zero and Span of 0V to +10V_{IN}, 0mA to 20mA Output Configuration (see Figure 5).

EXTENDED SPAN

For spans beyond 40mA, the internal 50Ω resistor (R_9) may be replaced by an external resistor connected between pins 13 and 16.

Its value can be calculated as follows:

$$R_{EXT} = R_9 \ (Span_{OLD}/Span_{NEW})$$

Since the internal thin-film resistors have a 20% absolute value tolerance, measure R_9 before determining the final value of R_{EXT}. Self-heating of R_{EXT} can cause nonlinearity. Therefore, choose one with a low TC and adequate power rating. See Figure 10 for application.

TYPICAL APPLICATIONS

The XTR110 is ideal for a variety of applications requiring high noise immunity current-mode signal transmission. The precision +10V reference can be used to excite bridges and transducers. Selectable ranges make it very useful as a precision programmable current source. The compact design and low price of the XTR110 allow versatility with a minimum of external components and design engineering expense.

Figures 8 through 10 show typical applications of the XTR110.

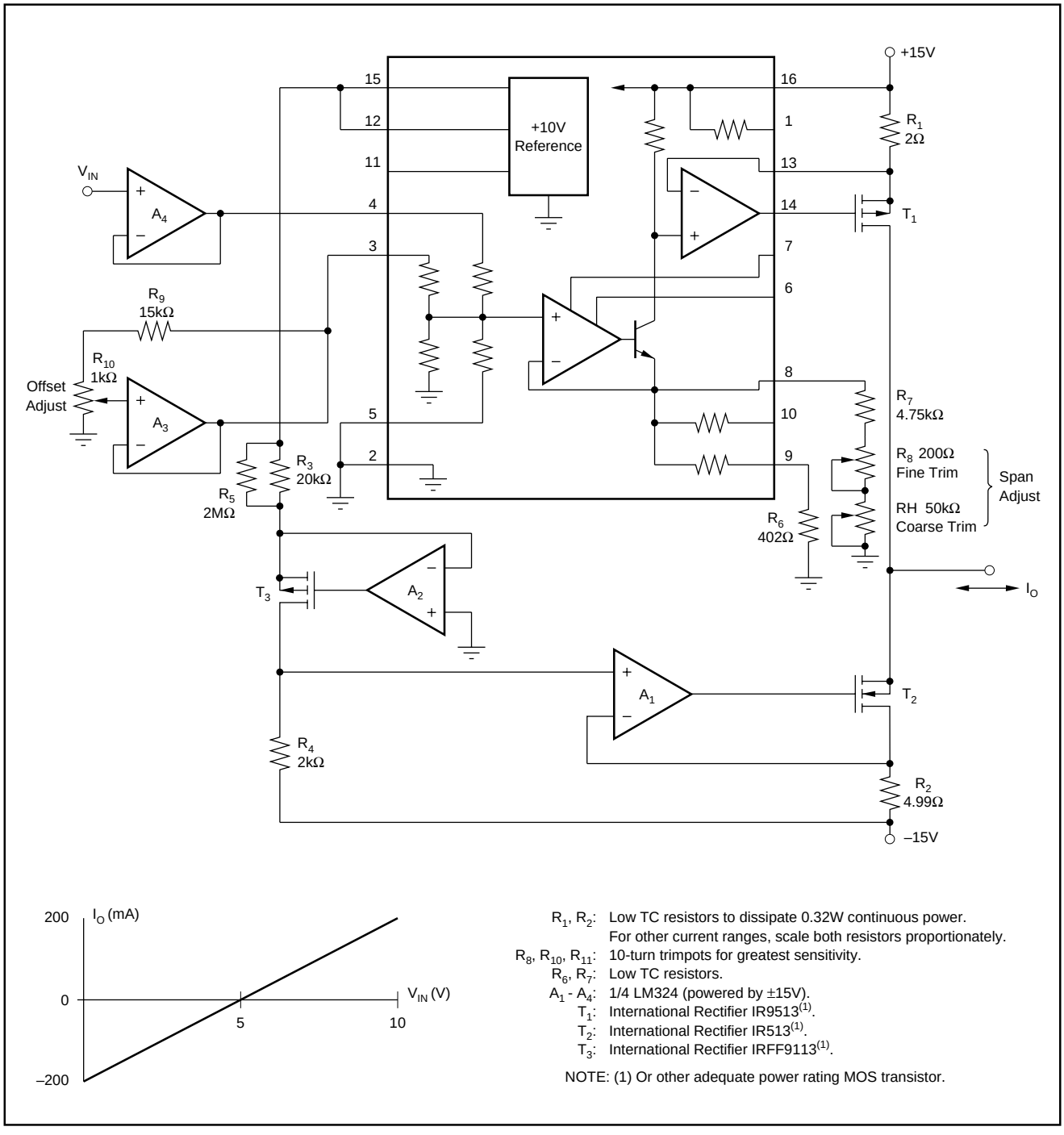

FIGURE 8. ±200mA Current Pump.

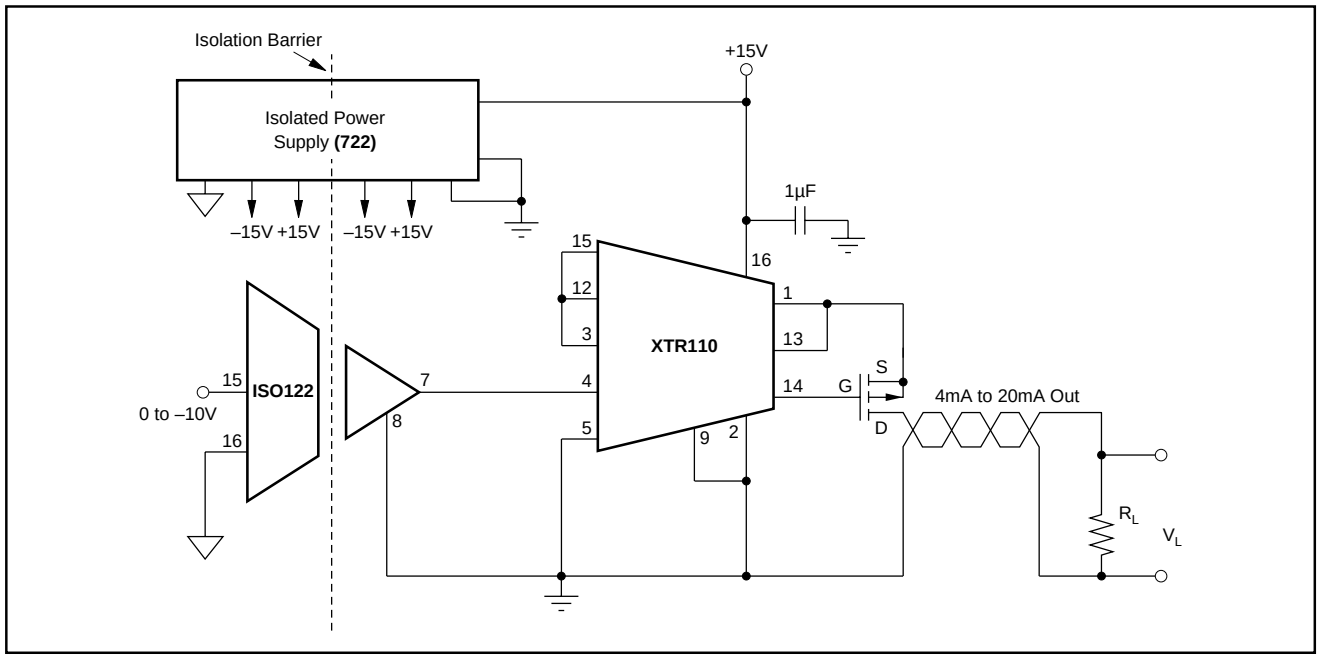

FIGURE 9. Isolated 4mA to 20mA Channel.

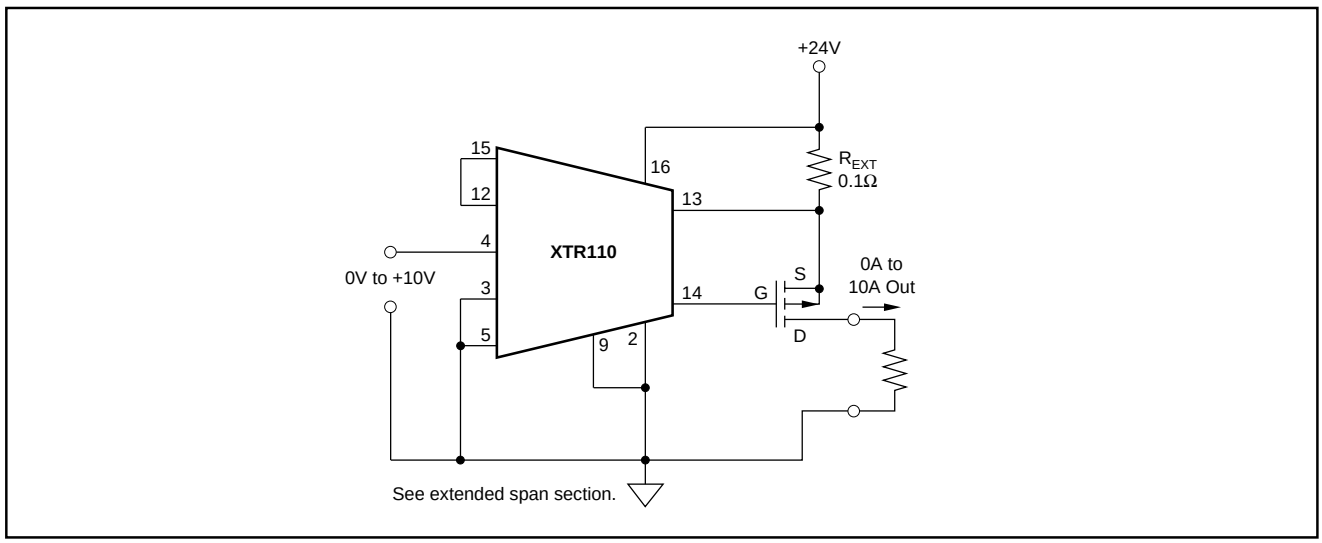

FIGURE 10. 0A to 10A Output Voltage-to-Current Converter.

N (R–PDIP–T**)

PLASTIC DUAL–IN–LINE PACKAGE

16 PINS SHOWN

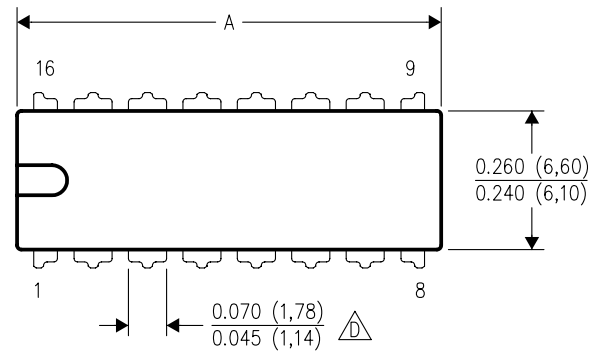

DIM \ PINS **	14	16	18	20
A MAX	0.775 (19,69)	0.775 (19,69)	0.920 (23,37)	1.060 (26,92)
A MIN	0.745 (18,92)	0.745 (18,92)	0.850 (21,59)	0.940 (23,88)
C MS–001 VARIATION	AA	BB	AC	AD

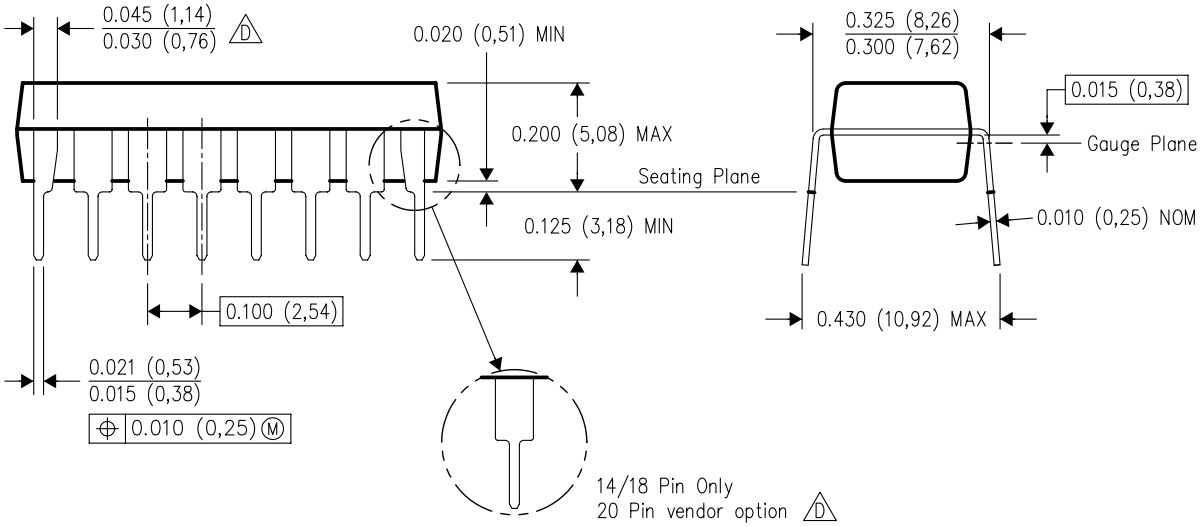

4040049/E 12/2002

NOTES:
A. All linear dimensions are in inches (millimeters).
B. This drawing is subject to change without notice.
C. Falls within JEDEC MS–001, except 18 and 20 pin minimum body length (Dim A).
D. The 20 pin end lead shoulder width is a vendor option, either half or full width.

C Fairchild FQP17P06

FAIRCHILD SEMICONDUCTOR®

March 2013

FQP17P06

P-Channel QFET® MOSFET

- 60 V, - 17 A, 120 mΩ

Description

This P-Channel enhancement mode power MOSFET is produced using Fairchild Semiconductor®'s proprietary planar stripe and DMOS technology. This advanced MOSFET technology has been especially tailored to reduce on-state resistance, and to provide superior switching performance and high avalanche energy strength. These devices are suitable for switched mode power supplies, audio amplifier, DC motor control, and variable switching power applications.

Features

- - 17 A, - 60 V, $R_{DS(on)}$ = 120 mΩ (Max.) @ V_{GS} = - 10 V, ID = - 8.5 A
- Low Gate Charge (Typ.21 nC)
- Low Crss (Typ. 80 pF)
- 100% Avalanche Tested
- 175°C Maximum Junction Temperature Rating

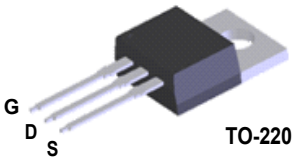

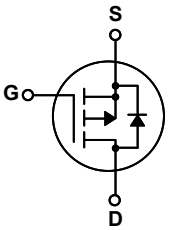

Absolute Maximum Ratings

T_C = 25°C unless otherwise noted

Symbol	Parameter			FQP17P06	Unit
V_{DSS}	Drain-Source Voltage			-60	V
I_D	Drain Current	- Continuous (T_C = 25°C)		-17	A
		- Continuous (T_C = 100°C)		-12	A
I_{DM}	Drain Current	- Pulsed	(Note 1)	-68	A
V_{GSS}	Gate-Source Voltage			± 25	V
E_{AS}	Single Pulsed Avalanche Energy		(Note 2)	300	mJ
I_{AR}	Avalanche Current		(Note 1)	-17	A
E_{AR}	Repetitive Avalanche Energy		(Note 1)	7.9	mJ
dv/dt	Peak Diode Recovery dv/dt		(Note 3)	-7.0	V/ns
P_D	Power Dissipation (T_C = 25°C)			79	W
	- Derate above 25°C			0.53	W/°C
T_J, T_{STG}	Operating and Storage Temperature Range			-55 to +175	°C
T_L	Maximum lead temperature for soldering purposes, 1/8" from case for 5 seconds			300	°C

Thermal Characteristics

Symbol	Parameter	FQP17P06	Unit
$R_{\theta JC}$	Thermal Resistance, Junction-to-Case, Max.	1.9	°C/W
$R_{\theta CS}$	Thermal Resistance, Case-to-Sink, Typ.	0.5	°C/W
$R_{\theta JA}$	Thermal Resistance, Junction-to-Ambient, Max.	62.5	°C/W

©2001 Fairchild Semiconductor Corporation

Elerical Characteristics

T_C = 25°C unless otherwise noted

Symbol	Parameter	Test Conditions	Min	Typ	Max	Unit
Off Characteristics						
BV_{DSS}	Drain-Source Breakdown Voltage	V_{GS} = 0 V, I_D = -250 μA	-60	--	--	V
ΔBV_{DSS} / ΔT_J	Breakdown Voltage Temperature Coefficient	I_D = -250 μA, Referenced to 25°C	--	-0.06	--	V/°C
I_{DSS}	Zero Gate Voltage Drain Current	V_{DS} = -60 V, V_{GS} = 0 V	--	--	-1	μA
		V_{DS} = -48 V, T_C = 150°C	--	--	-10	μA
I_{GSSF}	Gate-Body Leakage Current, Forward	V_{GS} = -25 V, V_{DS} = 0 V	--	--	-100	nA
I_{GSSR}	Gate-Body Leakage Current, Reverse	V_{GS} = 25 V, V_{DS} = 0 V	--	--	100	nA
On Characteristics						
$V_{GS(th)}$	Gate Threshold Voltage	V_{DS} = V_{GS}, I_D = -250 μA	-2.0	--	-4.0	V
$R_{DS(on)}$	Static Drain-Source On-Resistance	V_{GS} = -10 V, I_D = -8.5 A	--	0.094	0.12	Ω
g_{FS}	Forward Transconductance	V_{DS} = -30 V, I_D = -8.5 A	--	9.3	--	S
Dynamic Characteristics						
C_{iss}	Input Capacitance	V_{DS} = -25 V, V_{GS} = 0 V, f = 1.0 MHz	--	690	900	pF
C_{oss}	Output Capacitance		--	325	420	pF
C_{rss}	Reverse Transfer Capacitance		--	80	105	pF
Switching Characteristics						
$t_{d(on)}$	Turn-On Delay Time	V_{DD} = -30 V, I_D = -8.5 A, R_G = 25 Ω (Note 4)	--	13	35	ns
t_r	Turn-On Rise Time		--	100	210	ns
$t_{d(off)}$	Turn-Off Delay Time		--	22	55	ns
t_f	Turn-Off Fall Time		--	60	130	ns
Q_g	Total Gate Charge	V_{DS} = -48 V, I_D = -17 A, V_{GS} = -10 V (Note 4)	--	21	27	nC
Q_{gs}	Gate-Source Charge		--	4.2	--	nC
Q_{gd}	Gate-Drain Charge		--	10	--	nC
Drain-Source Diode Characteristics and Maximum Ratings						
I_S	Maximum Continuous Drain-Source Diode Forward Current		--	--	-17	A
I_{SM}	Maximum Pulsed Drain-Source Diode Forward Current		--	--	-68	A
V_{SD}	Drain-Source Diode Forward Voltage	V_{GS} = 0 V, I_S = -17 A	--	--	-4.0	V
t_{rr}	Reverse Recovery Time	V_{GS} = 0 V, I_S = -17 A, dI_F / dt = 100 A/μs	--	92	--	ns
Q_{rr}	Reverse Recovery Charge		--	0.32	--	μC

Notes:
1. Repetitive Rating : Pulse width limited by maximum junction temperature
2. L = 1.2mH, I_{AS} = -17A, V_{DD} = -25V, R_G = 25 Ω, Starting T_J = 25°C
3. I_{SD} ≤ -17A, di/dt ≤ 300A/μs, V_{DD} ≤ BV_{DSS}, Starting T_J = 25°C
4. Essentially independent of operating temperature

Package Dimensions

TO-220

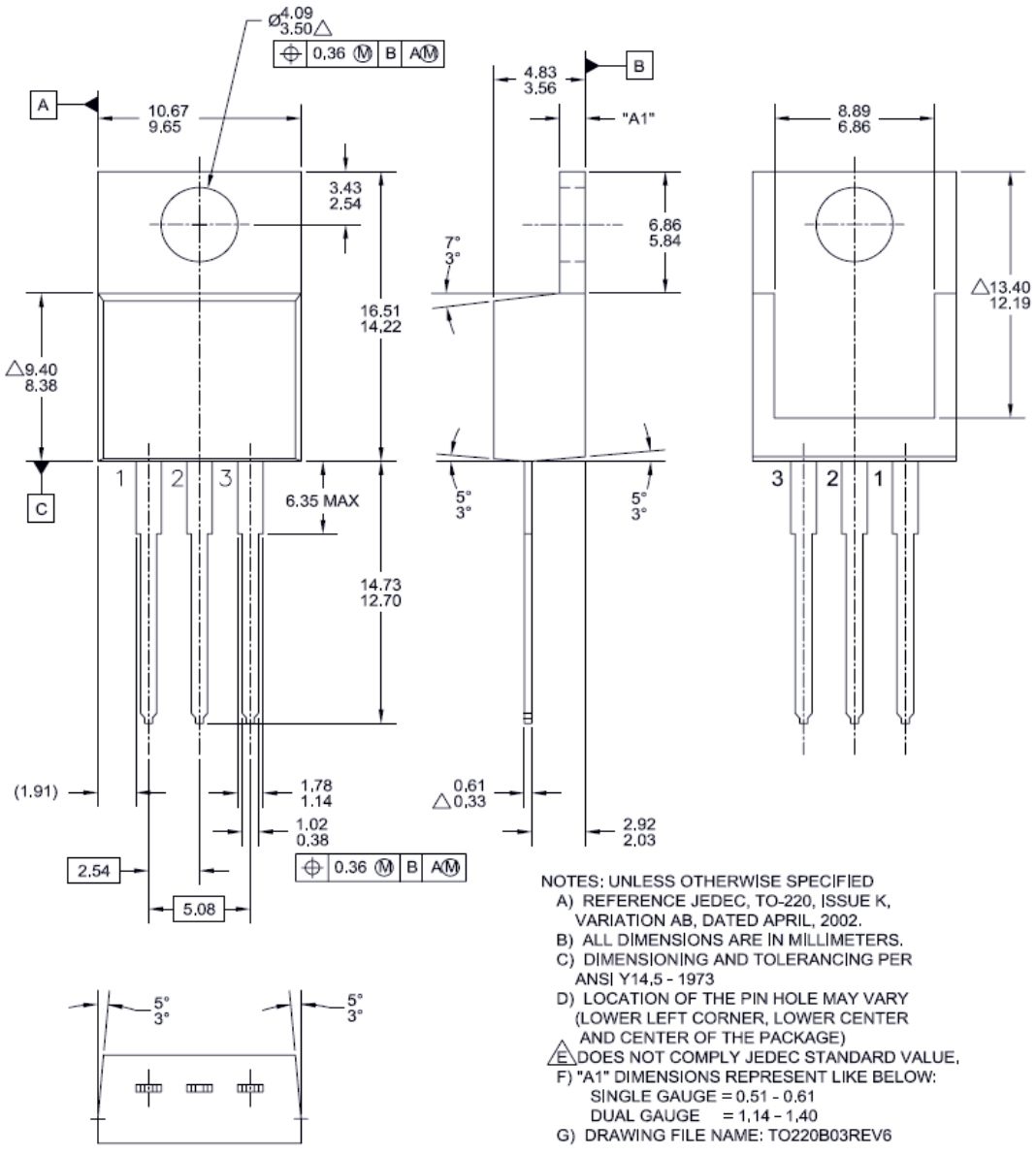

NOTES: UNLESS OTHERWISE SPECIFIED

A) REFERENCE JEDEC, TO-220, ISSUE K, VARIATION AB, DATED APRIL, 2002.
B) ALL DIMENSIONS ARE IN MILLIMETERS.
C) DIMENSIONING AND TOLERANCING PER ANSI Y14,5 - 1973
D) LOCATION OF THE PIN HOLE MAY VARY (LOWER LEFT CORNER, LOWER CENTER AND CENTER OF THE PACKAGE)
△E DOES NOT COMPLY JEDEC STANDARD VALUE,
F) "A1" DIMENSIONS REPRESENT LIKE BELOW:
SINGLE GAUGE = 0.51 - 0.61
DUAL GAUGE = 1,14 - 1,40
G) DRAWING FILE NAME: TO220B03REV6

D Arduino Code

```
#include <math.h>

int distancePin = A7;          // Input from distance sensor
int distanceRaw = 0;           // Raw data from distance sensor [bits]
float probeLength = 1200.0;    // Distance sensor to probe tip [mm]
float measuredDistance = 0.0; // From distance sensor to surface [mm]
float d1 = 50.0;               // Offset from centrum to distance sensor [mm]
float distance = 0.0;          // Distance after fixing error [mm]
float depth = 0.0;             // Depth in liquid
float density = 1000.0;        // Densitiy of the liquid
float pressure = 0.0;          // Pressure at probe tip
float g = 9.81;                // Gravity
int pwmOutputInt = 0;          // 10 bit pwm output
float pitch = 0.0;             // Pitch angle from IMU
float roll = 0.0;              // Roll angle from IMU
const int analogOutPin = 11;  // Output pin
float k = 0.9;                 // Constant for non-linear behaviour
int potPin = A0;               // Input pin for scaling constant 'k'
int counter = 0;               // Counter for printing values
float p = 1.0;                 // Adjusting for fast submerging
float velocity = 0.0;          // Velocity for 'p'
float maxVelocity = 800.0;     // Max velocity for 'p'
int led = 22;                  // Led pin
int sleep = 10;                // Software delay
float s1 = 0, s2 = 0;          // s1 and s2 are for velocity calculations
const float pi = 3.14;         // Pi for imu calculations
bool imu = false;              // Using IMU or not

void setup() {

  Serial.begin(57600);

  // Configuring analogOutPin to 10 bit
  TCCR1B &= ~(1 << CS12);
  TCCR1B |=  (1 << CS11);
  TCCR1B &= ~(1 << CS10);

  TCCR1B &= ~(1 << WGM13);
  TCCR1B |=  (1 << WGM12);

  TCCR1A |= (1 << WGM11);
  TCCR1A |= (1 << WGM10);
```

```
  pinMode(analogOutPin, OUTPUT);
  pinMode(led, OUTPUT);
}

void loop() {

    // Calculating the down velocity of the probe
    s1 = (float)analogRead(distancePin) * 1.3637 - 68.8295;
    velocity = (s2 - s1)*1000/sleep;
    if(velocity>=maxVelocity){
      p = 2.0;
      digitalWrite(led, HIGH);
    }
    else{
     p = 1.0;
     digitalWrite(led, LOW);
    }

  // Getting distance from US sensor
  distanceRaw = analogRead(distancePin);
  measuredDistance = (float)distanceRaw * 1.3868 -68.3981;

  // Constant from potentiometer for scaling
  k = (analogRead(potPin))*0.001172+0.4;

  // k is a constant to account for some non linearities
  k = k*(-0.0004*measuredDistance+0.9583); // With new PCB

  // Calculating depth with or without imu
  if(imu){
  // Reading angles from IMU and converting to radians
  pitch = (pi/180.0) * readPitch(); // Orientation about x
  roll = (pi/180.0) * readRoll();     // Orientation about y
  float d2 = probeLength -(measuredDistance-d1*tan(pitch));
  float temp1 = cos(pitch)*cos(roll);
  float temp2 = pow(sin(pitch),2)+pow(sin(roll),2);
  depth = d2*sin(atan(sqrt(temp1/temp2));
  }
  else{
  // Depth of tip if IMU is not used
  depth = probeLength - measuredDistance;
  }
```

```
  // Pressure at probe tip, in bars
  pressure = p * k * depth * density * g * pow(10,-8);

  // Calculating pwm output
  pwmOutputInt = (int)(pressure*2048);

  // Setting a minimum pressure if the probe is not in liquid
  if(measuredDistance >= probeLength ||  measuredDistance <= 200){
   pwmOutputInt = 0;
  }

  // Writing to the pressure regulator
  analogWrite(analogOutPin, pwmOutputInt);

  // Printing function, prints desired values/strings
  if(counter >= 1000/sleep){
  Serial.print(k);
  Serial.print('\t');
  Serial.print(measuredDistance);
  Serial.print('\t');
  counter = 0;
  }
  counter++;

  // s2 is for the velocity calculations
  s2 = (float)analogRead(distancePin) * 1.3637 - 68.8295;
  delay(sleep);
}

float readPitch() {
  Serial.write("#p");    // Requesting data from IMU
  int MSG_MAX = 100;
  char msg[MSG_MAX];
  char c;
  int i = 0;
  String msg_str;
  memset(msg,0,MSG_MAX);

  while(c != 10 && i <= MSG_MAX) {
    if(Serial.available() > 0) {
      c = Serial.read();
      msg[i] = c;
      i++;
    }
```

```
  }
  Serial.print(msg);
  return atof(msg);
  Serial.flush();
}

float readRoll() {
  Serial.write("#h");    // Requesting data from IMU
  int MSG_MAX = 100;
  char msg[MSG_MAX];
  char c;
  int i = 0;
  String msg_str;
  memset(msg,0,MSG_MAX);

  while(c != 10 && i <= MSG_MAX) {
    if(Serial.available() > 0) {
      c = Serial.read();
      msg[i] = c;
      i++;
    }
  }
  Serial.print(msg);
  return atof(msg);
  Serial.flush();
}
```

E Register Code

```
// This code goes into the void setup() function.
// This timer affects pins 11, 12 and 13 on Arduino Mega 2560
// To use these pins use analogWrite(pin, value)
// Value being between 0 - 1024

TCCR1B &= ~(1 << CS12);
TCCR1B  |=   (1 << CS11);
TCCR1B &= ~(1 << CS10);

TCCR1B &= ~(1 << WGM13);
TCCR1B |=  (1 << WGM12);

TCCR1A |= (1 << WGM11);
TCCR1A |= (1 << WGM10);

pinMode(pin, OUTPUT);
```

F Electrical Schematics

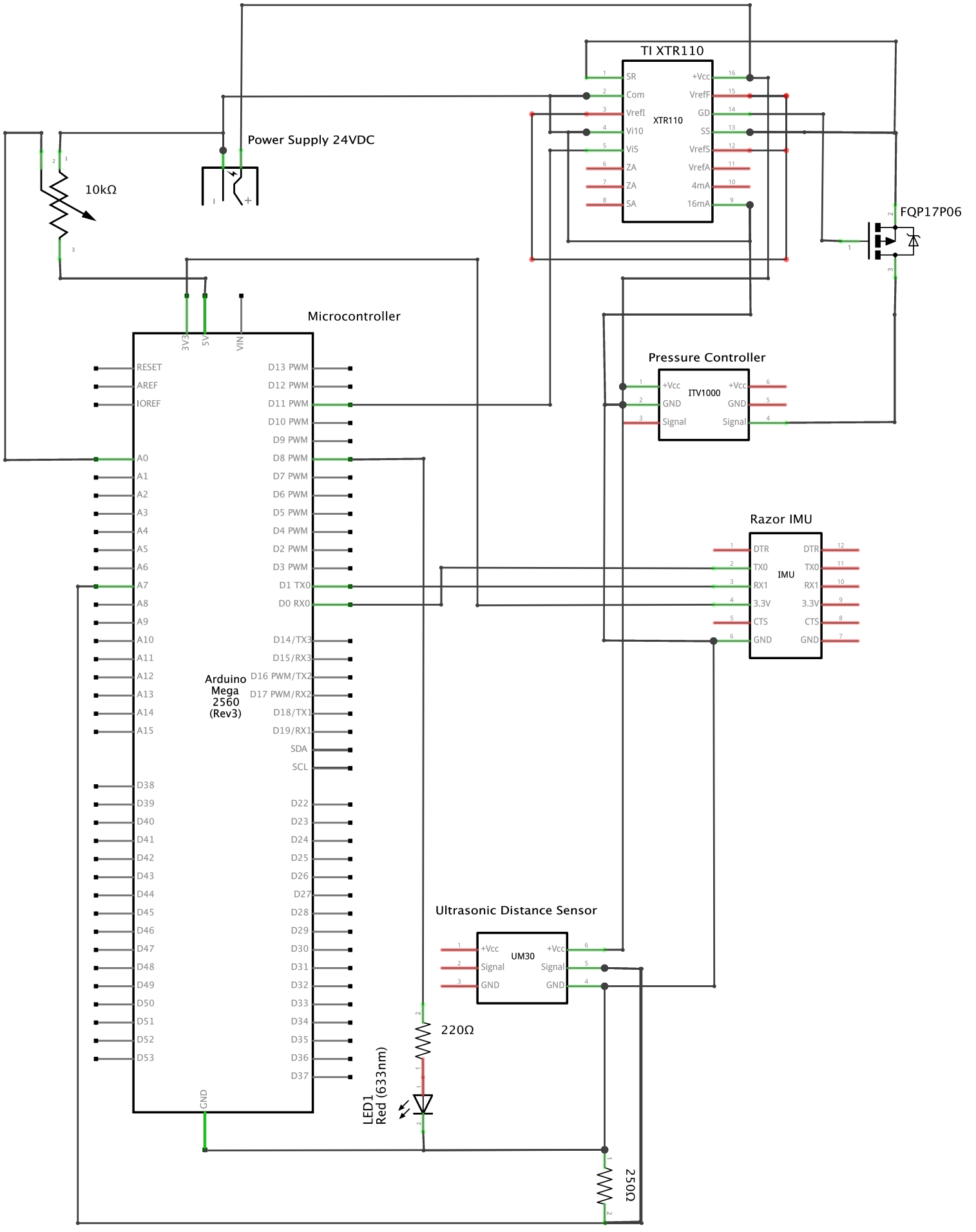
TI XTR110
XTR110
SR
Com
VrefI
Vi10
Vi5
ZA
ZA
SA
+Vcc
VrefF
GD
SS
VrefS
VrefA
4mA
16mA
Power Supply 24VDC
10kΩ
FQP17P06
Microcontroller
3V3
5V
VIN
RESET
AREF
IOREF
A0
A1
A2
A3
A4
A5
A6
A7
A8
A9
A10
A11
A12
A13
A14
A15
D13 PWM
D12 PWM
D11 PWM
D10 PWM
D9 PWM
D8 PWM
D7 PWM
D6 PWM
D5 PWM
D4 PWM
D2 PWM
D3 PWM
D1 TX0
D0 RX0
D14/TX3
D15/RX3
D16 PWM/TX2
D17 PWM/RX2
D18/TX1
D19/RX1
SDA
SCL
D38
D39
D40
D41
D42
D43
D44
D45
D46
D47
D48
D49
D50
D51
D52
D53
D22
D23
D24
D25
D26
D27
D28
D29
D30
D31
D32
D33
D34
D35
D36
D37
GND
Arduino Mega 2560 (Rev3)
Pressure Controller
ITV1000
+Vcc
GND
Signal
Razor IMU
IMU
DTR
TX0
RX1
3.3V
CTS
GND
Ultrasonic Distance Sensor
UM30
220Ω
LED1
Red (633nm)
250Ω

G PCB Top Layer

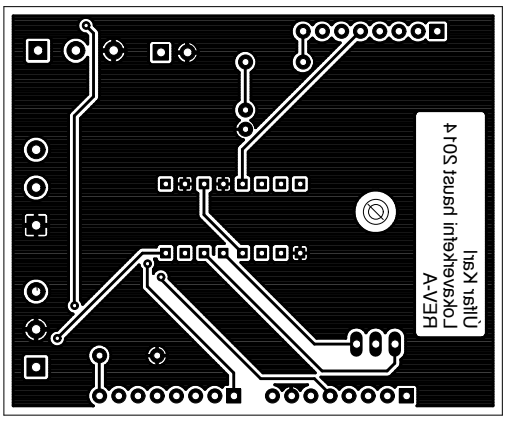
Ultar Kari
Lokavaheti trust 2014
REV-A

H PCB Bottom Layer

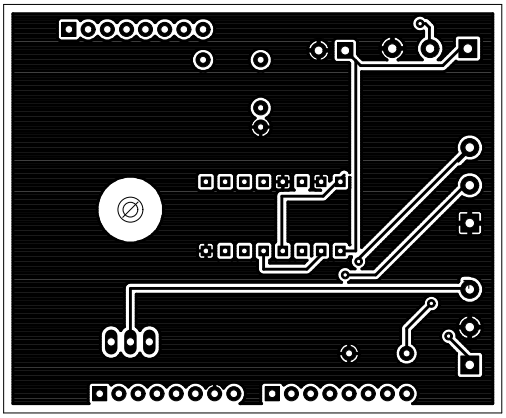

I Prototype Drawings

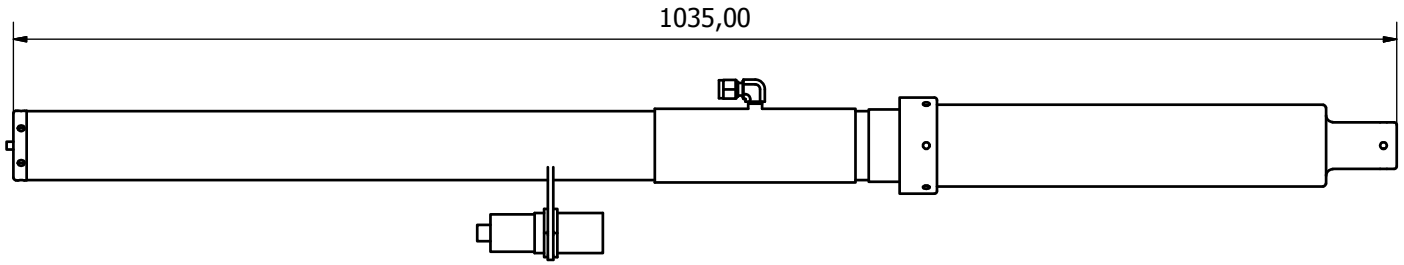

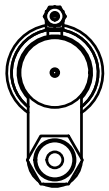

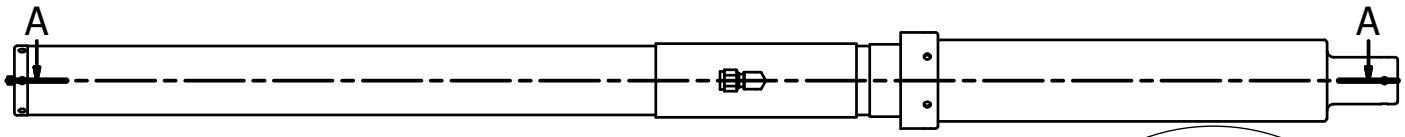

A-A (1:4)

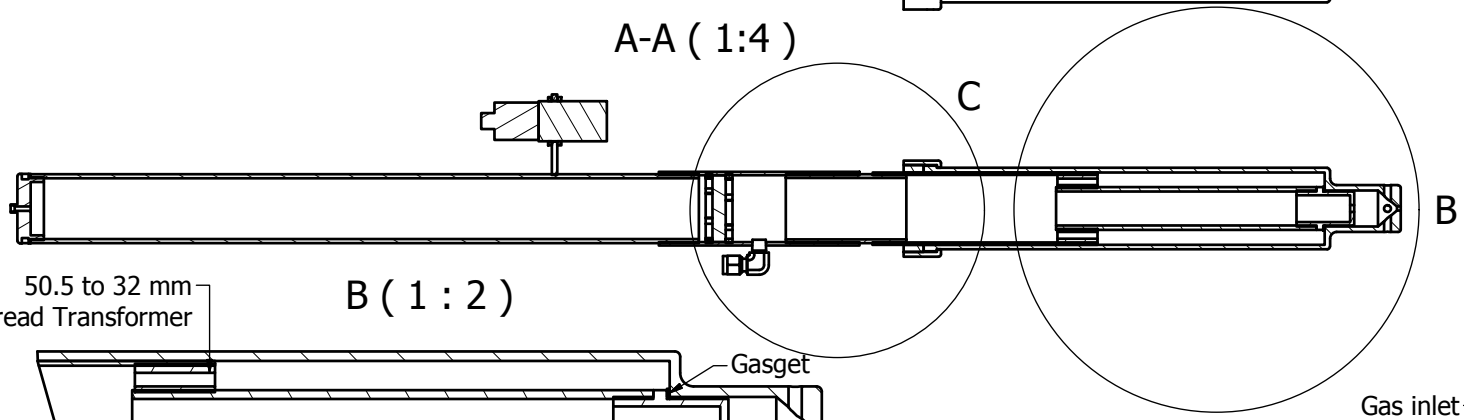

B (1 : 2)

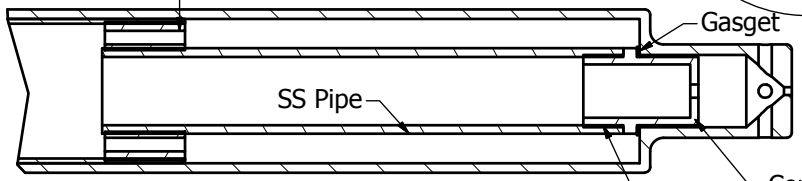

C (1 : 2)

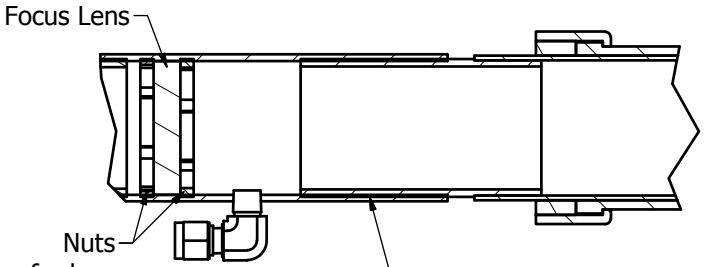

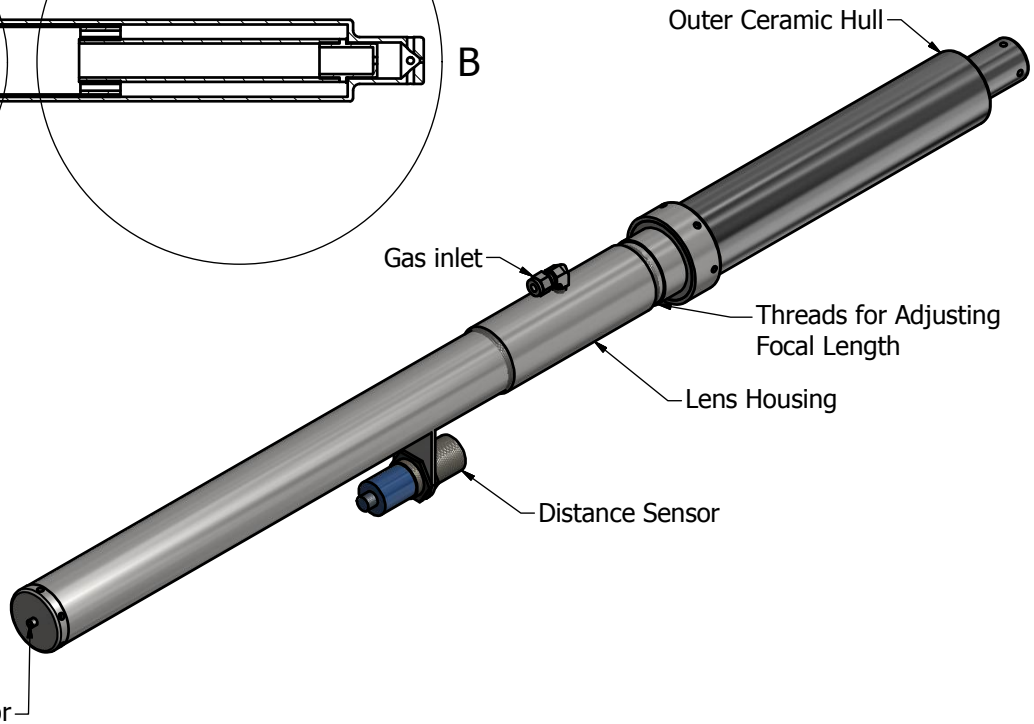

Designed by	Checked by	Approved by	Date		Date	Scale
Úlfar Karl	Sveinn Hinrik	Sveinn Hinrik	24.11.2014		15.11.2014	1 : 4

DTE DYNAMIC TECHNOLOGY EQUIPMENT

PEA-PROBE

Overview Ceramic

Edition	Sheet
C	1 / 16

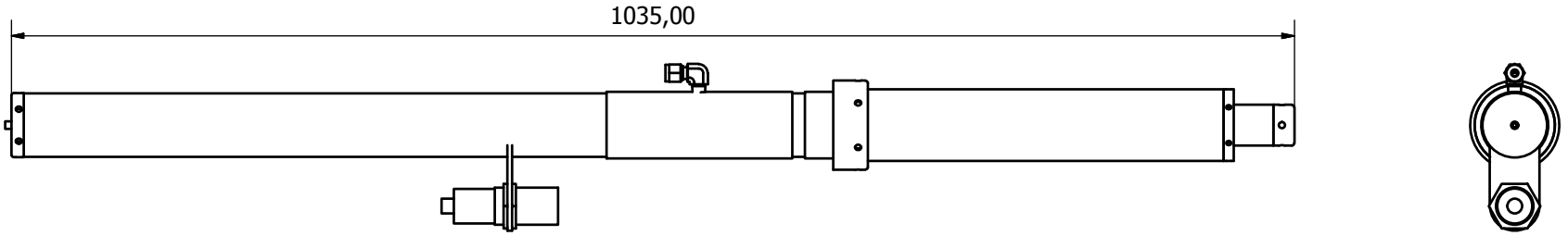

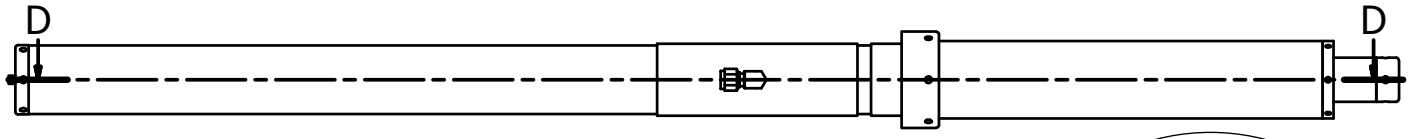

D-D (1:4)

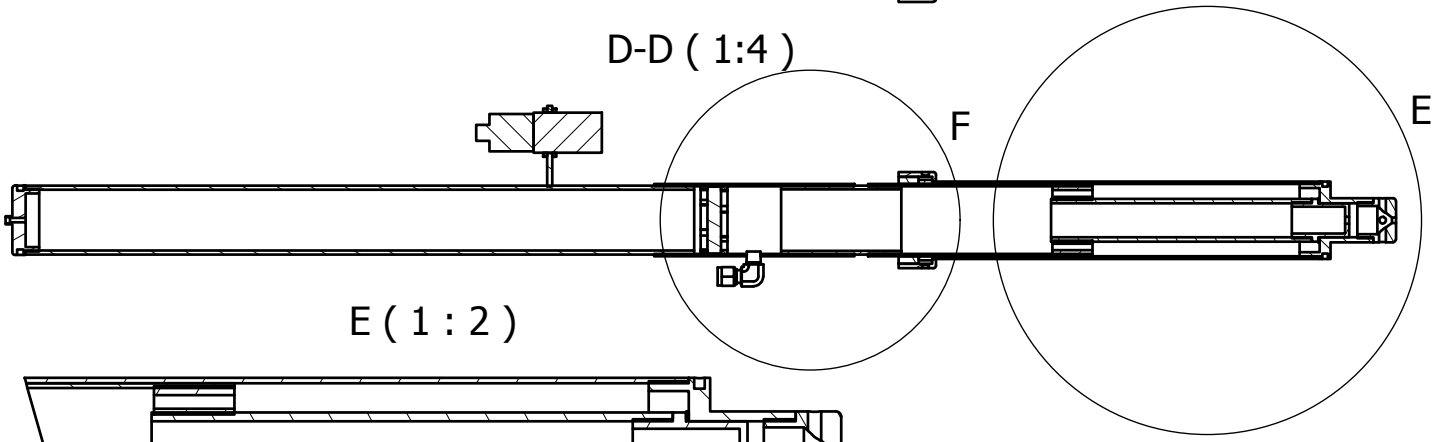

E (1 : 2)

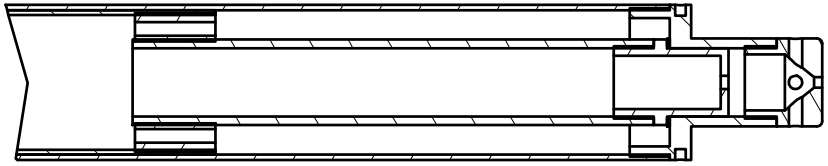

F (1 : 2)

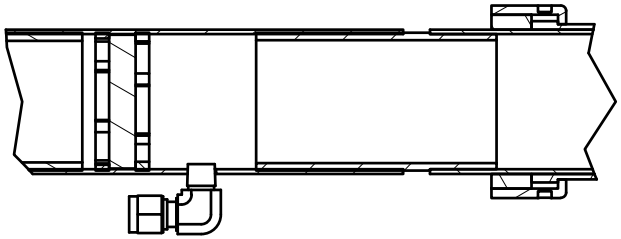

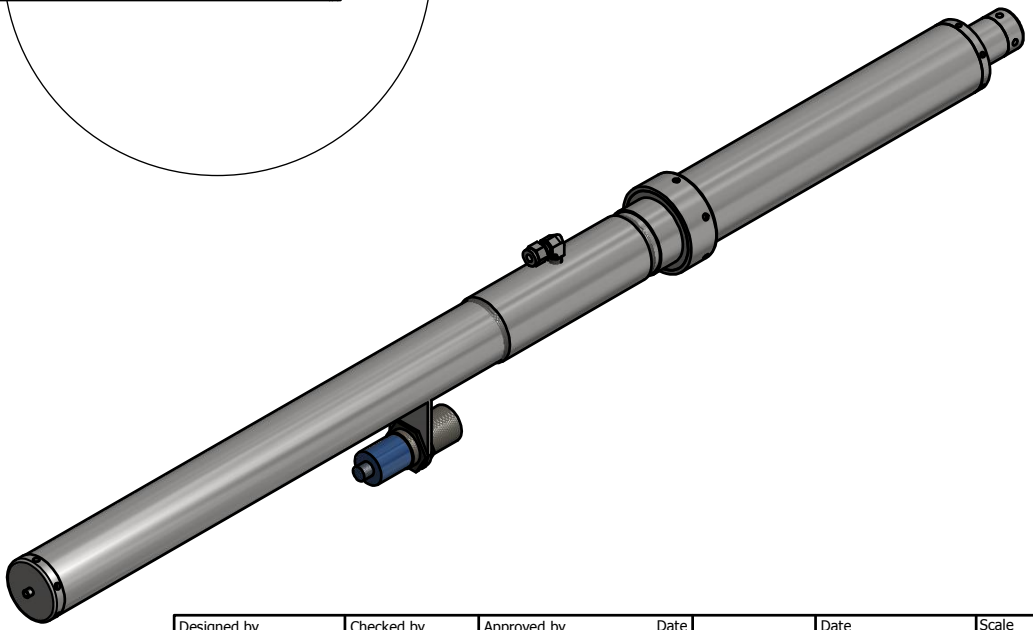

Designed by	Checked by	Approved by	Date		Date	Scale
Úlfar Karl	Sveinn Hinrik	Sveinn Hinrik	24.11.2014		15.11.2014	1 : 4

DTE DYNAMIC TECHNOLOGY EQUIPMENT

PEA-PROBE

Overview Steel	Edition	Sheet
	C	2 / 16

Probe with ceramic parts

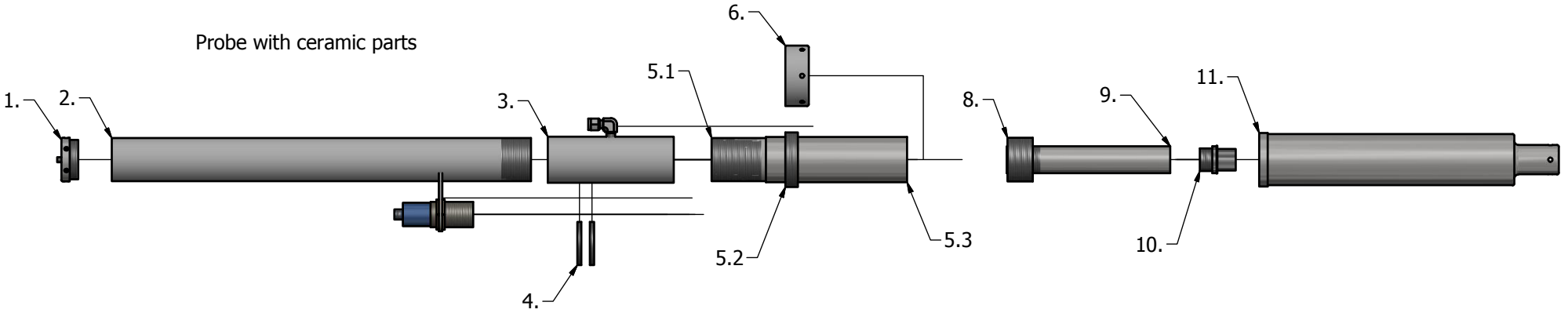

Probe with steel parts

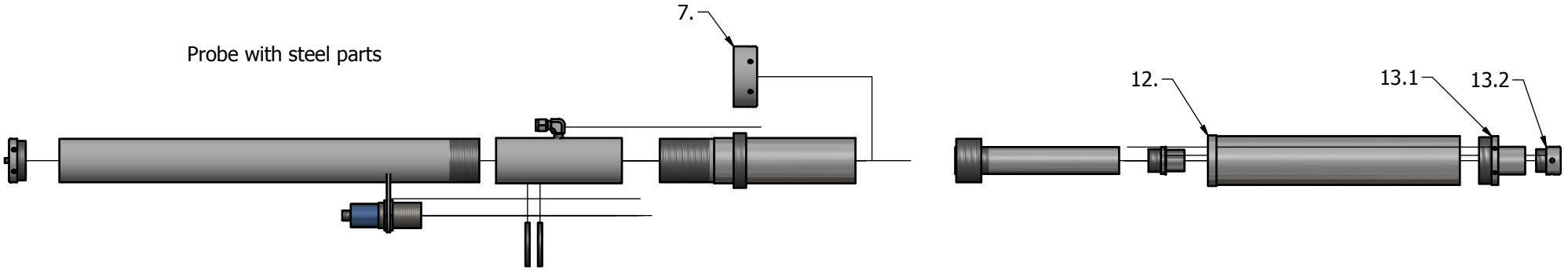

Designed by	Checked by	Approved by	Date		Date	Scale
Úlfar Karl	Sveinn Hinrik	Sveinn Hinrik	24.11.2014		15.11.2014	1 : 5

DTE DYNAMIC TECHNOLOGY EQUIPMENT

PEA-PROBE

Part List

Edition	Sheet
C	3 / 16

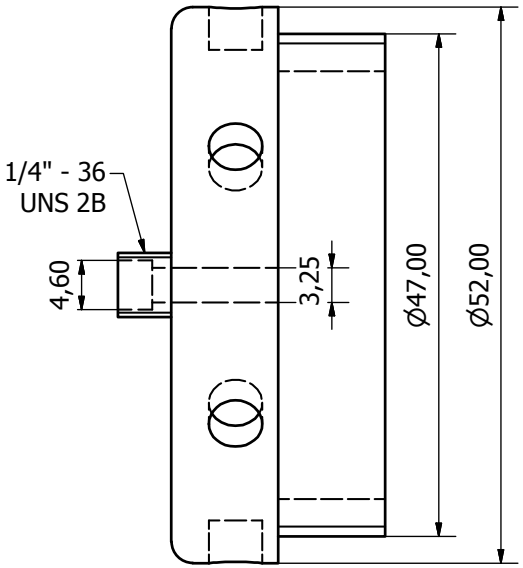

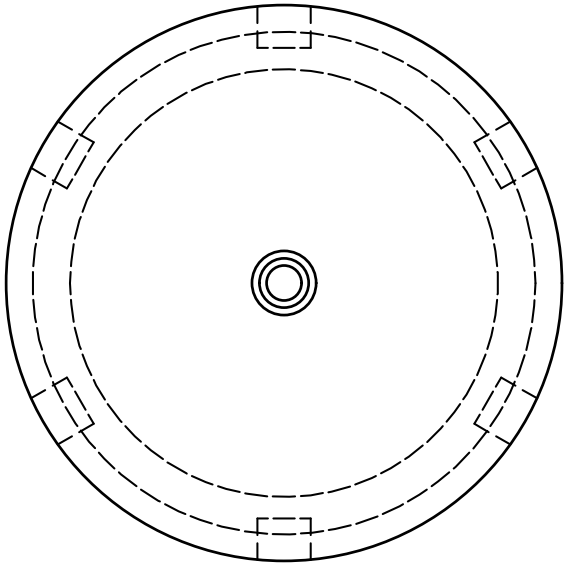

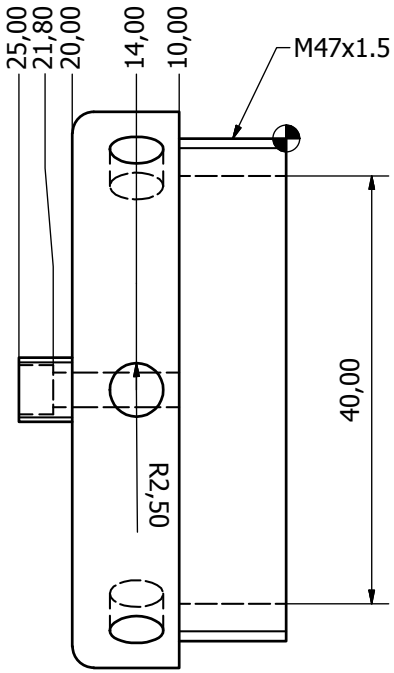

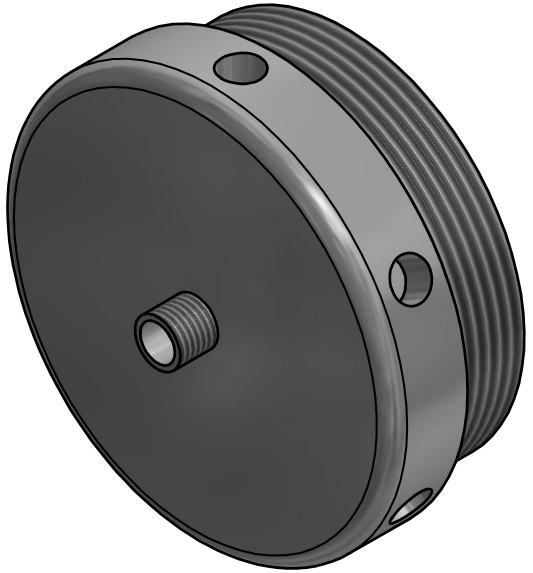

Designed by	Checked by	Approved by	Date		Date	Scale
Úlfar Karl	Sveinn Hinrik	Sveinn Hinrik	24.11.2014		15.11.2014	2 : 1

DTE DYNAMIC TECHNOLOGY EQUIPMENT

PEA-PROBE

1. OF Cap

Edition	Sheet
C	4 / 16

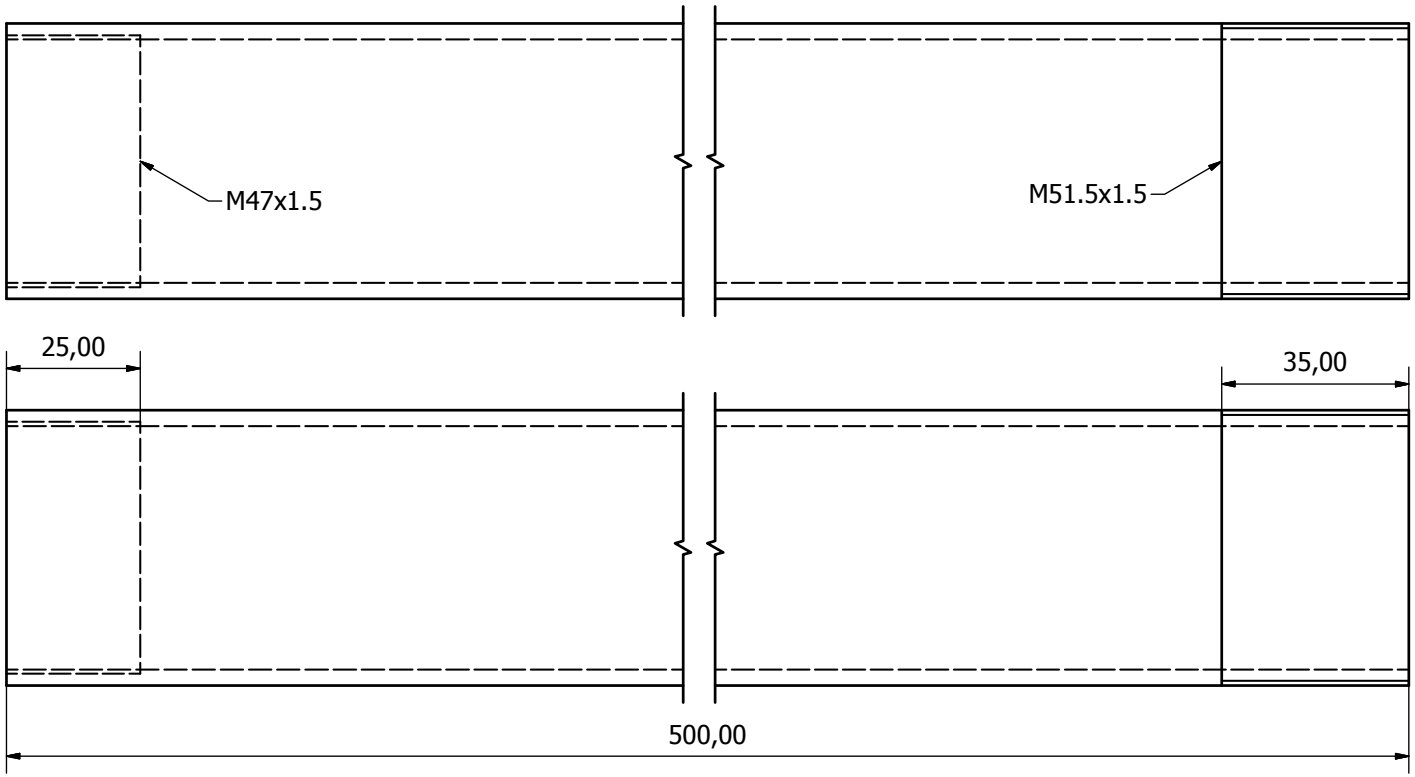

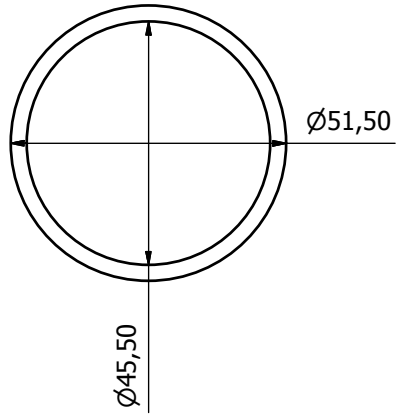

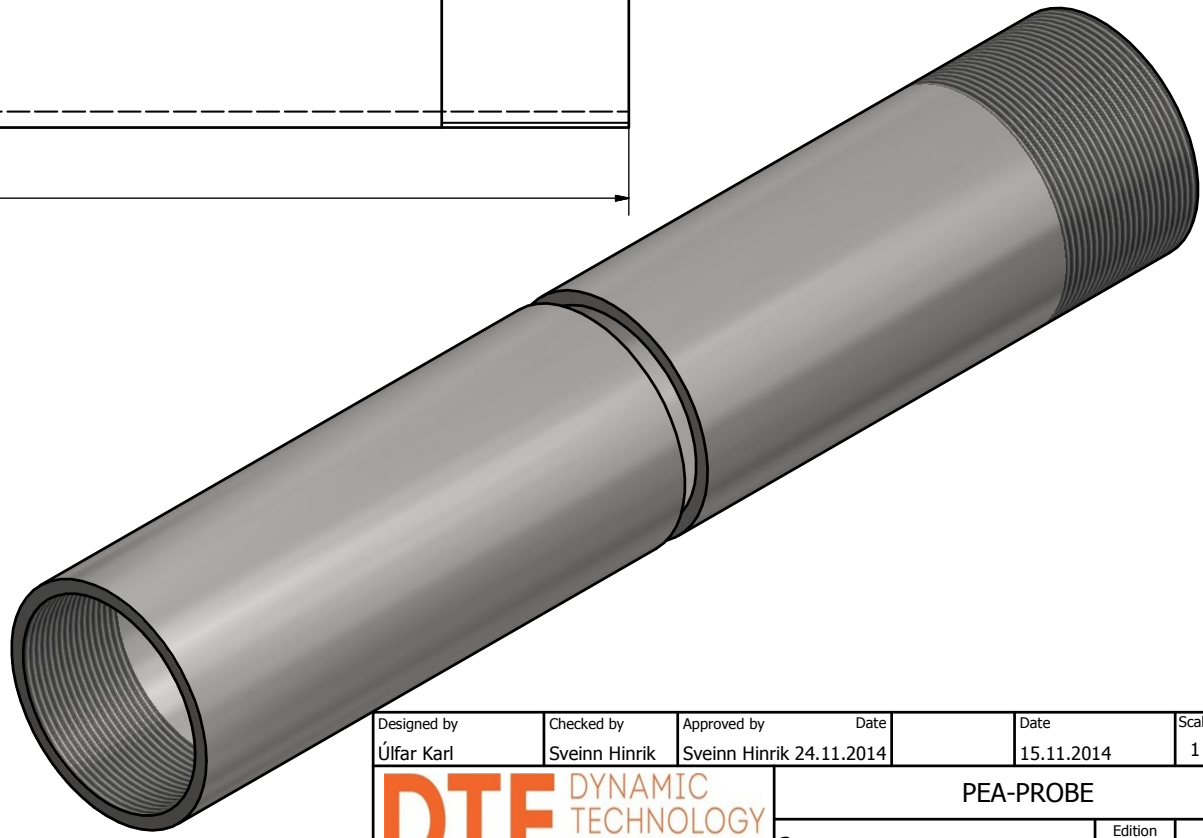

Designed by	Checked by	Approved by	Date		Date	Scale
Úlfar Karl	Sveinn Hinrik	Sveinn Hinrik	24.11.2014		15.11.2014	1 : 1

DTE DYNAMIC TECHNOLOGY EQUIPMENT

PEA-PROBE

2.	Edition C	Sheet 5 / 16

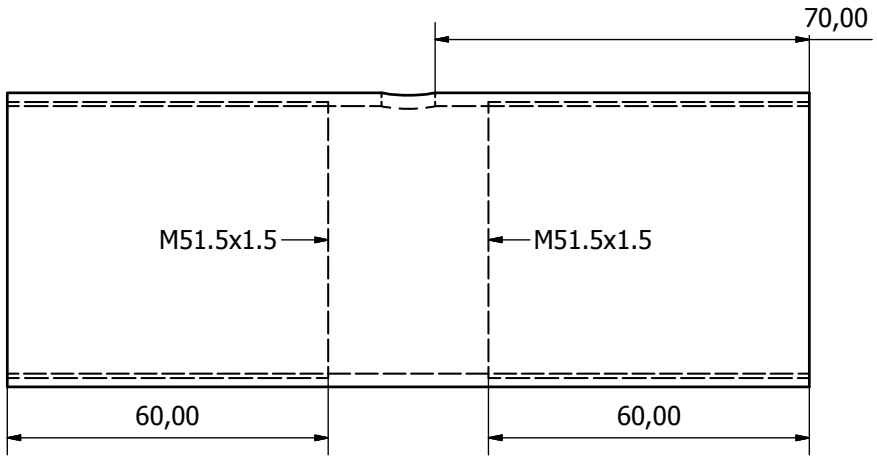

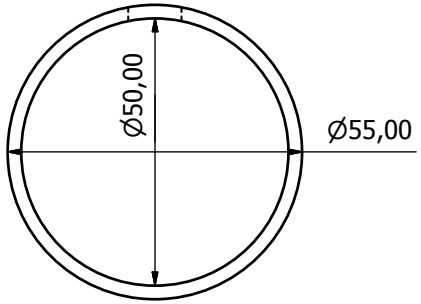

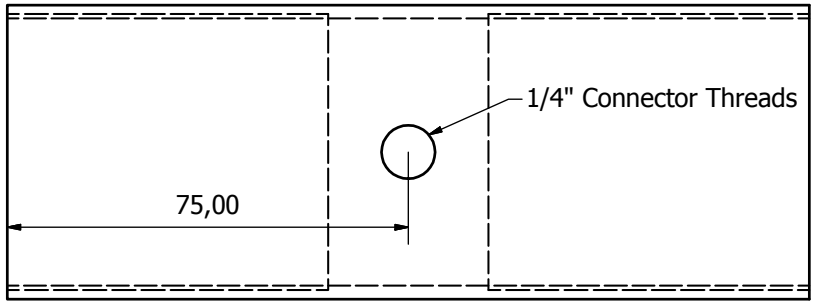

Designed by	Checked by	Approved by	Date		Date	Scale
Úlfar Karl	Sveinn Hinrik	Sveinn Hinrik	24.11.2014		15.11.2014	1 : 1

DTE DYNAMIC TECHNOLOGY EQUIPMENT

PEA-PROBE

3. Lens House

Edition	Sheet
C	6 / 16

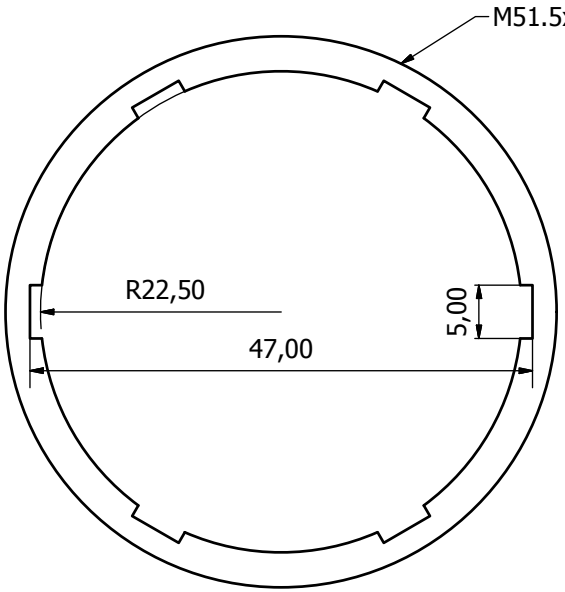

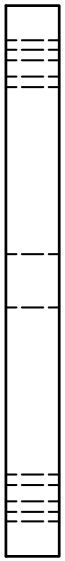

2 pieces.

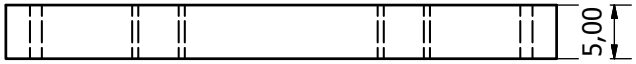

Designed by	Checked by	Approved by	Date		Date	Scale
Úlfar Karl	Sveinn Hinrik	Sveinn Hinrik	24.11.2014		15.11.2014	2 : 1

DTE DYNAMIC TECHNOLOGY EQUIPMENT

PEA-PROBE

4. Lens Nut

Edition C

Sheet 7 / 16

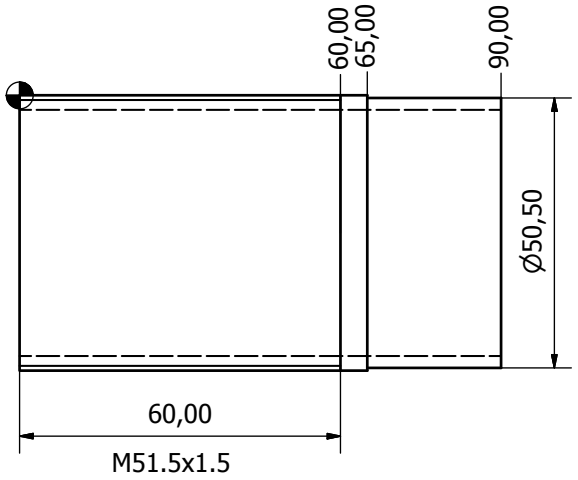

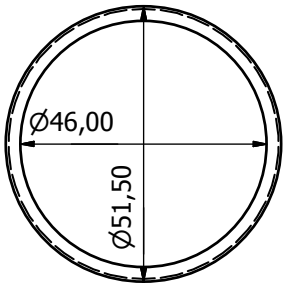

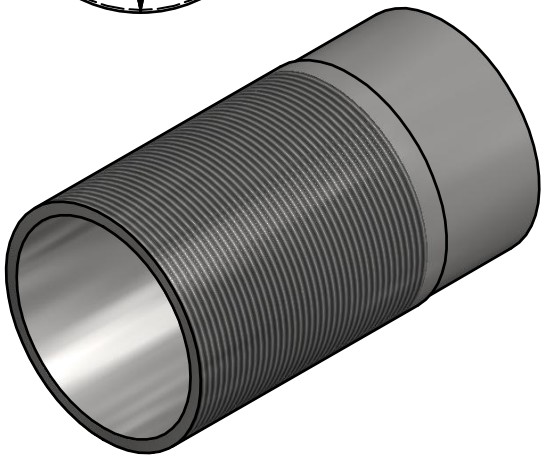

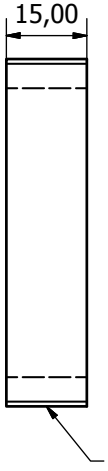

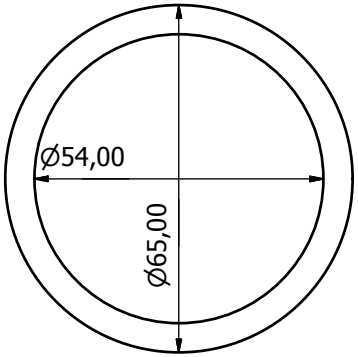

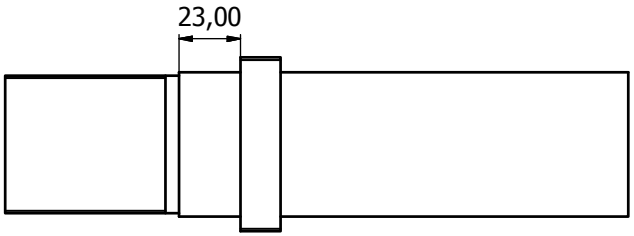

(1 : 2)

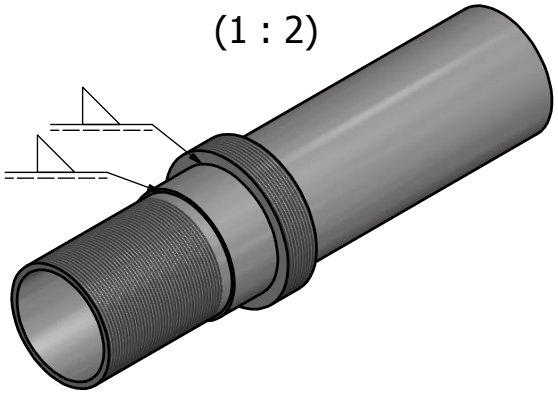

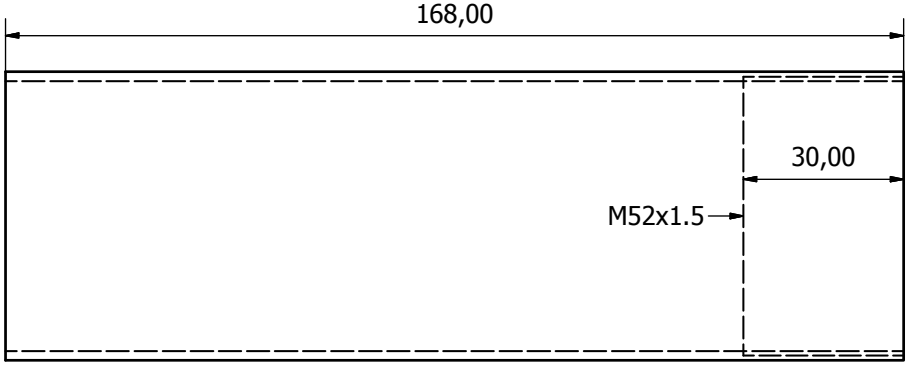

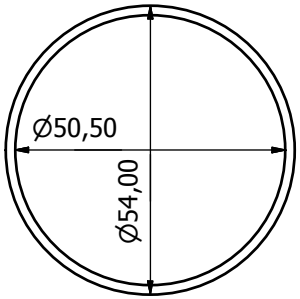

Designed by	Checked by	Approved by	Date		Date	Scale
Úlfar Karl	Sveinn Hinrik	Sveinn Hinrik	24.11.2014		15.11.2014	1 : 1

DTE DYNAMIC TECHNOLOGY EQUIPMENT

PEA-PROBE

5. Focus Adjuster

Edition	Sheet
C	8 / 16

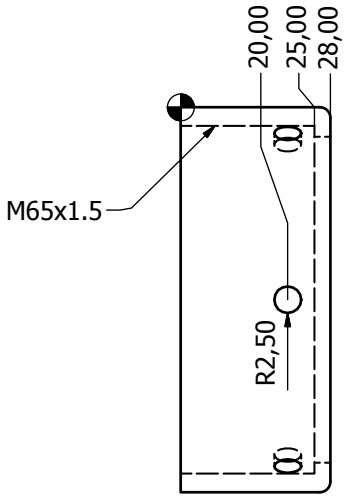

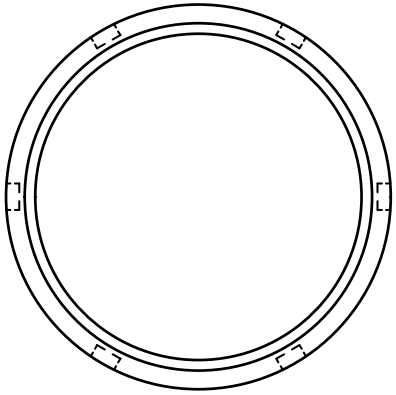

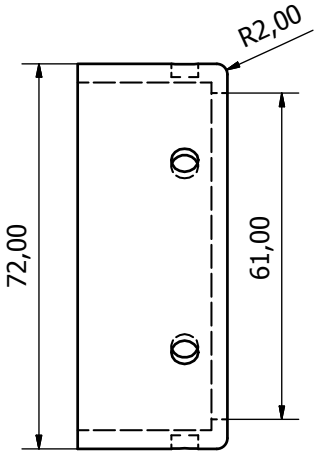

This part will only be made ones but the inside diameter will be changed when the ceramic parts are made

Designed by	Checked by	Approved by	Date		Date	Scale
Úlfar Karl	Sveinn Hinrik	Sveinn Hinrik	24.11.2014		15.11.2014	1 : 1

DTE DYNAMIC TECHNOLOGY EQUIPMENT

PEA-PROBE

6. Nut for Ceramic

Edition	Sheet
C	9 / 16

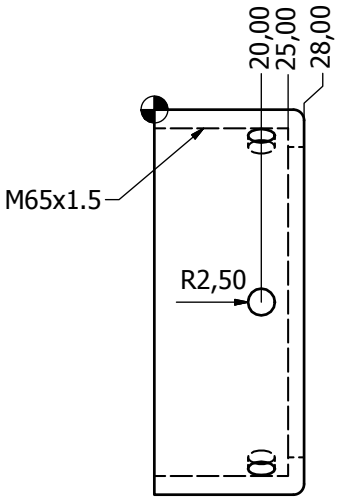

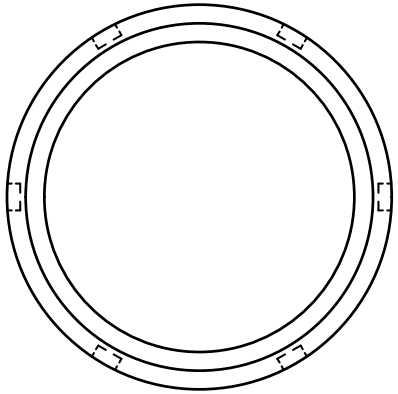

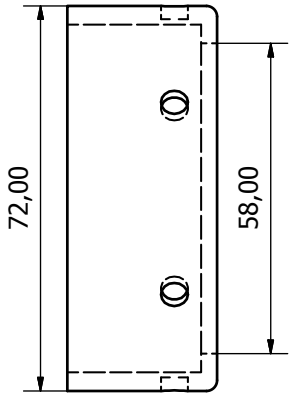

Designed by	Checked by	Approved by	Date		Date	Scale
Úlfar Karl	Sveinn Hinrik	Sveinn Hinrik	24.11.2014		15.11.2014	1 : 1

DTE DYNAMIC TECHNOLOGY EQUIPMENT

PEA-PROBE

7. Nut for Steel

Edition	Sheet
C	10 / 16

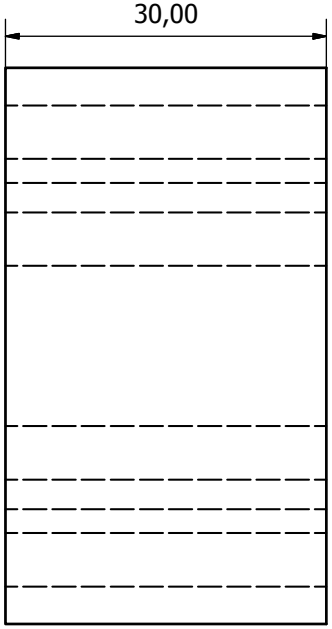

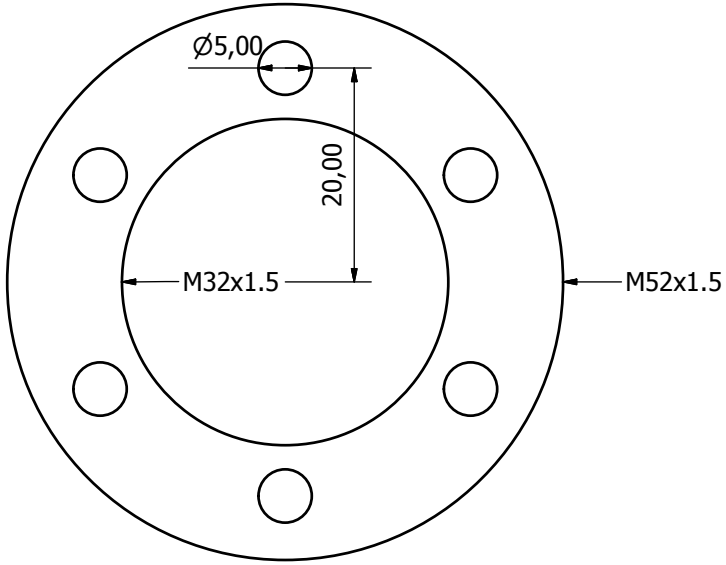

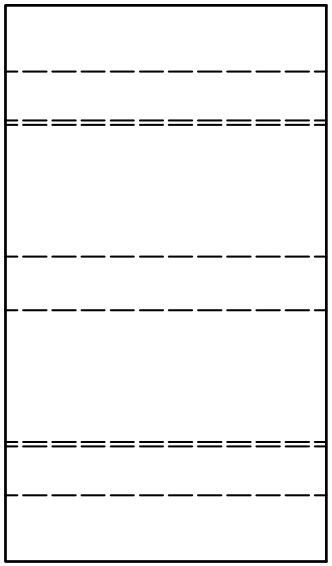

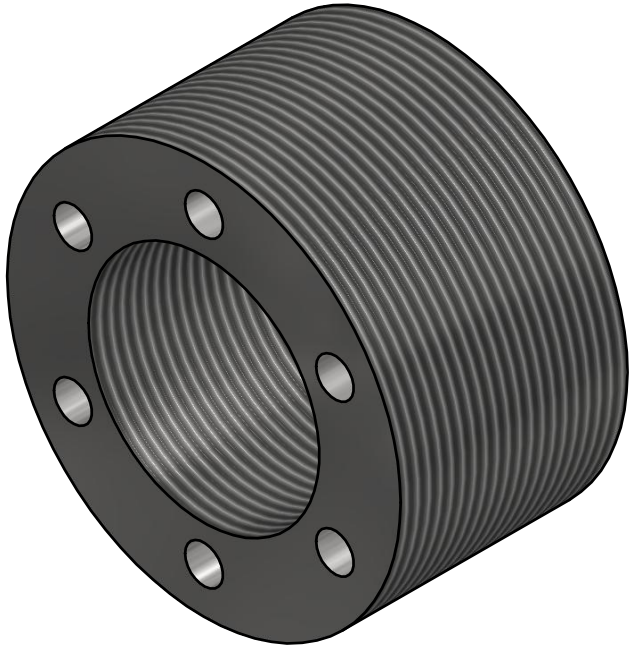

Designed by	Checked by	Approved by	Date		Date	Scale
Úlfar Karl	Sveinn Hinrik	Sveinn Hinrik	24.11.2014		15.11.2014	2 : 1

DTE DYNAMIC TECHNOLOGY EQUIPMENT

PEA-PROBE

8. Thread Transformer

Edition C

Sheet 11 / 16

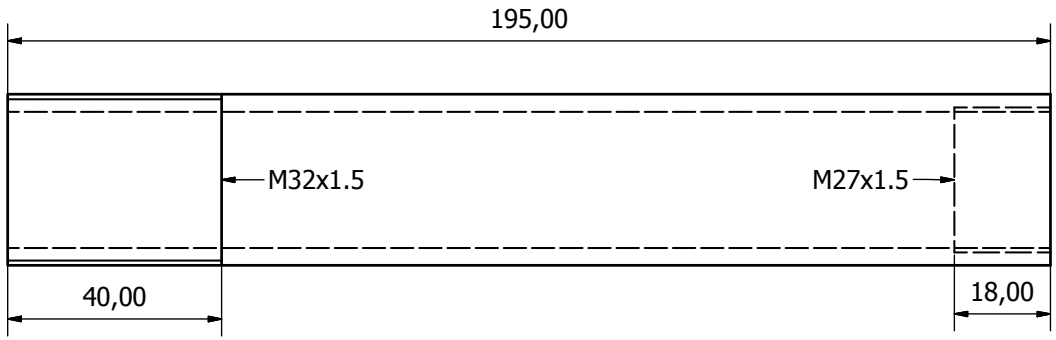

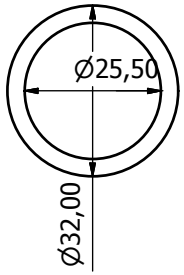

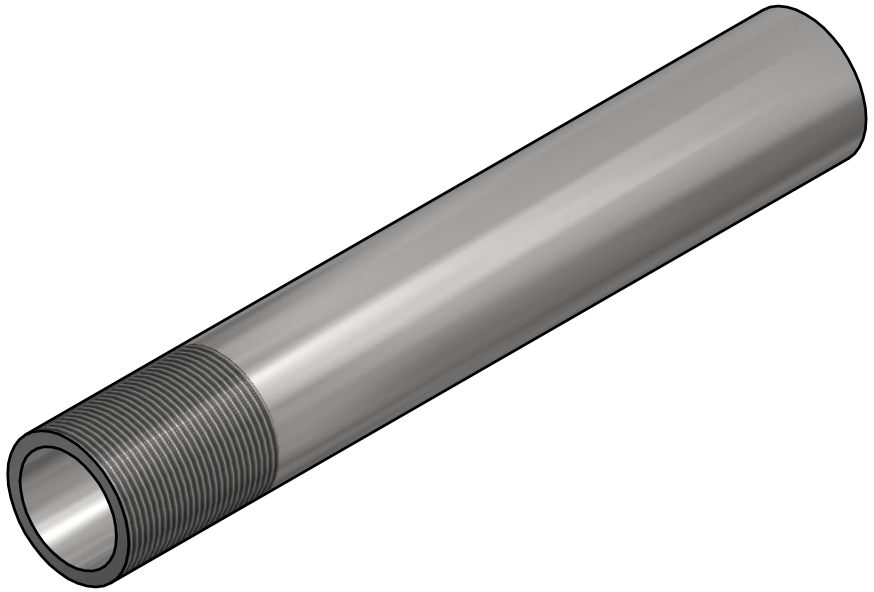

Designed by	Checked by	Approved by	Date		Date	Scale
Úlfar Karl	Sveinn Hinrik	Sveinn Hinrik	24.11.2014		15.11.2014	1 : 1

DTE DYNAMIC TECHNOLOGY EQUIPMENT

PEA-PROBE

9. Inner Steel Tube

Edition: C

Sheet: 12 / 16

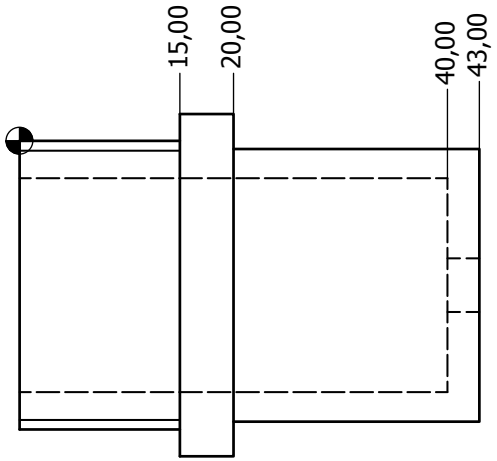

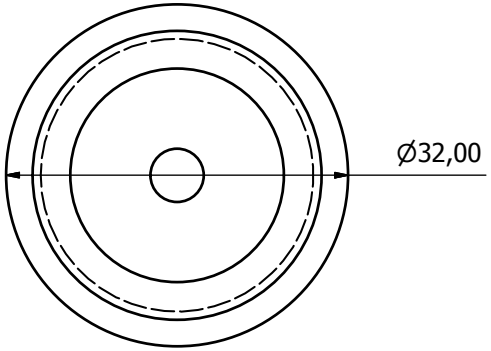

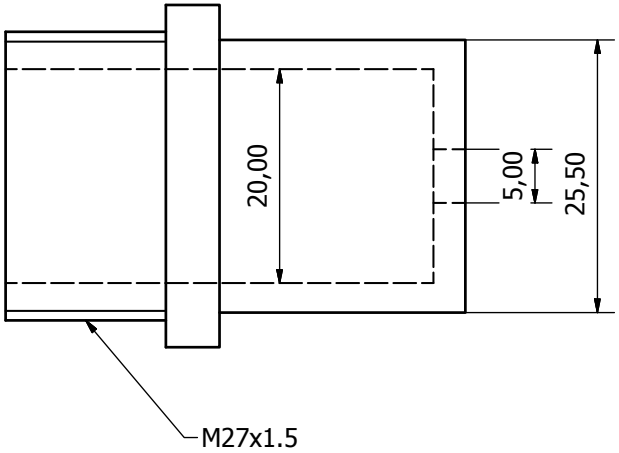

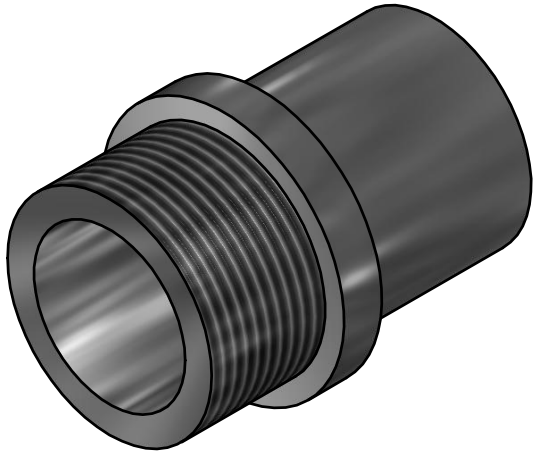

Designed by	Checked by	Approved by	Date		Date	Scale
Úlfar Karl	Sveinn Hinrik	Sveinn Hinrik	24.11.2014		15.11.2014	2 : 1

DTE DYNAMIC TECHNOLOGY EQUIPMENT

PEA-PROBE

10. Ceramic Cap

Edition	Sheet
C	13 / 16

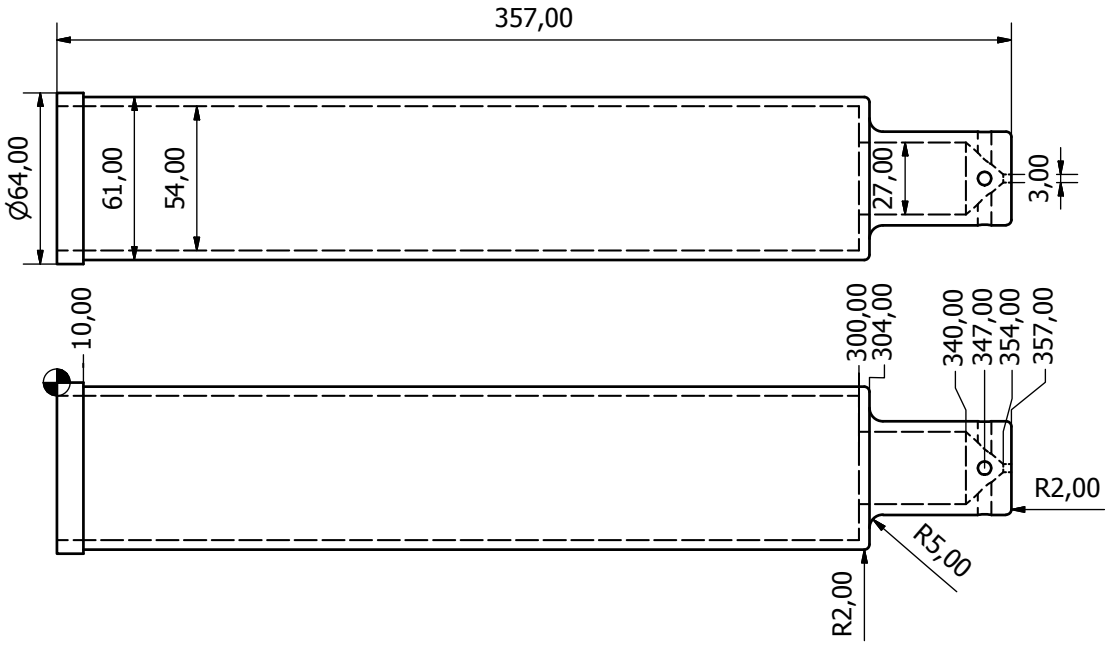

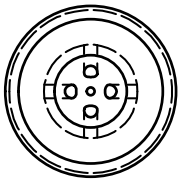

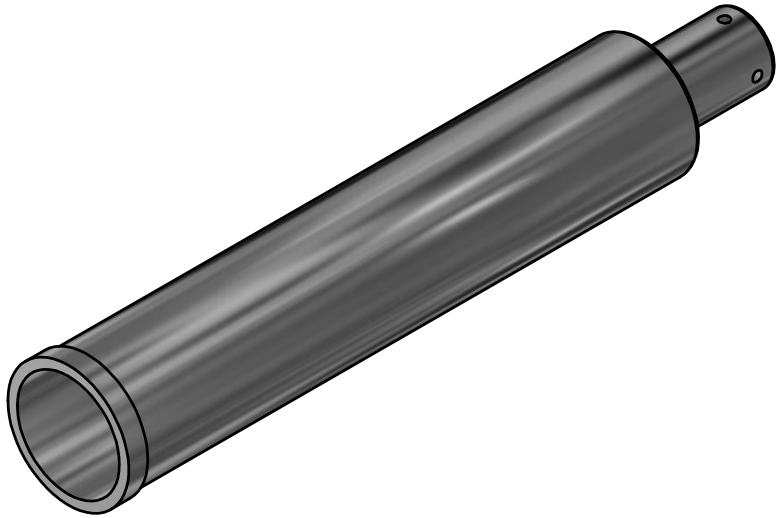

Designed by	Checked by	Approved by	Date		Date	Scale
Úlfar Karl	Sveinn Hinrik	Sveinn Hinrik	24.11.2014		15.11.2014	1 : 2

DTE DYNAMIC TECHNOLOGY EQUIPMENT

PEA-PROBE

11. Outer Ceramic Hull	Edition	Sheet
	C	14 / 16

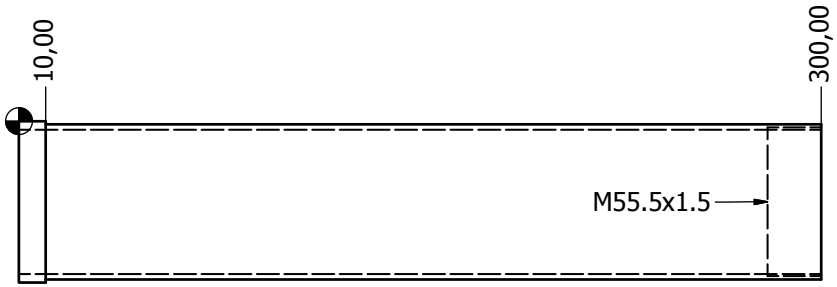

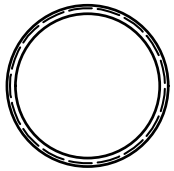

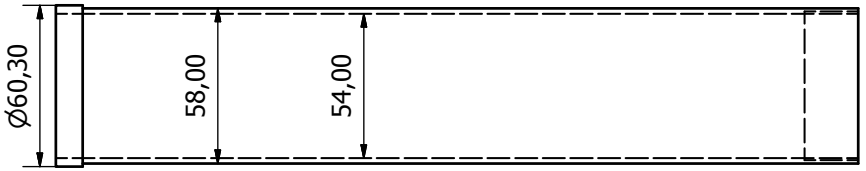

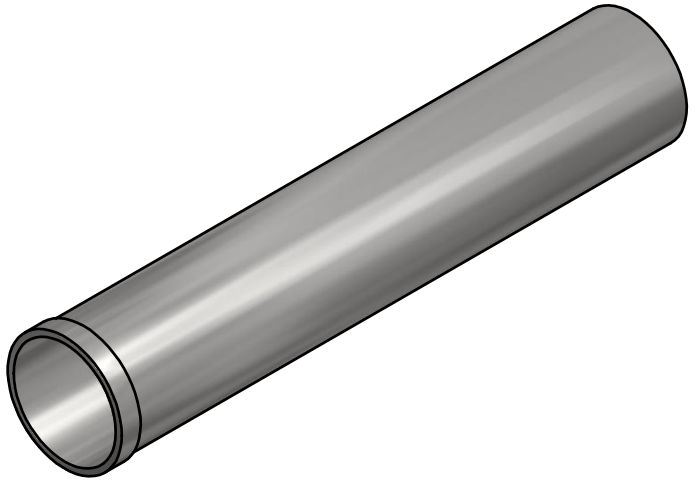

Designed by	Checked by	Approved by	Date		Date	Scale
Úlfar Karl	Sveinn Hinrik	Sveinn Hinrik	24.11.2014		15.11.2014	1 : 2

DTE DYNAMIC TECHNOLOGY EQUIPMENT

PEA-PROBE

12. Outer Steel Hull I

Edition	Sheet
C	15 / 16

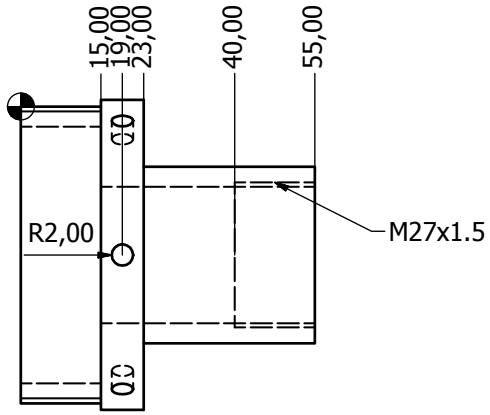

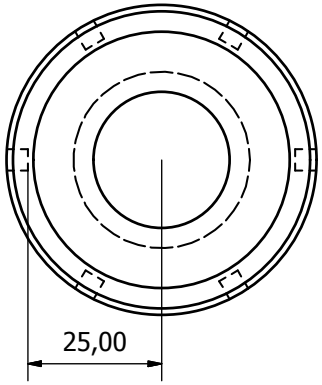

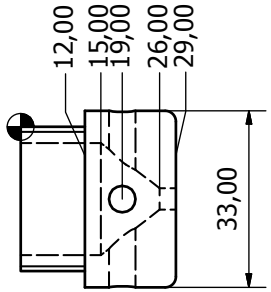

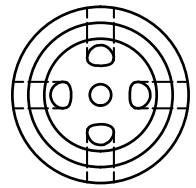

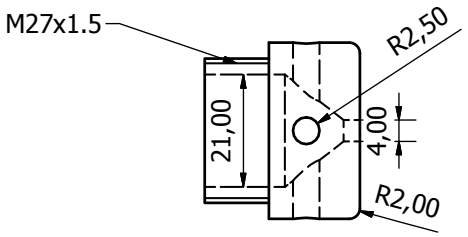

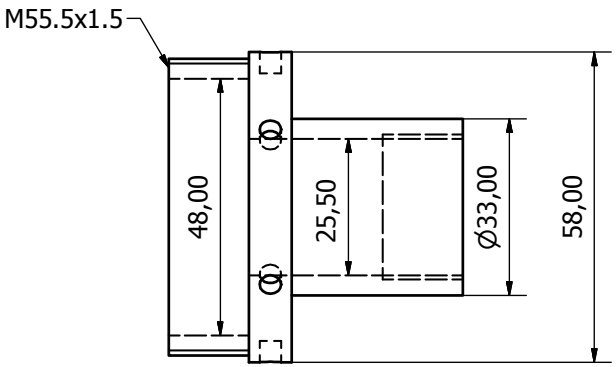

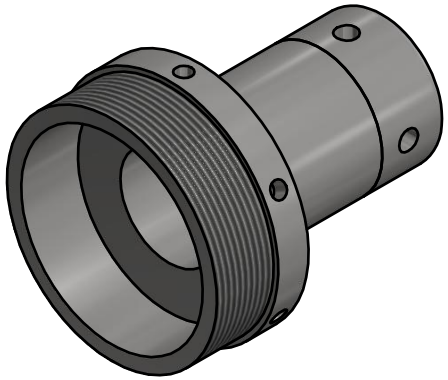

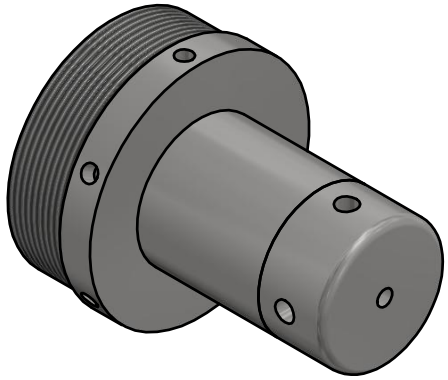

Designed by	Checked by	Approved by	Date		Date	Scale
Úlfar Karl	Sveinn Hinrik	Sveinn Hinrik	24.11.2014		15.11.2014	1 : 1

DTE DYNAMIC TECHNOLOGY EQUIPMENT

PEA-PROBE

13. Outer Steel Hull II

Edition C

Sheet 16 / 16